OUKA
Osaka University Knowledge Archive

Title	Crystal Sturcture Analysis of Cytochrome c553 from Desulfovibrio vulgaris Miyazaki F-An Application of the Multi-wavele-ngth Anomalous Dispersion Method-
Author(s)	中川, 敦史
Citation	大阪大学, 1989, 博士論文
Version Type	VoR
URL	https://hdl.handle.net/11094/2711
rights	
Note	

Osaka University Knowledge Archive : OUKA

https://ir.library.osaka-u.ac.jp/

Osaka University

Crystal Structure Analysis of Cytochrome c_{553} from *Desulfovibrio vulgaris* Miyazaki F

An Application of the Multi-wavelength Anomalous Dispersion Method

1989

Atsushi Nakagawa

Crystal Structure Analysis of Cytochrome c_{553} from *Desulfovibrio vulgaris* Miyazaki F

--- An Application of the Multi-wavelength Anomalous Dispersion Method ---

by

Atsushi Nakagawa

A Doctoral Thesis submitted to

Faculty of Science

Osaka University

1989

ABSTRACTS

Multi-wavelength anomalous dispersion phasing technique has been applied to the determination of three-dimensional structure of an electron transfer protein cytochrome c_{553} isolated from sulfate-reducing bacterium, *Desulfovibrio vulgaris* Miyazaki F. This novel method makes use of crystallographic phases determined from measurements made at several wavelengths. In contrast with all of the conventional methods of solving overall structures of biological macromolecular crystals, which require either multiple (or single) isomorphous derivatives or atomic coordinates of a similar structure for molecular replacement, this method does not need any other informations than diffraction intensities from native biological macromolecular crystals and allows direct solution of classical "phase problem". This result has proved successful through the use of intense and polychromatic synchrotron radiation at Photon Factory, National Laboratory for High Energy Physics, with accurate and high-speed data collection from the combination of the Weissenberg camera for macromolecular crystallography and the imaging plate, which is a flexible plate coated with photostimulable phosphor crystal and its sensitivity is several tens times higher than the conventional high sensitivity X-ray film. And local scaling procedure has succeeded to reduce systematic errors of data.

The model building of the structure has been carried out by the interpretation of the electron density map which was calculated by multiple anomalous dispersion technique using four native data sets taken at different wavelength below 2.2Å resolution. The structure has been refined by Hendrickson-Konnert's restrained parameter least-squares refinement proce-

dure to an R value of 0.226 at 6.0-1.6Å resolution including 63 water molecules.

The structure of cytochrome c_{553} has four α-helices, and about a half of all amino acid residues have α-helical conformations. The c-type heme group is attached covalently to the amino acid chain by thioether linkage from Cys10 and Cys13 to the heme vinyl groups at positions 2 and 4, respectively. Coordination bonds are also formed from the epsilon nitrogen of His14 and the sulfur of Met57 to the fifth and sixth coordination sites of the heme iron. The relative locations of two helices at both N-terminus and C-terminus and style of bonding and coordination to the heme group is similar to that of other cytochromes c. But other parts of the structure are quite different from that of other cytochromes c, and its function and physical properties, for example redox potential and so on, are also quite different from those of the others. In this sense, the folding pattern of cytochrome c_{553} shows "cytochrome c folding" like other cytochromes c superfamily but cytochrome c_{553} is not classified into the same class of the other small type cytochromes c, for example cytochrome c_{551} from *Pseudomonas aeruginosa* and so on. Its three-dimensional structure provides a novel insight into the physical and chemical properties and evolution of cytochromes c superfamily.

CONTENTS

ACKNOWLEDGMENT

I am deeply indebted to Professor Hideaki Chihara in Osaka University for his helpful suggestion and his heartily guidance throughout this work.

I am also deeply indebted to Professor Yukiteru Katsube and Professor Yoshimasa Kyogoku in Institute for Protein Research and Professor Yoshihiko Kushi in Osaka University for their helpful discussions and suggestions.

I am deeply indebted to Professor Noritake Yasuoka in Basic Research Laboratory, Himeji Institute of Technology, for his continuing help and encouragement throughout my research work.

I am deeply indebted to Professor Noriyoshi Sakabe in Photon Factory, National Laboratory for High Energy Physics (KEK), and Dr. Kiwako Sakabe for their continuing help and encouragement throughout my research work.

I am deeply indebted to Professor Tatsuhiko Yagi for his suggestion and advice on biochemistry and supplement of cytochrome c_{553}.

I am wish to thank to Dr. Yoshiki Higuchi in Basic Research Laboratory, Himeji Institute of Technology, for his continuing suggestion and advice and supplement of sample.

I wish to thank Dr. Keiichi Namba of Houtani Project in ERATO for using a Fuji BA-100 Imaging Plate read-out system.

I wish to thank Mr. Yuichi Iga for his technical suggestion and advise of computer programs.

I wish to thank Professor Nobuo Tanaka in Tokyo Institute of Technology, Dr. Yoshiki Matsuura, Dr. Masami Kusunoki and all members in Institute for Protein Research for their suggestion and assistance.

I wish to thank Dr. Yoshiyuki Amemiya for his helpful suggestion on

Imaging Plate, and I also thank to all members in Photon Factory.

I would like to thank to Dr. Nobuhisa Watanabe for his many assistance and Dr. Kyoyu Sasaki in Nagoya University for his helpful suggestion and assistance on computer programs.

I would also like to thank to Dr. Tsuneyuki Higashi for his suggestion and assistance on computer programs.

I would like to thank to use Facom M-360/MP computer of Photon Factory Computer System and VAX-11/750 (KEK750) of Tristan Computer Center in KEK.

Finally, I heartily thank to my parents and my wife, Noriko, for their continuing encouragement and unfailing assistance.

November, 1989 Atsushi Nakagawa

This work on multi-wavelength anomalous dispersion method has been performed under the approval of the Photon Factory Advisory Committee (Proposal No.87-028 and No.88-050).

ABBREVIATIONS

Ac	acetate
A.S.	ammonium sulfate
CNDP	4-carboxyl-2,6-dinitrophenol
DvH	*Desulfovibrio vulgaris* Hildenborough
DvM	*Desulfovibrio vulgaris* Miyazaki
EXAFS	extented X-ray absorption fine structure
IP	imaging plate
MAD	multi-wavelength anomalous dispersion
MIR	multiple isomorphous replacement
Mersalyl	[3-[[2-(carboxymethoxy)benzoyl]amino]-2-methoxypropyl]-hydoroxymercury monosodium salt
PCMB	*p*-chloromercuribenzoic acid
PHMB	*p*-hydroxymercuribenzoic acid
PHMBS	*p*-hydroxymercuribenzenesulfonic acid
PMA	phenylmercuric acetate
PTTC	platinum(II)(2,2',6',2"-terpyridine)chloride dihydrate
SIR	single isomorphous replacement
SIRA	single isomorphous replacement with anomalous dispersion effect
SR	synchrotron radiation
TFA	trifluoroacetate
TFC	trifluoromethylphenyl carbamate
oxi.	oxidized form (ferri form)
pI	isoelectric point
red.	reduced form (ferro form)

r.m.s. root-mean-square

Ala	A	alanine	Arg	R	arginine
Asn	N	asparagine	Asp	D	aspartic acid
Cys	C	cystein	Gln	Q	glutamine
Glu	E	glutamic acid	Gly	G	glycine
His	H	histidine	Ile	I	isoleucine
Leu	L	leucine	Lys	K	lysine
Met	M	methionine	Phe	F	phenylalanine
Pro	P	proline	Ser	S	serine
Thr	T	threonine	Trp	W	tryptophan
Tyr	Y	tyrosine	Val	V	valine

1 Å = 0.1 nm

1. INTRODUCTION

1-1. Protein Crystallography

Protein crystallography is the application of X-ray diffraction technique to crystals of proteins and it can determine three-dimensional structures of proteins, one of the most important kind of molecules in living system. It is advantageous to know how the atoms of major molecules of life - not only proteins but also nucleic acids - are disposed in space if the way they perform their vital function is to be understood in detail. Knowledge of three-dimensional structure will usually also be useful elucidating its function at the atomic level and to make the intelligent design of proteins with modification. At present, such structural information is most effectively obtained by analysis of diffraction from crystals of macromolecules. Even though the time-averaged structure might be determined by monochromatized X-ray diffraction technique and the environment around a proteins molecule may be a little different from that in solution, the structure information determined by X-ray diffraction method is very useful to study its function and mechanism. Protein crystals are highly hydrated - usually about half of the volume is due to solvent of crystallization - and for this reason molecular conformation in crystals are, for the most part, closely related to the situation in solution. And large part of the lattice interactions are mediated by water molecules. For this reason also, the environment of a protein molecule in crystal is quite similar to that in the solution in a living system.

Recent advances of in gene synthesis and genetic engineering have made it possible, in principle, to construct any desired amino acid sequences. To make more useful, more stable and more available proteins is one of the most important theme of protein engineering. So it is necessary to know relationship between structure and function of proteins in the native form as the first step. Although there are too many proteins to count in the nature, only less than 300 of coordinate sets from over 150 distinctive macromolecules have been deposited in the Protein Data Bank (Bernstein *et al.*, 1977).

Three-dimensional structures of proteins are restricted not only by its amino acid sequence but also by solvent-protein and protein-protein interactions. And it is very hard to predict its three dimensional structure only from the information about its amino acid sequence of the protein of which three-dimensional structure has been known. To determine three dimensional structures of proteins and to know relationship between structure and function of proteins are very important not only for protein engineering but also for molecular biology.

Recently because of the progress of mathematical procedure, computers and diffraction intensity measurement technique, the structure determination of proteins by X-ray diffraction technique became a very useful and powerful technique. If the crystal is nearly isomorphous with a known crystal structure of a similar protein, the difference Fourier method can be used with phases calculated from the known structure to show up the changes in structure. If the crystal is a novel one but is composed of molecules which are similar to those of known structure, the molecular replacement method following rotation and translation search can often be used to build a model of

properly positioned components from which phases can be computed by the structure factor equation. If the molecule is a novel one, the crystallographic phase problem must be solved *ab initio*. The method of isomorphous replacement has played a central role in the diffraction analysis of nearly all truly new protein structures. But many protein crystals do not give any good isomorphous derivatives to determine crystallographic phases by which unambiguous electron density map to elucidate three-dimensional structure can be calculated.

The most serious limitation for X-ray crystal structure analysis is the uncertainty of the crystallization of molecules. And the other serious problem for protein crystallography is to determine crystallographic phases of diffraction data, even if a large and well ordered native protein crystal is obtained.

1-2. Utilization of Synchrotron Radiation for Protein Crystallography

In 1912, M.Laue *et al.* discovered the X-ray diffraction phenomenon by crystals (Friedrich *et al.*, 1912). X-ray beam is scattered according to the three dimensional periodicity in a crystal. This phenomenon means that diffraction pattern of a crystal conveys information about an internal structure of a crystal. In other words, analysis of X-ray diffraction pattern should give an internal structure of a crystal. At the present time, X-ray crystal structure analysis is one of the most powerful techniques to determine crystal and molecular structure, not only of small molecules but also especially of biological macromolecules, such as proteins, viruses, DNA and

so on.

The most serious limitation for X-ray crystal structure analysis is the difficulty of obtaining good crystals. Success in crystallization of protein crystals depends on experience and fortune. It is not only neccesary to get a crystal but also the crystal must be grown to the size of 0.5 mm in all dimensions to get a good high resolution data. Even if we can get a good crystal, there are another problem on the structure analysis.

Suppose that there are some atoms in a crystal; number of atoms (N), coordinate of j-th atom (x_j, y_j, z_j); then the diffraction intensity for index hkl (I(hkl)) can be written as

$$I(hkl) = \mathbf{F}(hkl) \cdot \mathbf{F}^*(hkl) \qquad (1\text{-}1)$$

$$\mathbf{F}(hkl) = \sum_{J}^{N} f_j \exp(-B(\sin\theta/\lambda)^2) \cdot \exp(2\pi i(hx_j + ky_j + lz_j)) \qquad (1\text{-}2)$$

We can observe the only intensities, $|I(hkl)|$, by X-ray diffraction technique, not the structure factors F(hkl). In other words, phase angles of structure factors, $\alpha(hkl)$, are lost on intensity measurement. The most difficult problem to determine structure by the X-ray diffraction method is how we can determine crystallographic phases for the Fourier series calculation. Crystallographers call this problem the "PHASE PROBLEM".

To determine a structure of small molecular crystal, the direct method is very useful and very powerful technique. By this method, phase angles are calculated *ab initio* using only the intensity relationship between reflections. Recently, it has become possible to determine a crystal structure of small molecule fully automatically by the progress of computer technology and mathematical techniques. But to determine a macromolecule crys-

tal structure, it is very difficult to determine phases only by direct method, although many crystallographers have been trying to solve the phase problem and have also been trying to determine the structure using only native crystal data by the direct method. So some empirical methods must always be employed for phase determination in biological macromolecular crystallography. Isomorphous replacement technique is the most useful method to determine crystallographic phases of diffraction intensities from macromolecular crystal. In isomorphous replacement technique, phases are determined from the intensity difference between the native and the derivative(s). This technique is very useful when good isomorphous derivatives can be prepared. Another technique, molecular replacement method, may be the most useful when three-dimensional structure of a similar protein has been solved because it is then not necessary to prepare any isomorphous derivative. Molecular replacement may be very useful for protein engineering.

When the structure of a similar protein is not understood and it is very hard or it is not able to prepare isomorphous derivative, it should be very difficult to determine the structure of macromolecule by X-ray diffraction technique.

Recently a new type of light source called synchrotron radiation (SR) has been widely used for many fields in which photons were used.

When electronic particle, such as electron or positron, is accelerated close to the light speed and changed its direction by a magnetic field, very strong electromagnetic wave is observed toward its tangent direction. This electromagnetic wave is called "Synchrotron Radiation". This synchrotron radiation has some special characters compared with X-rays from a conven-

tional X-ray generator. These characteristics include

1. Very high brightness
2. Polychromatic beam
3. Small divergency
4. Pulse beam
5. Polarized light

The synchrotron radiation beam is also very useful for protein crystallography. With regard to the first advantage, the high power X-ray beam, high resolution data can be obtained and even if the size of crystal is small, for example 0.2 mm in all directions, it is possible to get high resolution data. Although protein crystals are very easy to get radiation damage by X-ray beam, a shorter exposure time helps make radiation damage to a smaller extent, even though the intensity of the beam may be higher. With regard to the second advantage, polychromatic X-rays, the Laue method, which is the technique to get many reflections at the same time using white X-rays, may become the best technique for time-resolved macromolecule crystal structure analysis. Another usage of the second advantage is that we can choose any wavelength of the X-rays. Tunability of wavelength is very useful for anomalous dispersion technique. Even for isomorphous replacement method, anomalous dispersion effect is very useful for crystallographic phase determination. For protein crystals which have heavy atom(s) in its native form, they have an ability to determine crystallographic phases without heavy atom derivatives and to determine three-dimensional structure. By a conventional X-ray generator, characteristic X-ray is strong but white X-ray is very weak. So it is impossible to get any wavelength of X-ray other than characteristic X-ray of target, CuKα is always used for protein

crystallography (1.54 Å), using a conventional X-ray generator. Because of the synchrotron radiation is a polychromatic beam, we can choose any wavelength of X-ray. For anomalous dispersion experiment, this wavelength tunability is very useful because any wavelength of X-ray can be chosen including that near absorption edge which is used in the anomalous dispersion experiments. The third advantage, small divergency, is that the beam divergency is very close to parallel and when it is monochromatized by a monochromator, the energy dispersion of beam will be small. In the energy region of near absorption edge, real part of the anomalous scattering factor ($\Delta f'$) varies dramatically. In other words, when energy resolution of X-ray beam is not very good, it is difficult to use real term of the anomalous difference efficiently. The fourth advantage, the pulse beam, also provides a possibility for time-resolved measurement, but averaged X-ray beam is always used for static structure determination of biological macromolecule crystals. The fifth advantage, polarization of X-ray beam does not give any information of the static protein structure. But recently, elliptically polarized synchrotron beam for X-ray region has been obtained using undulator constructed in the Accumulation Ring (AR) in KEK, National Laboratory for High Energy Physics, and is will be possible to give some informations of protein structure.

The crystal of cytochrome c_{553} diffracts data at quit high resolution, that means the quality of cytochrome c_{553} crystal is good. But it was very difficult to get good isomorphous derivatives and to determine the three-dimensional structure of cytochrome c_{553}.

In this thesis, the three-dimensional structure of cytochrome c_{553} has been determined by the multi-wavelength anomalous dispersion method using

anomalous dispersion effect of the iron atom of the heme group in the native protein, and this method does not require to prepare any isomorphous derivative. The multi-wavelength anomalous dispersion method provides a possibility to determine the three-dimensional structure of any kind of metallo-proteins which contain heavy atoms, of which atomic number ranges from ^{29}Cu to ^{47}Ag and from ^{50}Sn to ^{92}U, in the native form.

1-3. Structure study of cytochrome c_{553}

The sulfate-reducing bacteria were discovered by Beijerinck in 1895 (Beijerinck, 1895). Sulfate-reducing bacteria are classified as a group of microbes which conduct dissimilatory sulfate reduction. In the metabolism of a sulfate-reducing bacterium, the sulfate ion acts as a terminal electron acceptor, as oxygen acts in conventional respiration, and therefore it has been called "sulfate respiration", analogous to "nitrate respiration" found among nitrate-reducing bacteria. The sulfate-reducing bacteria have been considered to consist of a small group of highly specialized anaerobic bacteria with similar phylogenetical and bioenergetic systems. As oxygen always inhibits their growth, they always live in the anaerobic environment such as a marshy place and so on.

Today at least seven genera of sulfate-reducing bacteria are discovered and confirmed. The two genera of sulfate-reducing bacteria, *Desulfovibrio* and *Desulfotomaculum*, are well established, and these two species seem to be closed in the phylogenetic tree. *Desulfotomaculum* involves spore forming. *Desulfovibrio* contains methophilic and halophilic bacteria and

they do not form spores. *Desulfovibrio* is the best known, because it is easy to isolate and purify. The cytochrome c_{553} of which three-dimensional structure is discussed in this thesis comes from *Desulfovibrio vulgaris* Miyazaki F (IAM no. 12604, Kobayashi and Skyring, 1982). This strain was initially isolated from a paddy field in Miyazaki Prefecture, Japan (Ishimoto and Koyama, 1953), and its enzymes have been investigated by various biochemical methods.

These bacteria are Gram-negative and tend to have single polar flagella with an average size of 0.4X10μm.

Electron transfer system of *Desulfovibrio vulgaris* is not well known, but Figure (1-1) shows a tentative scheme for it, Aerobes reduce oxygen to water, whereas the sulfate-reducing bacteria reduce sulfate to water and sulfide.

Desulfovibrio have many *c*-type cytochromes although they are anaerobic bacteria. It was the first anaerobic bacterium which involved cytochromes *c* in its metabolic path (Ishimoto *et al.*, 1954, Postgate, 1954). At least three kinds of *c*-type cytochromes, having the heme *c* in a molecule, are found in *Desulfovibrio vulgaris* Miyazaki F. They are cytochrome c_{553}, cytochrome c_3 and high molecular weight cytochrome *c*, and their properties are summarized in Table (1-1).

Cytochrome c_3 acts as an electron transfer protein to hydrogenase, and its electrochemical, physicochemical and other properties are well studied from many facets (Ishimoto *et al.*, 1954, Postgate, 1954, Yagi and Maruyama, 1971). The three-dimensional structure of cytochrome c_3 from *Desulfovibrio vulgaris* Miyazaki (Higuchi *et al.*, 1981, Higuchi *et al.*, 1981, Higuchi *et al.*, 1984) and *Desulfovibrio denitrofricans* Norway (Haser *et al.*, 1979,

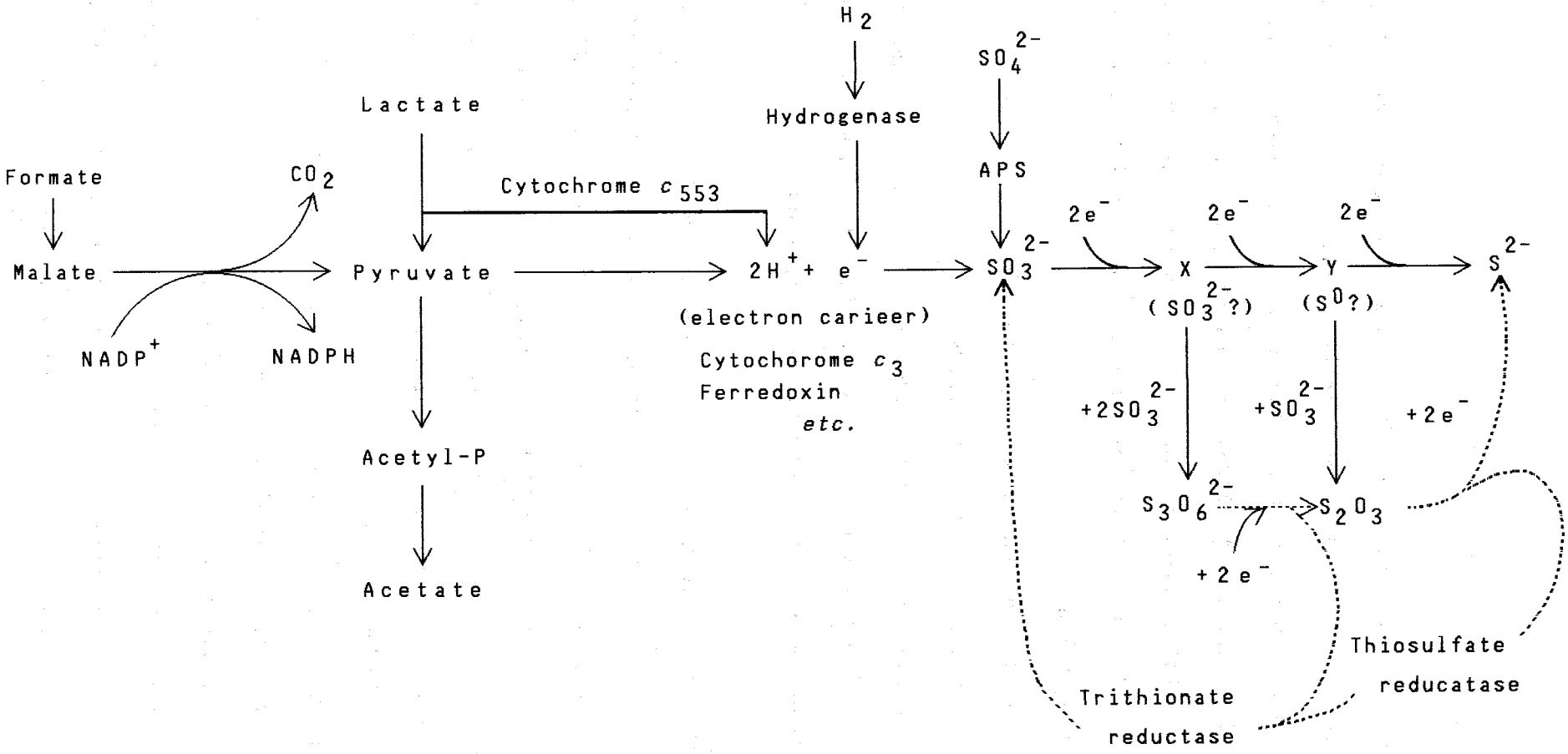

Figure 1-1

The tentative scheme for electron transfer system of cytochrome c_{553}

	M.W.	No. of residues	Heme contents
Cytochrome c_{553}	9,000	79	1
Cytochrome c_3	14,000	107	4
High molecular weight cytochrome *c*	70,000	?	12?

Table 1-1

Cytochromes in *Desulfovibrio vulgaris* Miyazaki

Pierrot *et al.*) has already been determined and the structure of cytochrome c_3 from *Desulfovibrio vulgaris* Miyazaki has been refined to 1.8Å resolution (Higuchi *et al.*, 1984).

High molecular weight cytochrome *c*, which was at first separated from extracts of *Desulfovibrio vulgaris* Miyazaki F by Yagi (Yagi, 1969), is composed of two subunits and has a molecular weight of about 70000. Its purification and crystallization has been successful (Higuchi *et al.*, 1987).

Cytochrome c_{553} (Le Gall and Bruschi-Heriand, 1968; Bruschi *et al.*; Yagi, 1969; Yagi, 1979; Bruschi and Le Gall, 1972; Peck and Le Gall, 1982) is reported to act as an electron carrier protein for formate dehydrogenase (Yagi, 1979) and lactate dehydrogenase (Ogata *et al.*, 1981) at the starting point of carbon and energy metabolism. It accepts electrons from lactate and transfers them to cytochrome c_3 and the other enzymes involved in the inorganic sulfur metabolism. Cytochrome c_{553} from *Desulfovibrio vulgaris* Miyazaki has a single polypeptide chain containing 79 amino acids residues and one heme group (Table (1-2)). And it is the smallest cytochrome *c* that has been isolated so far (Nakano *et al.*, 1983). This suggests that cytochrome c_{553} is one of the most primitive *c*-type cytochrome of the known members of cytochromes *c* super family.

The amino acid sequence of cytochrome c_{553} from *Desulfovibrio vulgaris* Hildenborough strain was determined by Bruschi and Le Gall (Bruschi and Le Gall, 1972). Dickerson proposed the alignment of amino acid sequence of cytochrome c_{553} and other *c*-type cytochromes and, on the basis of that, the location of sulfate-reducing bacteria in the phylogenetic tree (Dickerson, 1980). However a comparison of amino acid sequences of cytochrome c_{553} from *Desulfovibrio vulgaris* Miyazaki and *Desulfovibrio vul-*

Molecular weight	9000 dalton	
Number of residues	79 amino acids	
Heme content	1	
pI	10.5	
Absorption spectra (molar absorbance)	(red.) 553nm	(23.9)
	(red.) 524nm	(16.2)
	(red.) 417nm	(142.0)
	(red.) 317nm	(32.1)
	(oxi.) 525-526nm	(10.6)
	(oxi.) 410 nm	(109.0)
	(oxi.) 360 nm	(27.8)
	(oxi.) 227-280nm	(193.0)
Redox potential (pH 7.0)	0 mV	

Table 1-2

Physicochemical Properties of
cytochrome c_{553}
from *Desulfovibrio vulgaris* Miyazaki

garis Hildenborough does not show any similarity except for several residues at the N- and C-terminal although amino acid composition of both species is quite similar to each other (Table (1-3)). Yagi and his colleague has suggested a new alignment of the primary structures of cytochrome c_{553} from *Desulfovibrio vulgaris* Miyazaki and other small type cytochromes *c* (Nakano *et al.*, 1983). Comparison of tertiary structures will give a new insight to the alignment of cytochromes *c* superfamily.

The redox potential of cytochrome c_{553} from *Desulfovibrio vulgaris* Miyazaki was measured by Niki (Niki, *unpublished result*) and it is about 0mV, whereas other cytochromes *c* have values about 200-400mV. This unusually low redox potential must depend on its structure. It is also necessary to know the three-dimensional structure for understanding of the relationship between structure and redox potential.

	DvMF	DvH
Lys	12	12
His	2	1
Arg	1	1
Asp + Asn	6 + 1	5 + 1
Thr	1	1
Ser	5	6
Glu + Gln	4 + 2	5 + 1
Pro	0	1
Gly	11	12
Ala	11	14
Cys	2	2
Val	5	2
Met	5	6
Ile	0	1
Leu	5	5
Tyr	5	6
Phe	1	0
Trp	0	0

Table 1-3

Amino acid Composition of cytochrome c_{553}
from two strains,
Desulfovibrio vulgaris Miyazaki F (DvMF)
and
Desulfovibrio vulgaris Hildenborough (DvH)

2. PRELIMINARY STAGE OF STRUCTURE ANALYSIS

2-1. Crystallization

2-1-1. Purification and Crystallization

The purification of cytochrome c_{553} was carried out according to the method reported by Yagi (Yagi, 1979). The procedure for purification is described in Figure (2-1). Just before crystallization, the solution of cytochrome c_{553} was purified by gel-filtration with Sephacryl S-200 gel. The fractions having the value of the purity index[1] greater than 1.2 were collected and then condensed by ultrafiltration.

As cytochrome c_{553} is soluble in Tris-HCl buffer saturated with ammonium sulfate at the neutral pH, it could be crystallized by the combined method of the salting out by ammonium sulfate and the vapor diffusion of ammonia to make the pH of the protein solution close to the isoelectric point (10.5) of the protein. A solution of purified cytochrome c_{553} (10%(W/V)) was used for crystallization. Ammonium sulfate powder was added stepwise to make the solution saturated on cooling with crushed ice. This solution was then centrifuged (15000rpm, 30min.) to remove insoluble ammonium sulfate powder. This purified protein solution was put in the microdialysis cell

---

1. The purity index is defined as:

Absorbance at 553 nm (red.)/Absorbance at 280 nm (oxi.)

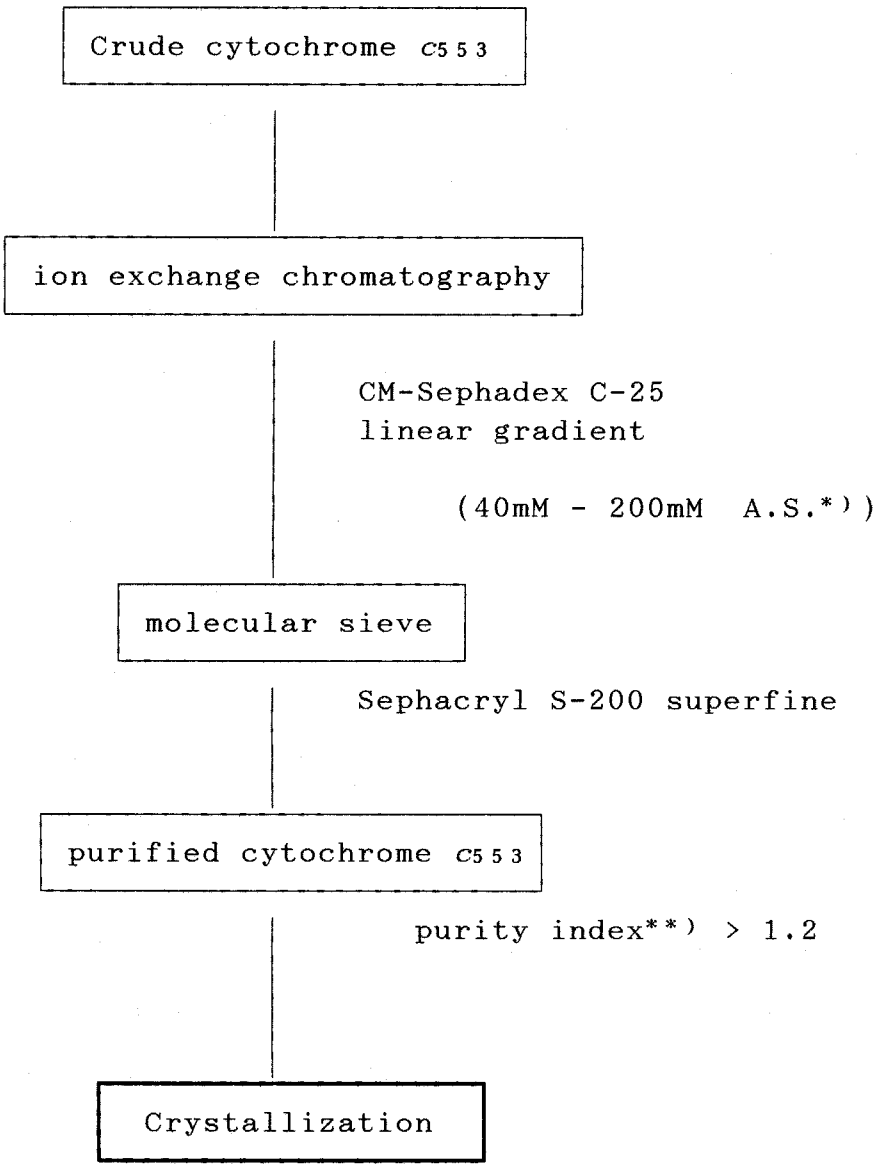

Figure 2-1

Flow chart of the purification
of cytochrome c_{553}

*) Ammonium sulfate
**) Absorbance at 553nm(red.) / Absorbance at 280nm(oxi.)

(crystallization button) and was dialyzed against 50 mM of the ammonium sulfate-saturated Tris-HCl buffer solution (pH 8.0) and placed in an air-tight box with another 50 mM of the ammonium sulfate-saturated Tris-HCl buffer solution (pH 9.0) containing ammonia (Figure (2-2)). After about 10 days at 15 °C, as the pH of the protein solution increased and approached its isoelectric point, some crystals suitable for X-ray analysis were grown. The crystals were red tetragonal bipyramid, and their typical dimensions were approximately 0.8X0.8X1.0mm^3 (Figure (2-3)).

2-1-2. Crystallographic Study of Cytochrome c_{553}

The crystal data were determined with Ni-filtered CuKα radiation on a four-circle diffractometer. The X-ray generator was a rotating-anode type RIGAKU RU-200 (40 kV,200 mA), and the diffractometer was the Rigaku AFC-5 system. The tentative cell parameters were determined by using the vector minimum method from 15 reflections collected by the diffractometer using the peak search system. Then preliminary measurement of intensities of Bijvoet pairs was carried out at 5 Å resolution. From the inspection of the symmetry of diffraction intensities and systematic absences of diffraction, the space group was determined as $P4_32_12$ (or its enantiomorph $P4_12_12$). Unit cell parameters were reduced from Bragg angles of twenty reflections carefully measured on the diffractometer; a=b=42.7 Å, c=103.4 Å. The correct enantiomorph, $P4_32_12$, was determined by the inspection of two Fourier maps with SIR phases (see Chapter 2-2-3); one of them was calculated for the space group $P4_32_12$ and the other was calculated for the space group $P4_12_12$.

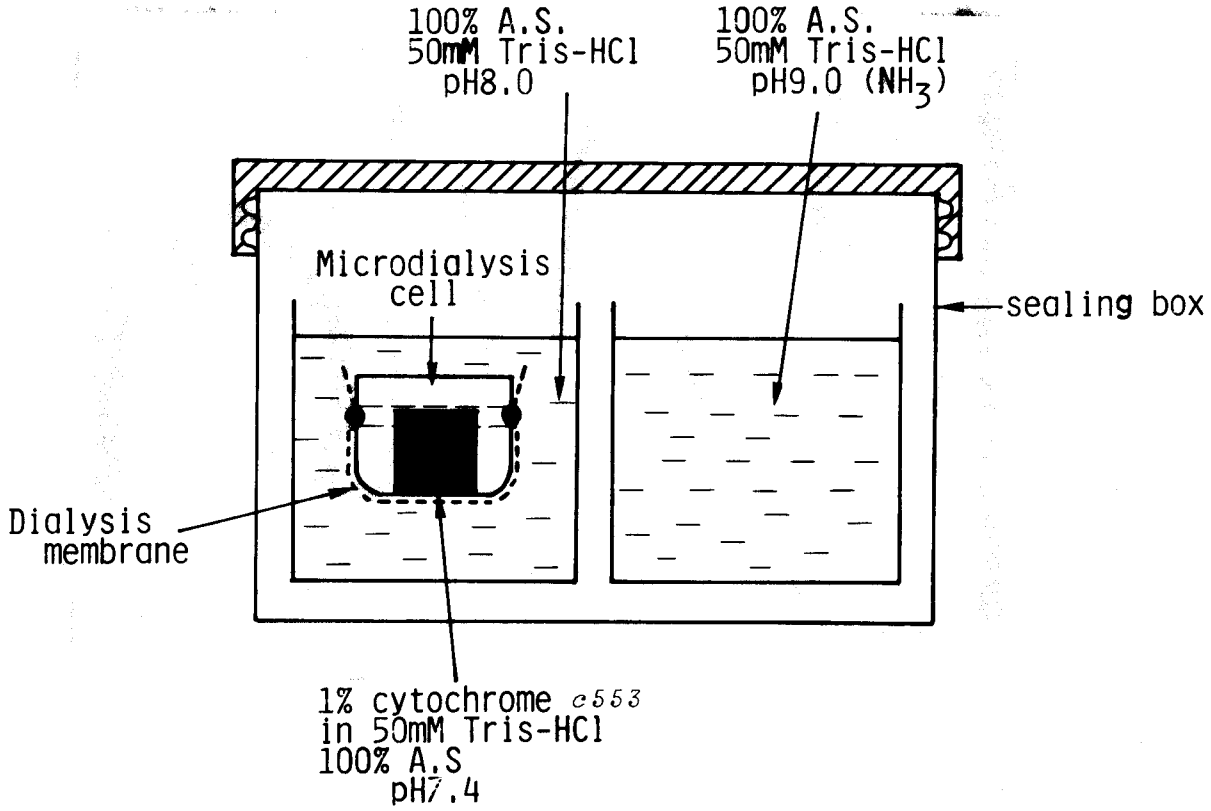

Figure 2-2

Crystallization of cytochrome c_{553}
by the combined method of the salting-out and
the vapor diffusion technique

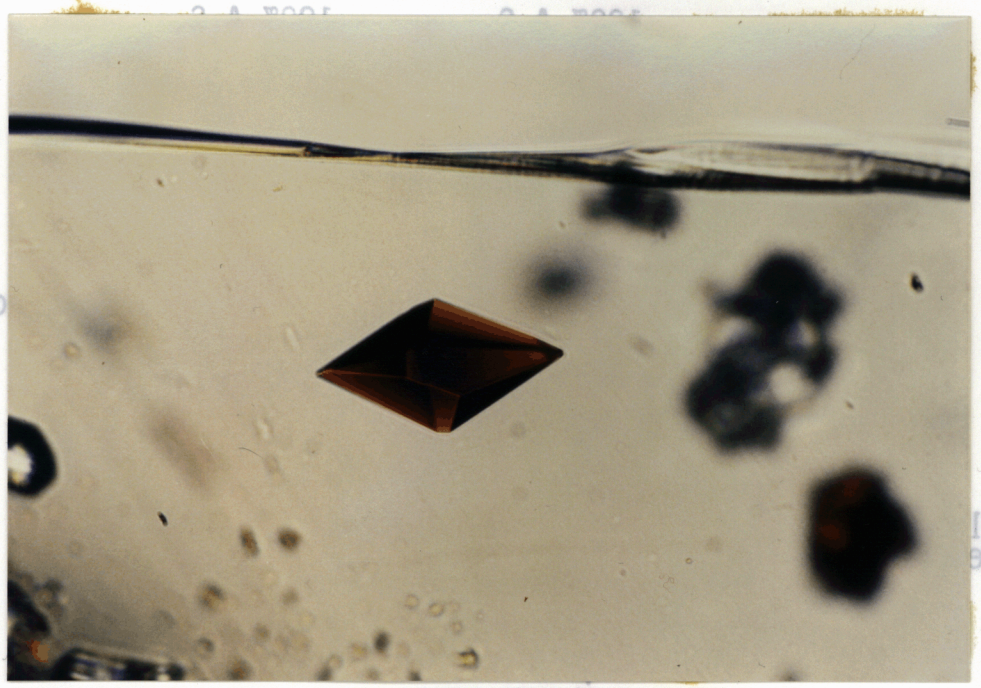

Figure 2-3

Crystal of cytochrome c_{553}
Approximate crystal size is 0.4X0.4X0.7 mm^3

The consideration of anomalous scattering effect supported this selection of enantiomorph. If there is one molecule in an asymmetric unit, a V_M value of 2.61 $Å^3$/dalton is obtained, which is a reasonable value for a commonly found protein crystal (Matthews, 1968). Table (2-1) summarizes the crystallographic data of a cytochrome c_{553} crystal.

2-2. Single Isomorphous Replacement Method

2-2-1. Theoretical Background

Suppose that there are N atoms in a unit cell of a crystal and the coordinate of j-th atom in a crystal is (x_j, y_j, z_j) in the fractional coordinates system, the structure factor of particular reflection which has a Miller index hkl is described as

$$F(hkl) = \sum_{j}^{N} f_j \cdot \exp 2\pi i(hx_j + ky_j + lz_j) \qquad (2\text{-}1)$$

where f_j is the atomic scattering factor of j-th atom. Alternatively, the structure factor is given using phase, α, as follows,

$$F(hkl) = |F(hkl)| \cdot \exp i\alpha \qquad (2\text{-}2)$$

An inversed Fourier transformation of equation (2-1) is written as

$$\rho(x,y,z) = \frac{1}{V} \sum_{h} \sum_{k} \sum_{l} F(hkl) \cdot \exp -2\pi i(hx+ky+lz) \qquad (2\text{-}3)$$

Crystal system	Tetragonal
Space group	$P4_32_12$
Cell Constants	$a = b = 42.7$ Å $c = 103.4$ Å
Volume	$V = 188 \times 10^3$ Å^3
Number of molecule in one unit cell (1 molecule per asymmetric unit)	$Z = 8$
Volume per 1 dalton	$V_M = 2.61$
Volume of solvent	$V_{solv.} = 0.53$

Table 2-1

Crystallographic data of cytochrome c_{553} crystal

Equation (2-3) shows that if the structure factors F(hkl) are known, then electron density at point (x,y,z) can be calculated.

By X-ray diffraction method, only an intensity I(hkl) can be observed. The intensity I(hkl) is given by

$$I(hkl) = \mathbf{F}(hkl) \cdot \mathbf{F}^*(hkl) \qquad (2\text{-}4)$$

where $\mathbf{F}^*(hkl)$ denotes the conjugate complex of a structure factor F(hkl).

Equation (2-2) shows that structure factor has both amplitude term and phase term. As the intensity I(hkl) can be described by equation (2-4), the phase term of a structure factor vanishes in the diffraction intensity measurement. Thus it is necessary to determine phases of each reflections for structure determination.

For structure analysis of a protein crystal, the isomorphous replacement method is mainly used for phase determination.

Assume that $\mathbf{F}_P$, $\mathbf{F}_{PH}$, $\mathbf{f}_H$ are structure factors of a protein, a heavy atom derivative and a heavy atom itself, respectively. Here these three terms are related as follows,

$$\mathbf{F}_{PH} = \mathbf{F}_P + \mathbf{f}_H \qquad (2\text{-}5)$$

If the positions of heavy atoms are reduced from the difference Patterson maps, the structure factor of heavy atom can be calculated by

$$\mathbf{f}_H = \sum_j G_j \cdot T_j \cdot f_j \cdot \exp(2\pi i(hx_j + ky_j + lz_j)) \qquad (2\text{-}6)$$

here,

$$T_j = \exp(-B_j(\sin\theta/\lambda)^2) \qquad (2\text{-}7)$$

where $G_j, B_j, f_j, (x_j, y_j, z_j)$ are the occupancy, the isotropic temperature factor, the atomic scattering factor and the fractional coordinates of j-th atom of each heavy atom, respectively.

As shown in Figure (2-4), if modulus of structure factor of the native protein crystal and both modulus and phase of the heavy atom derivative are known and the structure factor of the heavy atom is also known, the phase angle of structure factor of protein can be calculated. But in this method, there is an ambiguity of selecting the correct phase from two possible phases, P and Q in Figure (2-5).

To resolve phase ambiguity inherent in the single isomorphous replacement method (SIR), either of the two methods is usually employed. One is the multiple isomorphous replacement method (MIR) and the other is the single isomorphous replacement method with anomalous scattering effect (SIRA).

Figure (2-6) shows a Harker diagram of MIR case and Figure (2-7) shows a Harker diagram of SIRA case. Combination of MIR and anomalous scattering effect are always used to get a better result than MIR only.

In an actual experiment, many kinds of errors are included in data. Therefore all circles do not cross at the one unique phase on the Harker's diagram, and the correct phases are hard to determine uniquely and phases can only be determined with assessed probability. The lack of closure error can be expressed as the difference between the observed and the calculated

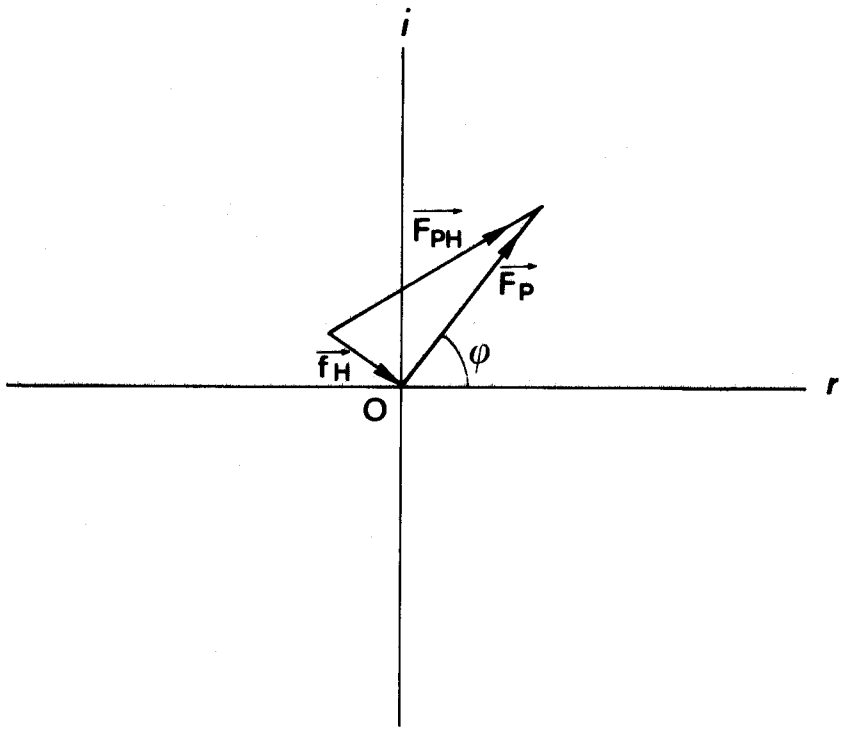

Figure 2-4

Vector diagram
showing single isomorphous replacement case

F_P : Sturcure factor of protein
F_{PH} : Structure factor of isomorphous derivative
f_H : Structure factor of heavy atom(s)

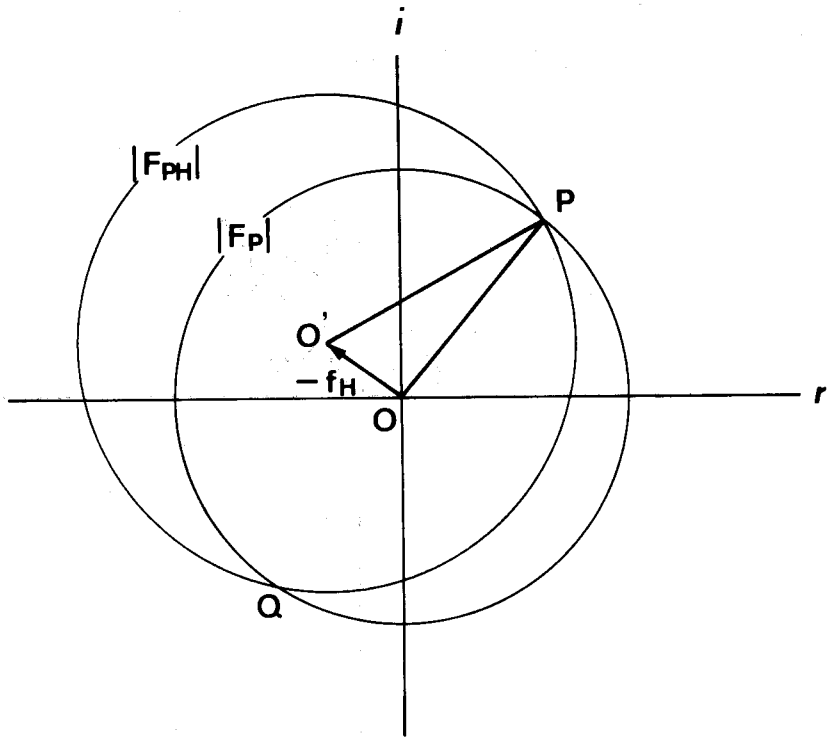

Figure 2-5

Harker diagram showing SIR case

Two possible phases (P and Q) are obtained and it is not possible to select the correct phase

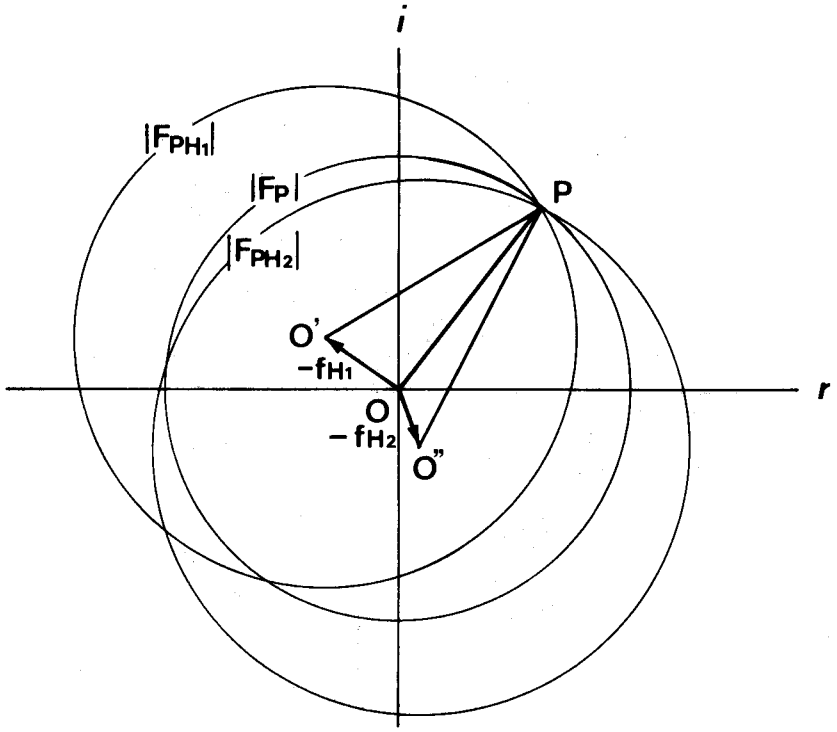

Figure 2-6

Harker diagram showing MIR case

In this case, correct phase can be selected without ambiguity

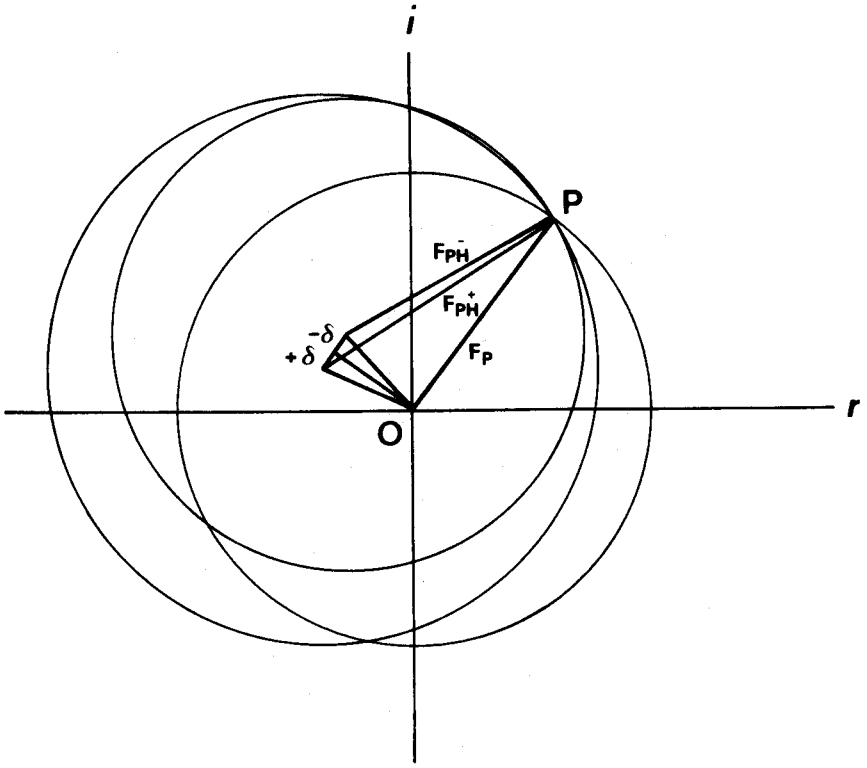

Figure 2-7

Harker diagram showing SIRA case

F_P : Structure factor of protein

F_{PH} : Structure factor of isomorphous derivative

δ : Imaginary part of anomalous term of heavy atom

value of the structure factor as follows.

$$\varepsilon = |F_{obs}| - |F_{calc}| \qquad (2\text{-}8)$$

For the isomorphous replacement with anomalous difference phase calculation case, the lack of closure error is defined as follows (Matthews, 1966),

$$\begin{aligned} \varepsilon_+^2 + \varepsilon_-^2 &= \{(\varepsilon_+ + \varepsilon_-)^2 + (\varepsilon_+ - \varepsilon_-)^2\}/2 \\ &= (\chi_{iso}^2 + \chi_{ano}^2) \end{aligned} \qquad (2\text{-}9)$$

Assume a Gaussian distribution in the lack of closure errors, the probability of a phase angle for the protein structure factor, α, is given by

$$P_j(\alpha) = \exp[-\varepsilon_j(\alpha)^2/2E_j^2] \qquad (2\text{-}10)$$

for the j-th heavy atom derivative.

When several heavy atom derivatives are used for phase calculation, the overall probability of a phase angle is given by the product of individual probabilities

$$P(\alpha) = \prod_j P_j(\alpha) = \exp[-\sum_j \varepsilon_j(\alpha)/2E_j^2) \qquad (2\text{-}11)$$

Blow and Crick had shown that the centroid of the phase distribution is a better choice to get a good result (Blow and Crick, 1959). Suppose the

true structure factor $\mathbf{F}_t$, that can be written as

$$\mathbf{F}_t = |\mathbf{F}_P| \cdot \exp(i\alpha) \qquad (2\text{-}12)$$

where $|\mathbf{F}_P|$ is an amplitude of protein structure factor and α is a phase angle. Then the mean squares error of electron density over the unit cell from this reflection is

$$\langle \Delta\rho^2 \rangle = \frac{1}{V} \left(|\mathbf{F}_S| - |\mathbf{F}_t| \right) \qquad (2\text{-}13)$$

where $\mathbf{F}_S$ is the value of the coefficient used in the synthesis. To minimize the error of electron density, $\langle \Delta\rho^2 \rangle$, $\mathbf{F}_S$ should be expressed as,

$$\mathbf{F}_S(\text{best}) = \frac{|\mathbf{F}_P| \cdot \int \exp(i\alpha) \cdot P(\alpha) d\alpha}{\int P(\alpha) d\alpha}$$

$$= \mathbf{m} \cdot |\mathbf{F}_P| \cdot \exp(i\alpha_{best}) \qquad (2\text{-}14)$$

Here, α_{best} is known as the "best phase". This equation (2-14) means that the centroid of the probability distribution can be expressed as polar coordinate $(\mathbf{m} \cdot |\mathbf{F}_P|, \alpha)$. The $\mathbf{m}$ value is known as the "figure of merit", and has a value between 0 and 1 and m=1 means there are no errors in the phase angle.

The mean square error of the electron density can be expressed using figure of merit

$$\langle \Delta\rho^2 \rangle = \frac{1}{V} \sum \mathbf{F}_h^2 \cdot (1-\mathbf{m}) \qquad (2\text{-}15)$$

Refinement of heavy atom parameters of each derivative uses minimiza-

tion of the lack of closure error for each derivatives.

Following parameters should be refined,

1. Relative scale factor and temperature factor to native data : K, ΔB
2. Coordinates of each heavy atom sites : (x_j, y_j, z_j)
3. Temperature factor of each heavy atom : B_j
4. Occupancy of each heavy atom : G_j

Two refinement techniques are always used for the refinement of heavy atom parameters. One is FHLE refinement, or centric refinement as its modification, and the other is phase refinement.

2-2-2. Heavy Atom Reagents Survey

At first, in the structure determination of cytochrome c_{553}, the author has been tried to determine phases by the isomorphous replacement technique as it is the best procedure in many cases.

As described in Chapter 2-2-1, cytochrome c_{553} was crystallized in ammonium sulfate saturated Tris-HCl(50mM) buffer at pH 9.0. Few heavy atom reagents are dissolved in basic buffer solution and many heavy atom ions form complexes with sulfate ion. Thus it was very hard to get good isomorphous derivatives. More than twenty heavy atom reagents were surveyed (Table (2-2)). Only mersalyl derivative could be successfully used for phase determination (Nakagawa *et al.*, 1979).

At first, diffraction data sets of native and mersalyl derivative were collected on a four-circle diffractomator (RIGAKU AFC-5) with rotating anode X-ray generator (RIGAKU RU300; CuKα).

Reagent	Conc. (mM)	Time (day)	PH
$K_3UO_2F_5$	sat.	30	9.0
UO_2Ac_2	sat.	10	9.0
$UO_2(NO)_2$	sat.	10	9.0
$HgAc_2$	2.0	9	9.0
Mersalyl	4.0	12	9.0
PCMB	2.0	10	9.0
PHMB	sat.	30	9.0
PHMBS	sat.	30	9.0
PMA	sat.	14	9.0
K_2HgBr_4	sat.	20	2.0
Mercurochrome	sat.	30	9.0
K_2PtCl_4	sat.	6	8.8
K_2PtCl_6	sat.	9	9.1
PTTC	4.0	3	9.0
$LaCl_3$	sat.	12	9.0
$SmCl_3$	sat.	7	9.0
$NaAuCl_6$	2.0	9	9.0
$PdCl_2$	2.0	11	9.0
$OsCl_3$	2.0	8	9.0
CsCl	10.0	12	9.0
$AgNO_3$	5.0	12	9.1
$Th(NO_3)_4$	sat.	11	9.0
WO_3	2.0	13	9.0
K_3IrCl_6	4.0	11	9.0

Table 2-2

Soaking Conditions for Heavy Atom Derivatives

Only mersalyl derivative can be used
for phase determination process

Figure (2-8(a)) and Figure (2-8(b)) show difference Patterson maps of modulus $|F_{PH}-F_P|^2$ and $|F_{PH}^+-F_{PH}^-|^2$, respectively.

2-2-3. Selection of Space Group Enantiomorph

From the interpretation of the difference Patterson map using the mersalyl derivative, the author found one reasonable peak for a heavy atom site. After the refinement of the atomic parameter by phase refinement method (program : LS3DA; Matsuura, 1976, *private communication*), native Fourier maps with SIRA phases were calculated both in the space group $P4_12_12$ and $P4_32_12$. Only the map that was calculated in the space group $P4_32_12$ shows molecular boundary at 6Å resolution map.

2-2-4. Native Anomalous Scattering Effect for Phase Calculation

If we could get one good isomorphous derivative, with large anomalous dispersion effect, we would be able to calculate a good electron density map which leads to the interpretation of molecular folding. However mersalyl derivative of cytochrome c_{553} crystal was not good enough to get an electron density map by which the molecular folding can be visualized. So it was necessary to get phase information from other sources.

Though the imaginary term of the anomalous scattering effect ($\Delta f''$) of heme iron of these data was not so large (3.2 electrons at 1.54 Å), native anomalous difference Patterson map, modulus $(F_P^+-F_P^-)^2$, showed an Fe-Fe self

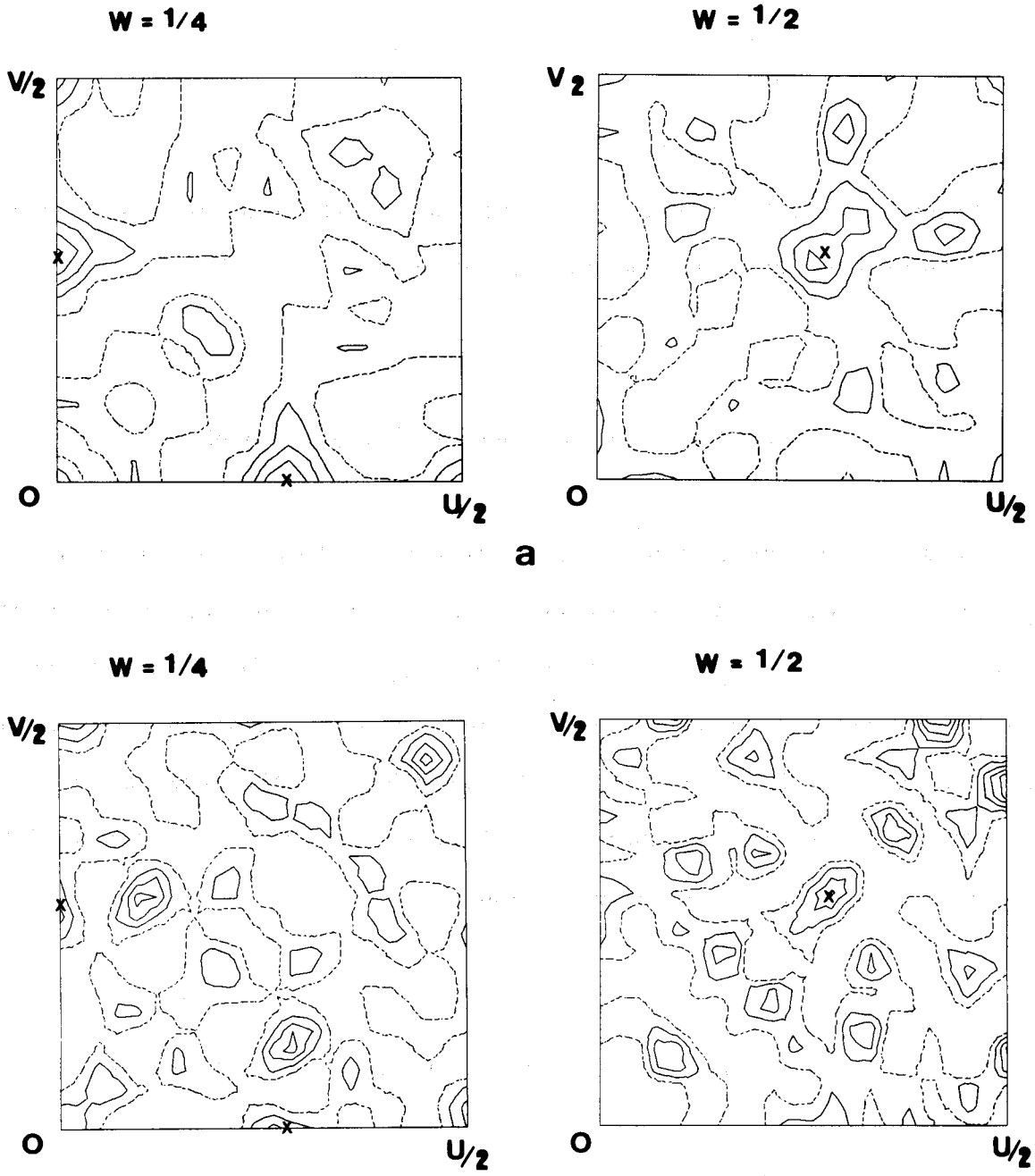

Figure 2-8

Difference Patterson maps of mersalyl derivative showing Harker sections

(a) Isomorphous difference with coefficient of $|F_{PH}-F_P|^2$

(b) Anomalous difference with coefficient of $|F_{PH}^+-F_{PH}^-|^2$

Dashed line shows zero level and these maps are contouring of equal intervals in arbitrary unit

vector on the Harker section (Figure (2-9)). To use the phase information from the native anomalous scatterer, the author coded a program for phase refinement which can accept native anomalous scattering effect (program : LS3DN, Nakagawa, 1984, *unpublished result*).

The lack of closure error of the native anomalous case is defined as follows (Argos and Mathews, 1973),

$$\varepsilon = (|F^{+}_{c}| - |F^{-}_{c}|) - (|F^{+}_{o}| - |F^{-}_{o}|) \qquad (2\text{-}16)$$

Total phase probability distribution is calculated by the product of individual probabilities of isomorphous and anomalous difference of mersalyl derivative and native anomalous difference.

After heavy atom parameters were refined, native Fourier map was calculated.

To build a molecular model from the interpretation of electron density map, the author used the random stroke type monochrome three-dimensional graphic display (VG/3) and model building program PTNFITG (Iga *et al.*, *private communication*).

But electron density map calculated by crystallographic phases using SIRA of mersalyl derivative and native anomalous dispersion effect was not good enough to trace the main chain folding.

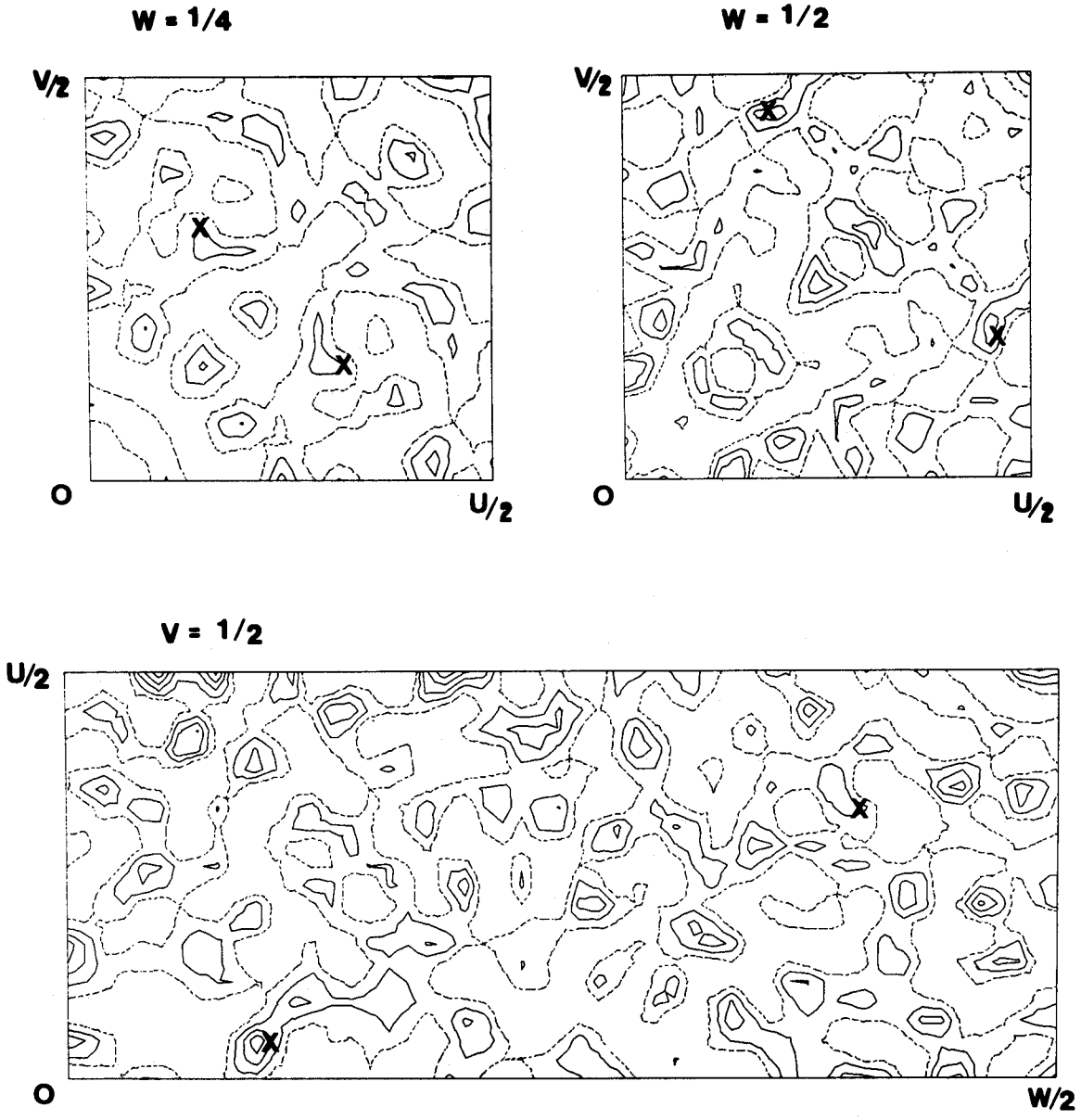

Figure 2-9

Harker sections of native anomalous difference Patterson map with coefficient of $|F_P^+ - F_P^-|^2$ using data collected by a four-circle diffractometer

Dashed line shows zero level and these maps are contouring of equal intervals in arbitrary unit

3. MULTI-WAVELENGTH PHASE DETERMINATION STAGE OF STRUCTURE ANALYSIS

3-1. Data Collection

3-1-1. Apparatus and Equipment

3-1-1a. X-ray Source

All diffraction data for multi-wavelength anomalous dispersion method were collected at Photon Factory using synchrotron radiation source.

There are two main accelerators in Photon Factory, one is a linear accelerator and the other is a storage ring. The liner accelerator is called Linac and is 200m long. Electron or positron beam is accelerated to 2.5GeV and is injected to storage ring. Electron or positron beam is stored in PF ring at 2.5GeV. Electron beam was used to get synchrotron radiation at the time when all data for this study were collected. Since July, 1988, positron beam has been stored. Positron beam is more stable than electron beam because of lack of ion trapping effect. But when all diffraction data were collected using synchrotron radiation, PF ring was operated using electron beam.

Normal bending magnets and some insertion devices, such as undulator, vertical wiggler and multi-pole wiggler, are used as light sources in Photon Factory. All diffraction data were collected at branch beamline BL-6A$_2$, and the light source of BL-6A$_2$ is produced by a normal bending magnet.

As synchrotron radiation is polychromatic beam, any wavelength of X-

ray beam can be chosen.

3-1-1b. Beamline Optics at BL-6A2

The branch beam line BL-6A2 is mainly used for macromolecular crystallography using camera method. The light source of this beamline is a normal bending magnet. At this station, continuous X-ray beam can be used for various experiments. The hutch is placed 15m far from the light source point. At 11.8m from the light source point, the fused quartz mirror is placed to focus X-ray beam and to reduce high order X-ray. This mirror is 100cm long and two types of mirror, one is a flat type and the other is a cylindrical type, can be used (Satow *et al.*, 1989). To collect diffraction data from macromolecular crystals, the flat type mirror with bending to focus vertical direction is always used (Figure (3-1)).

The optical bench with a single plate monochromator is placed in this hutch to collect diffraction data by the Weissenberg method. When diffraction data will be collected by Laue method, the monochromator should be removed to get white X-ray radiation.

The monochromator is a triangle-shaped Si(111) plane. It is an asymmetrical cut type with small bending, α=7.8°, to focus horizontal direction of X-ray.

The vertical divergence of beam is focused by the mirror and the horizontal direction is focused by the asymmetrical cut bending monochromator.

Air in the slit and monochromator chamber are replaced by helium gas

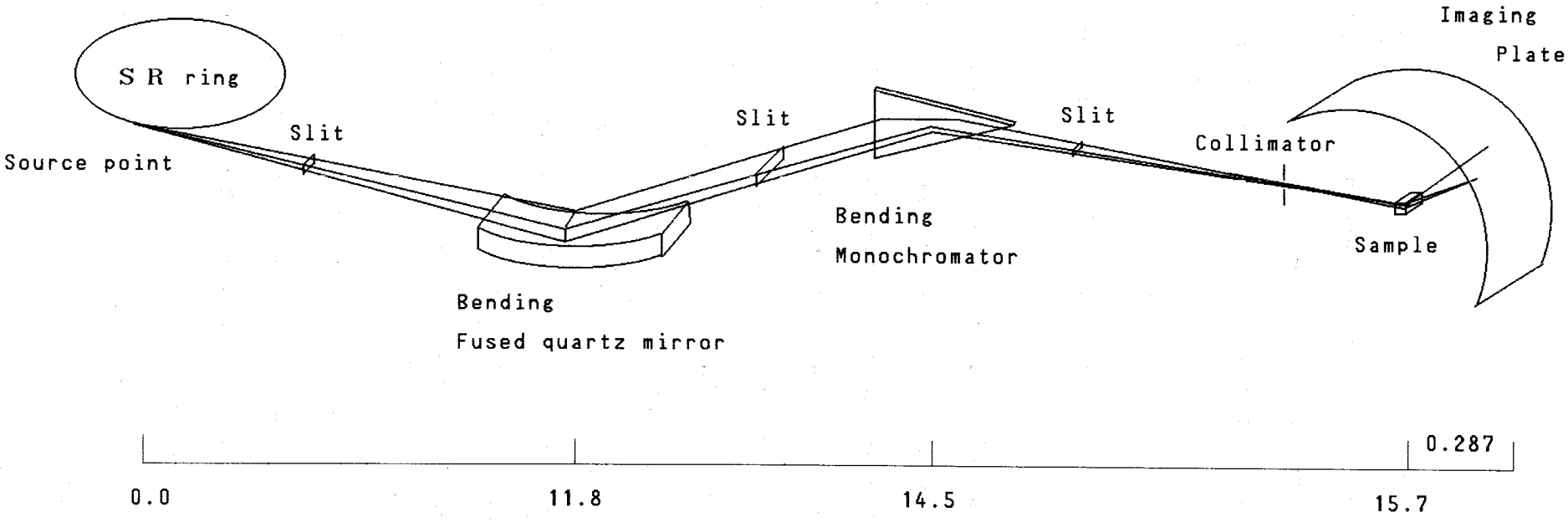

Figure 3-1

Beamline components at BL-6A2 at Photon Factory

Vertical direction is focused by the bending mirror and
horizontal direction is focused by the asymmetrical cut bending monochromator

to reduce absorption and scattering by air.

The slit and the optical bench, those were designed by Kamiya and constructed by KEK workshop, are controlled by the personal computer NEC PC-9801E placed outside of the hutch with a program coded by the author.

3-1-1c. The Weissenberg Camera for Macromolecular Crystallography

The weissenberg camera for macromolecular crystallography was used to collect diffraction data in this study. An advantage of the camera method is to allow us to collect many reflections at a same time. This Weissenberg type camera to adopt for data collection in macromolecular crystallography was designed by Sakabe (Sakabe, 1979), and the modified type-II is now working at BL-6A2 hutch at Photon Factory (Sakabe *et al.*, 1989).

A conventional Weissenberg camera for crystals of small molecules (Weissenberg, 1924) has a single layer-line screen to get only one layer data on one film and to spread these data two-dimensionally on a film. But this camera has no screen or multilayer-line screen, which is used to reduce background noise and not to select any layer-lines of diffraction. All layer data should be recorded on one film.

Ardnot-Wonacott type oscillation camera (Ardnot and Wonacott, 1977) is widely used to collect reflection data of biological macromolecular crystal in the world. This Weissenberg camera has many advantages compared with the Ardnot-Wonacott type oscillation camera.

Advantages of this type Weissenberg camera are,

- Wide oscillation range

· Bijvoet-paired data are recorded simultaneously, if symmetry is higher than monoclinic system.

· Easy to collect high angle (high resolution) data, on account of a cylindrical cassette

· Easy to replace to helium gas in the film cassette

Disadvantages of this camera are,

· Relatively high background, as oscillation range is wider than oscillation method

· Necessity of crystal alignment before data collection

The first disadvantage can be ignored by replacing to helium gas in the film cassette, which reduce scattering by air, and by large film cassette, because random scattering should be reduced according to $1/R^2$ (R : camera radius). Second disadvantage is related to the second advantage, simultaneous recording of Bijvoet-paired data. Practically, as crystal alignment is very easy and it usually takes less than one or two minutes for exposure, radiation damage during alignment is not a serious problem.

The type-II camera has six axes of motors to move

1. FIlm cassette movement : Z
2. Crystal rotation : ω
3. Inclination angle of the camera : μ
4. Crystal alignment axis of X-direction : X
5. Crystal alignment axis of Y-direction : Y
6. Crystal movement along rotation axis : Z'

These six motors are controlled by the personal computer NEC PC-9801E (Clock : 8MHz) and recently this camera can also be controlled by a new personal computer, NEC PC-9801RX4 (CPU : 80286, Clock : 12MHz), using the modified

version of the control program (Version 3.1). The control program was originally coded by Sakabe in Photon Factory and then it was modified and improved by the author. Synchronized movement of ω and Z results Weissenberg movement.

Now, any of four type camera cassettes can be chosen among 143.0, 286.5, 430.0 and 573.0 mm camera radius. The cassette of which camera radius was 286.5 mm was used to collect diffraction data of cytochrome c_{553}. When 200X400 mm^2 size the imaging plate (see chapter 3-1-1d) was mounted onto this cassette, the maximum resolution was above 1.5 Å with use of 1.38 Å X-ray beam. In the film cassette, air was replaced with helium gas to reduce background noise according to reducing scattering of X-ray by air.

Recorded image data on the imaging plate was read-out by the imaging plate system (BA-100, Fuji Photo Film Co.LTD.) and stored in magnetic tapes. These data were used to estimate intensity data. This process was done at the computer center at Photon Factory (FACOM M-360MP) using the program WEIS coded by Higashi (Higashi, 1989). This program at first refines the film setting matrix and the crystal setting matrix. Calculated and observed positions for any reflections should agree sufficiently to measure its intensity accurately. The initial film setting matrix is determined by positions of three fiducial marks, which are marked by very short-time exposure of the direct beam, which is attenuated by some metal sheets, with the detector appropriately translated in each case. The crystal and film setting matrices are refined from positions of reflections. Mis-indexing is avoided by monitoring the shape of the spot intensity profile, the percentage of reflections with intensities greater than background and the quality of agreement of intensities of symmetry-related reflections. Initially film

setting matrix is refined with low-resolution data. The mis-orientation matrices and the cell parameters are then included in the refinement. And the resolution limit of the data used increased in a stepwise manner after parameters are converged within each step.

Finally data up to 2.0 - 2.5 Å resolution were used for processing of intensities. Integrated intensities are calculated by the profile-fitting method (Rossmann, 1979), and the standard profiles are determined in nine different regions of the detector area.

3-1-1d. Imaging Plate

Normal X-ray film which uses silver compound have been usually used as the most useful detector of X-ray diffraction. But normal X-ray film has many disadvantages, such as low sensitivity, high background noise called chemical fog, narrow dynamic range, non-linearity of blacking of film by X-ray intensity, difficulty of uniform developing and so on. Since computer controlled four-circle diffractomator with scintillation counter was invented, it has been widely used in crystallography because all diffraction data are collected automatically with high precision. But scintillation counter has no spatial resolution and all reflections must be measured step by step. Recently, new type area detectors have been invented, such as multi-wire proportional counter (MWPC), TV detector, CCD and the imaging plate. The former three detectors can handle real-time data measurement but later one is similar to X-ray film in the sense of necessity of read-out system. But imaging plate has many advantages, such as high sensitivity, no

chemical fog, wide dynamic range, large detective area, linearity of response, no dead time and so on (Miyahara *et al.*, 1986).

The imaging plate is a flexible plate coated with fine photostimulable phosphor crystal, $BaFBr:Er^{2+}$, combined in an organic binder. X-ray image is stored as a distribution of F-centers in the photostimulable phosphor crystal. The stored image is read out by measuring the intensity of fluorescence stimulated by He-Ne laser beam scanned over the surface of the screen. And the image stored in a plate is erasable by irradiation of visible light. Performance of the imaging plate is summarized in Table (3-1).

In this study, all data were collected using the imaging plate which size was 200X400 mm^2.

The read-out system of the imaging plate image data was a BA-100 manufactured by Fuji Photo Film Co.LTD. Image data were read out as two-dimensional intensity data of 0.1X0.1mm^2 pixels and 10bit A/D converter iwas used to get digital data. Total of 16MByte data were stored on the disk and then saved on the magnetic tape.

3-1-2. Experiments

3-1-2a. Choice of Wavelengths

To determine the crystallographic phases of cytochrome c_{553} by the multi-wavelength anomalous dispersion method, following four different wave lengths were chosen for data collection.

(1) Active Area Size	...	400 x 200 mm^2 (max. size for BA-100)
(2) Pixel Size	...	0.1 x 0.1 mm^2 (min. size for BA-100)
(3) Spacial Resolution	...	< 0.2 x 0.2 mm^2
(4) Linearity of Response	...	4 order of magnitude
(5) Dynamic Range	...	5 order of magnitude
(6) Detective Quantum Efficiency	...	86 % (for MoKα-ray)
(7) Background Level	...	< 3 photons/pixel
(8) Dead Time	...	Zero

(9) The plate can be used REPEATEDLY

Table 3-1

Performance of imaging plate

- 1.040Å ($\Delta f'$= 0.197e, $\Delta f''$=1.664e) ... λ_1
- 1.380Å ($\Delta f'$=-0.440e, $\Delta f''$=2.678e) ... λ_2
- 1.743Å ($\Delta f'$=-9.211e, $\Delta f''$=3.951e) ... λ_3
- 1.746Å ($\Delta f'$=-6.299e, $\Delta f''$=0.469e) ... λ_4

Real and imaginary part of anomalous scattering terms are calculated by Cromer and Liberman's method (Sasaki, 1984). Gold foil was used to select 1.04 Å wavelength X-ray, copper foil was use to select 1.380 Å. Iron foil was used to select X-ray at absorption edge of iron, 1.7345 Å. 1.743 Å and 1.746 Å were selected by mechanical movement of monochromator from absorption edge of iron foil. As shown in Figure (3-2), λ_3 and at λ_4 are near to the K absorption edge of iron atom, and both $\Delta f'$ at λ_3 and $\Delta f'$ at λ_4 were quite large. And $\Delta f''$ at λ_3 was large, although $\Delta f''$ at λ_4 was negligible. The data at λ_1 is far from absorption edge and both $\Delta f'$ and $\Delta f''$ were negligible. The data at λ_2 was at first collected to use as native data for refinement. $\Delta f'$ at λ_2 was small and $\Delta f''$ was not so large but native anomalous difference Patterson $(F_P^+ - F_P^-)^2$ shows a significant peak corresponds to Fe-Fe self vector (see Chapter 3-1-2b) as this data set was merged by five crystals and non-systematic errors should be reduced.

Following differences were used for the crystallographic phase determination.

- $F^+(\lambda_2) - F^-(\lambda_2)$ ... $\Delta f''(\lambda_2)$
- $F^+(\lambda_3) - F^-(\lambda_3)$ ... $\Delta f''(\lambda_3)$
- $F(\lambda_3) - F(\lambda_1)$ ... $\Delta f'(\lambda_3 - \lambda_1)$
- $F(\lambda_4) - F(\lambda_1)$ ... $\Delta f'(\lambda_4 - \lambda_1)$

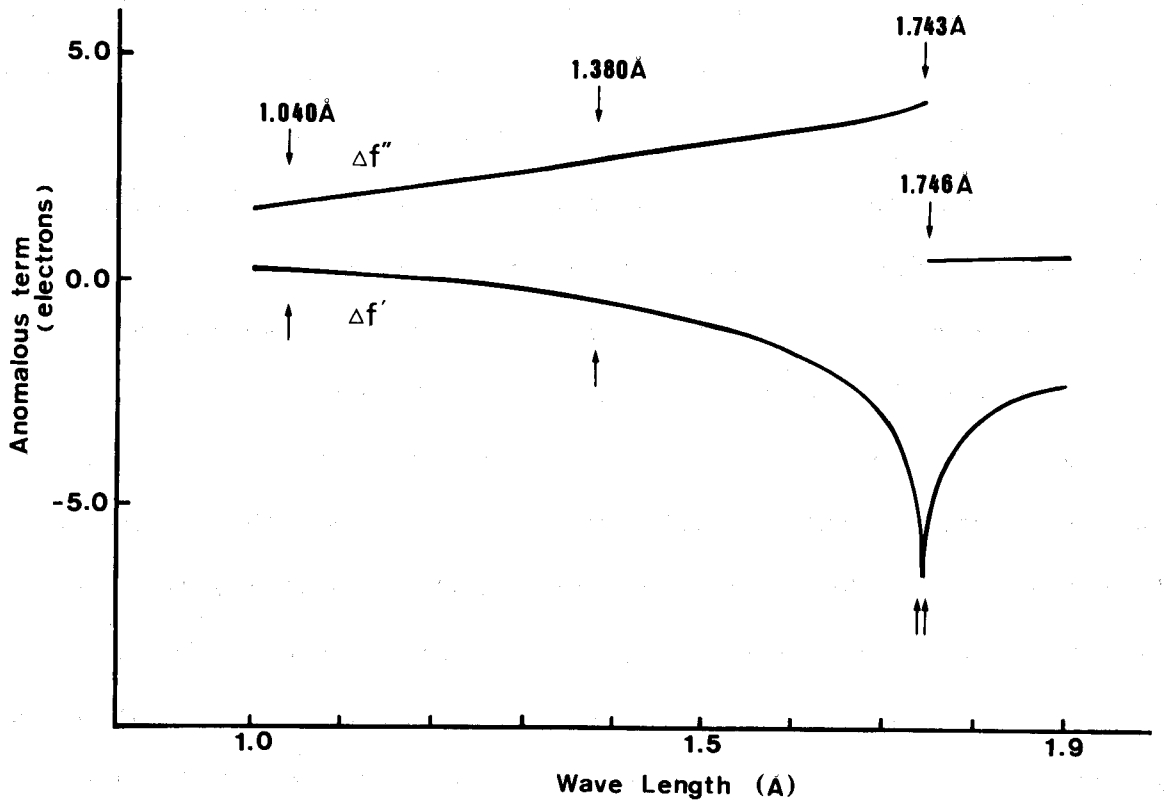

Figure 3-2

Wavelength dependence of anomalous terms of atomic scattering factor of iron

Arrows show wavelengths at which diffraction data was collected

These data are calculated by Cromer and Liberman's method (Sasaki, 1984)

3-1-2b. Condition of Data Collection

The conditions of data collection were summarize in Table (3-2). Monochromatized X-ray beam was collimated by the $0.2 \times 0.2 mm^2$ collimator just in front of the sample. Film cassette of which camera radius was 286.5mm was carried out for all data collection. The diffraction data sets at 1.380 Å were merged using data of five crystals both *a*- and *c*-axis rotation. The data near rotation axis which are taken using the Weissenberg geometry are not so good, because the shape of these data usually becomes worth than the other part of data. So usually it is neccesary to collect at least two data set rotating along two different directions. But the diffraction data of cytochrome c_{553} has 4/mmm symmetry and it means that intensity of the reflection of which the Miller index is hkl is equal intensity of the reflection of khl, I(hkl)=I(khl), thus it is enough for data collection of cytochrome c_{553} to rotate along only one axis which is not the unique axis (*c*-axis). Three data sets except for data at 1.380 Å were collected using only one crystal for each data set.

As the author wanted to get higher resolution data at 1.380 Å as can as possible, total exposure time for these data sets were relatively longer than those for other data sets.

Crystal number	Wavelength(Å)	Rotation axis	ϕ-range(°)	exposure time	irradiated power(mA·min.)*)
1	1.380	*c*	103.9	54'27"	9796
2	1.380	*a*	118.25	63'42"	12421
3	1.380	*c*	57.75	18'15"	3921
4	1.380	*a*	129.0	34'00"	9537
5	1.380	*c*	60.75	21'21"	4792
6	1.743	*a*	220.6	18'50"	4765
7	1.040	*a*	200.5	13'52"	2665
8	1.746	*a*	198.6	20'24"	3765

Table 3-2

Conditions of data collection for multi-wavelength anomalous dispersion method

All data are collected at BL-6A2 at Photon Factory
using the Weissenberg camera for
macromolecular crystallography and imaging plates

*) Irradiated power is defined as
Ring current(mA) X Exposure time(min.)

3-2. Data Handling

3-2-1a. Data Reduction -- Indexing --

The program system WEIS (Higashi, 1989) was used to get integrated intensity data of each Miller index from two dimensional image data of Weissenberg type diffraction pattern. Conditions of data reduction and their results were summarized on Table (3-3). Crystals those data were collected at 1.380 Å diffracted better than 1.5 Å resolution, that was limited by the size of an imaging plate, but diffraction data below 1.6 Å resolution were indexed and collected to avoid the data at the edge of a imaging plate.

Lorentz and polarization corrections for each reflections were applied at the same time when each reflections were indexed and integrated.

Polarization factor P is defined as

$$P = (I(h)-I(v))/(I(h)+I(v)) \qquad (3-1)$$

where I(h) and I(v) are intensities of horizontally and vertically polarized X-ray, respectively. As synchrotron radiation is highly linear polarized, polarization correction is effective for accuracy of data. It was used 0.92 for polarization correction from the measurement using powder diffraction (Sakabe, *private communication*). Relatively large effective mosaic spread of Δ=0.3 were used, and this value was large enough to avoid true partial reflections being classified as full reflections even if the crystal setting matrix has a little error. Size of measurement box was changed according to the size of diffraction spot, and from 9X9 to 13X13 pixels of measurement

Wave length (Å)	IDENT	RSET[1]	RINT[2]	DR[3]	DS[4]	No.of refln.	R_{merge}[5]
1.380	101	2.0	1.6	0.23	0.16	4886	6.2
	102			0.29	0.17	4940	7.5
	103			0.25	0.17	5814	5.7
	104			0.26	0.19	5004	6.0
	105			0.34	0.22	4972	5.8
	106			0.35	0.20	5460	5.8
	107			0.28	0.19	5294	5.7
	108			0.29	0.17	4888	6.0
	109			0.25	0.25	3902	7.7
	110			0.22	0.15	5114	5.3
	111			0.27	0.19	5098	5.9
	201	2.0	1.6	0.25	0.15	9030	6.9
	202			0.32	0.19	6066	6.0
	203			0.30	0.22	10018	6.0
	204			0.36	0.21	4992	5.6
	205			0.29	0.17	12582	5.8
	206			0.28	0.16	13134	5.4
	301	1.6	1.6	0.33	0.21	2726	6.9
	302			0.20	0.13	2840	7.2
	303			0.36	0.21	2772	6.3
	304			0.28	0.20	2840	6.6
	305			0.32	0.19	2544	8.4
	306			0.29	0.18	2728	6.6
	307			0.27	0.16	2936	6.1
	308			0.29	0.21	2480	7.7
	309			0.31	0.19	3012	6.3
	310			0.25	0.12	2768	6.9
	311	2.0	1.6	0.26	0.14	3026	5.8
	312	1.6	1.6	0.26	0.18	2516	9.6
	313			0.25	0.17	2902	5.7
	314			0.31	0.18	2666	6.1

Table 3-3

Data reduction of cytochrome c_{553} on each films

Wave length (Å)	IDENT	RSET[1]	RINT[2]	DR[3]	DS[4]	No.of refln.	R_{merge}[5]
1.380	401	2.0	1.6	0.26	0.17	10828	6.1
	402			0.21	0.19	10374	5.7
	403			0.20	0.15	10680	6.4
	404			0.21	0.14	10646	6.8
	405			0.22	0.14	10334	6.6
	406			0.19	0.12	9236	7.1
	407			0.27	0.23	8538	7.3
	408			0.24	0.14	5188	6.1
	501	2.0	1.6	0.18	0.11	5078	6.8
	502			0.20	0.13	5258	5.9
	503			0.21	0.16	5284	4.9
	504			0.19	0.13	5126	5.7
	505			0.18	0.13	5150	5.1
	506			0.27	0.14	4600	6.9
	507			0.22	0.13	4694	6.8
	508			0.21	0.14	4390	7.1
1.743	601	2.2	2.0	0.45	0.29	6152	6.4
	602			0.37	0.27	6544	6.5
	603			0.34	0.18	6170	6.5
	604			0.34	0.22	5710	6.8
	605			0.44	0.25	4348	7.1
	606			0.32	0.17	6098	6.2
	607			0.41	0.26	5990	6.7
	608			0.48	0.21	6424	6.9
	609			0.30	0.18	6708	6.1
	610			0.51	0.27	6768	7.0

Table 3-3
(*continued*)

Wave length (Å)	IDENT	RSET[1]	RINT[2]	DR[3]	DS[4]	No.of refln.	R_{merge}[5]
1.040	701	2.2	1.6	0.24	0.22	9516	6.4
	702			0.18	0.14	10148	5.7
	703			0.19	0.16	9992	5.5
	704			0.19	0.16	9982	5.8
	705			0.17	0.14	9222	5.5
	706			0.18	0.14	8758	5.8
	707			0.18	0.14	7974	5.5
	708			0.17	0.14	6846	5.3
	709			0.23	0.18	7190	6.5
	710			0.22	0.18	6328	6.1
	711			0.20	0.19	7454	6.3
	712			0.19	0.17	7780	6.5
	713			0.21	0.16	8136	5.7
	714			0.20	0.15	9004	6.1
	715			0.22	0.16	9102	5.9
	716			0.18	0.15	9436	6.1
1.746	801	2.2	2.0	0.24	0.20	6024	6.3
	802			0.33	0.22	5982	6.8
	803			0.24	0.16	6548	6.1
	804			0.41	0.27	6212	7.0
	805			0.42	0.33	5366	7.3
	806			0.23	0.12	5822	6.1
	807			0.29	0.18	4798	6.4
	808			0.38	0.24	4982	6.5
	809			0.22	0.18	5362	6.5

Table 3-3
(continued)

1) Resolution limit to determine setting matrix
2) Resolution limit to collect diffraction data
3) r.m.s. deviation along R-direction
4) r.m.s. deviation along S-direction
5) R_{merge} is defined as

$$R_{merge} = \frac{\Sigma \Sigma |I_{hj} - \langle I \rangle_h|}{\Sigma \Sigma \langle I \rangle_h}$$

box was used for integration of intensities.

3-2-1b. Absorption Correction and Local Scaling

Observed diffraction data should be included both systematic and non-systematic errors.

Non-systematic errors should be reduced by averaging of many symmetry-related reflections. But some correction technique should be neccesary to reduce systematic errors. Absorption effect by crystal, mother liquor and glass capillary and difference of diffraction volume according to its rotation angle should be the most serious parts of systematic errors. The scaling program in the WEIS system, named SCALE, can reduce these errors using Katayama's method (Katayama *et al.*, 1972). This method needs some symmetry related reflections, but camera method is suitable for this purpose as many symmetry related reflections can be collected at a same time. This correction was applied to the data set at 1.380 Å using the data collected by diffractometer, which was applied absorption correction by described North & Phillips (North *et al.*, 1968), as reference data.

Matthews suggested that local scaling method was very useful to reduce systematic errors (Matthews and Czerwinski, 1975). Modified technique of this method was attempted to the data collected by this Weissenberg method. Small differences $\Delta f'$ and $\Delta f''$ are used for phase determination by the multi-wavelength anomalous dispersion method, it was neccesary to reduce systematic errors as could as possible.

In this local scaling procedure, scaling factors applied to each shell

were determined by the following procedure,

1. Blocking reflection data according to their polar coordinates (ϕ,ψ) in the reciprocal space (Figure (3-3(a))).
2. For each shell, the scale factor k_j of j-th shell will be calculated as follows,

$$\left(\sum_h \sum_k \sum_l \left(F_{obs}(hkl)/F_{ref}(hkl)\right)\right)/N = 1/k_j \qquad (3\text{-}2)$$

where N is number of reflections in the j-th shell

The reference data must be needed for this method. The reflection data set collected at 1.040 Å was used as reference data. Figure (3-3(b)) shows an example of distribution of polar angles of reflections on a film. Figure (3-4) shows an example of distribution of local scale factors according to ϕ angles.

To calculate local scale factors, the following equation were also tried to apply,

$$\left(\sum_h \sum_k \sum_l \left(F_{obs}(hkl)/\sum_h \sum_k \sum_l F_{ref}(hkl)\right)\right)/N = 1/k_j \qquad (3\text{-}3)$$

but this scale factor did not show so much improvement. The equation (3-2) gave much weight to weak reflections. Anomalous effect is more effective to higher resolution data and higher resolution data is always weaker than lower resolution data. That was because the equation (3-2) gave better result in this study.

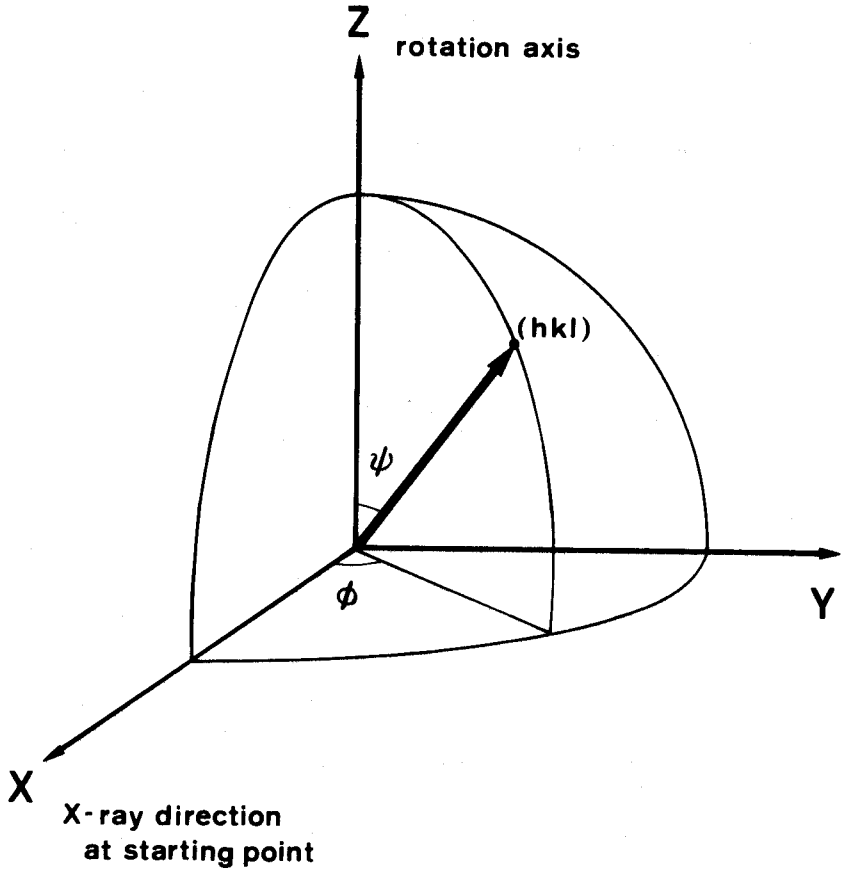

Figure 3-3

(a) Polar coordinates (ϕ,ψ) to determine diffraction point for Local scaling

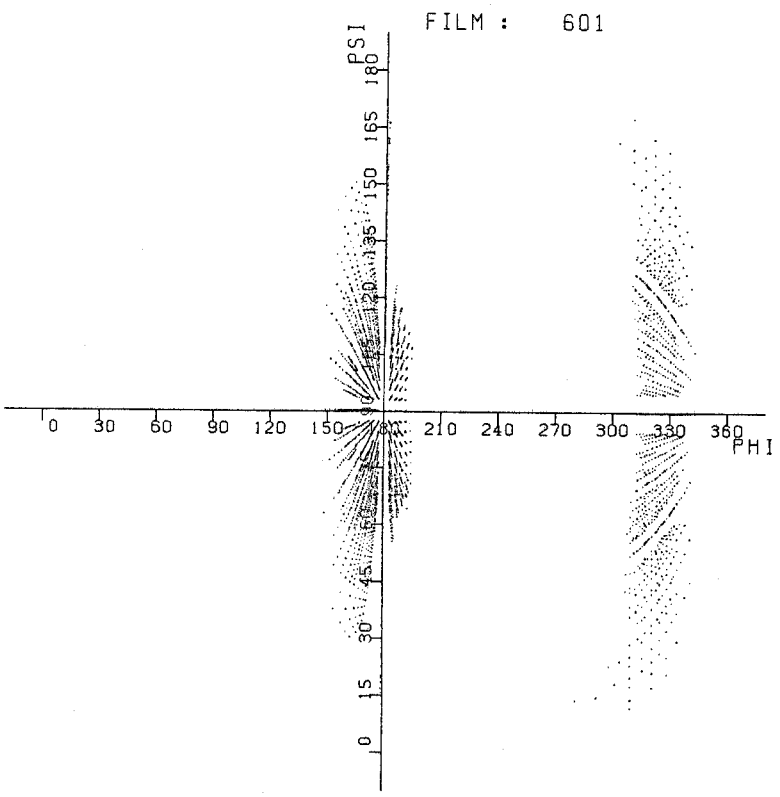

Figure 3-3
(*continued*)

(b) An example of distribution of polar angles of diffractions on a film

Each point shows a polar coordinate of a diffraction spot

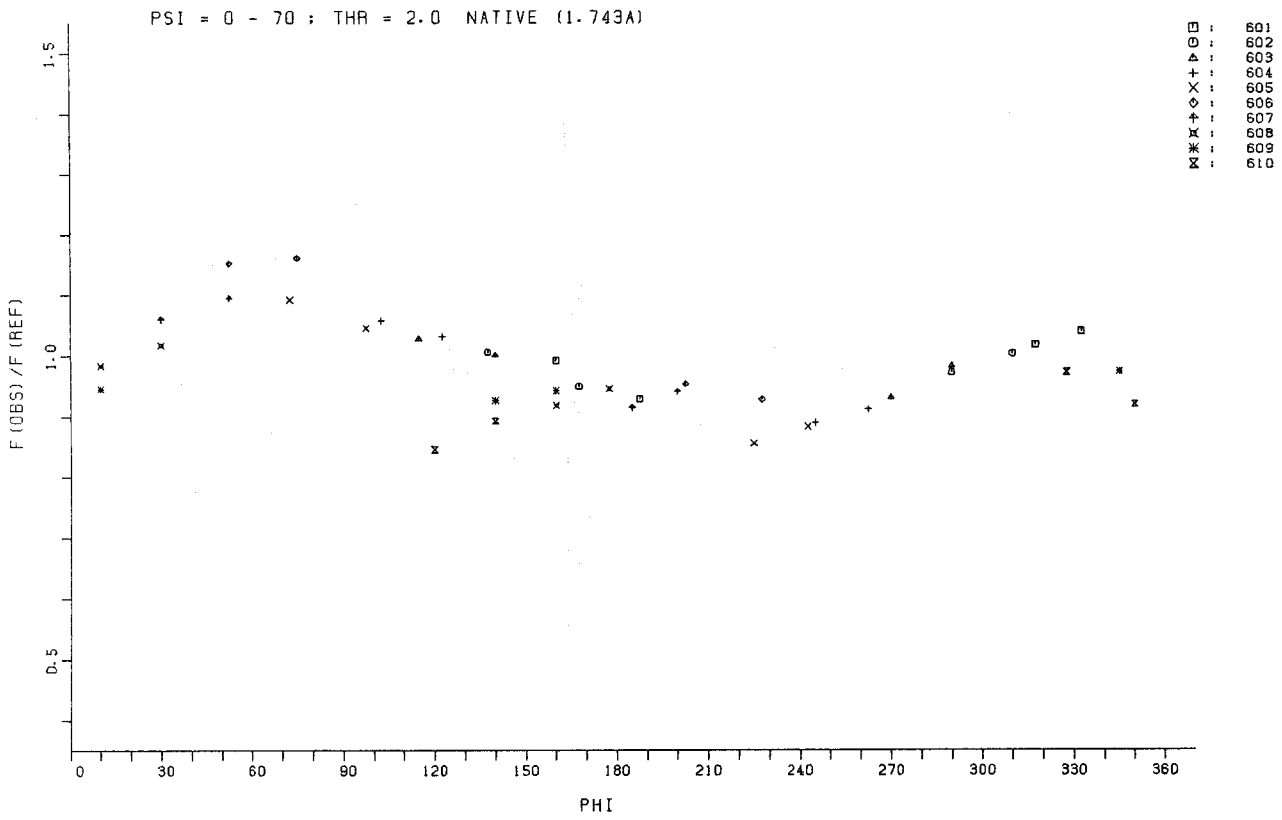

Figure 3-4

An example of angle distribution of Local scale factors

Figure (3-5(a)) and Figure (3-5(b)) showed anomalous difference Patterson maps of the data at 1.743 Å without the local scaling. The Patterson coefficient of former was corresponds to $\Delta f'$ term and that of later was corresponds to $\Delta f''$ term. The former Patterson map did not show clear Fe-Fe self vector on the Harker section, although the later showed clear peaks. The difference of qualities of these maps was due to film-to-film scaling problem. The later coefficient, $F_P^+ - F_P^-$, was used differences on the same film of only one crystal, although the former included scaling problem between two different crystals. To reduce this scaling error, the local scaling procedure was very effective for improvement of quality of map. Figure (3-6) showed Patterson maps with both before and after local scaling data. The coefficient of both two maps was $|F_P(1.743) - F_P(1.380)|^2$. Apparently, after local scaling data showed high signal-to-noise ratio peak at the position corresponding to Fe-Fe self-vector of heme iron. And Table (3-4) shows an example of changes of R_{merge} according to the local scaling procedure.

Since the intensities recorded on the imaging plate would correspond to the average intensities from the crystal during the exposure time, radiation damage correction was difficult to be applied. But as the exposure time to take intensities on one sheet of imaging plate was very short, radiation damage must be negligible on one sheet. Difference of diffraction patterns which were cause by radiation damage on the first and the last sheet could not recognized in the same crystal, and small radiation damage might be corrected by the film to film scaling based on equivalent reflections.

Table (3-5) shows final data statistics for multi-wavelength anomalous

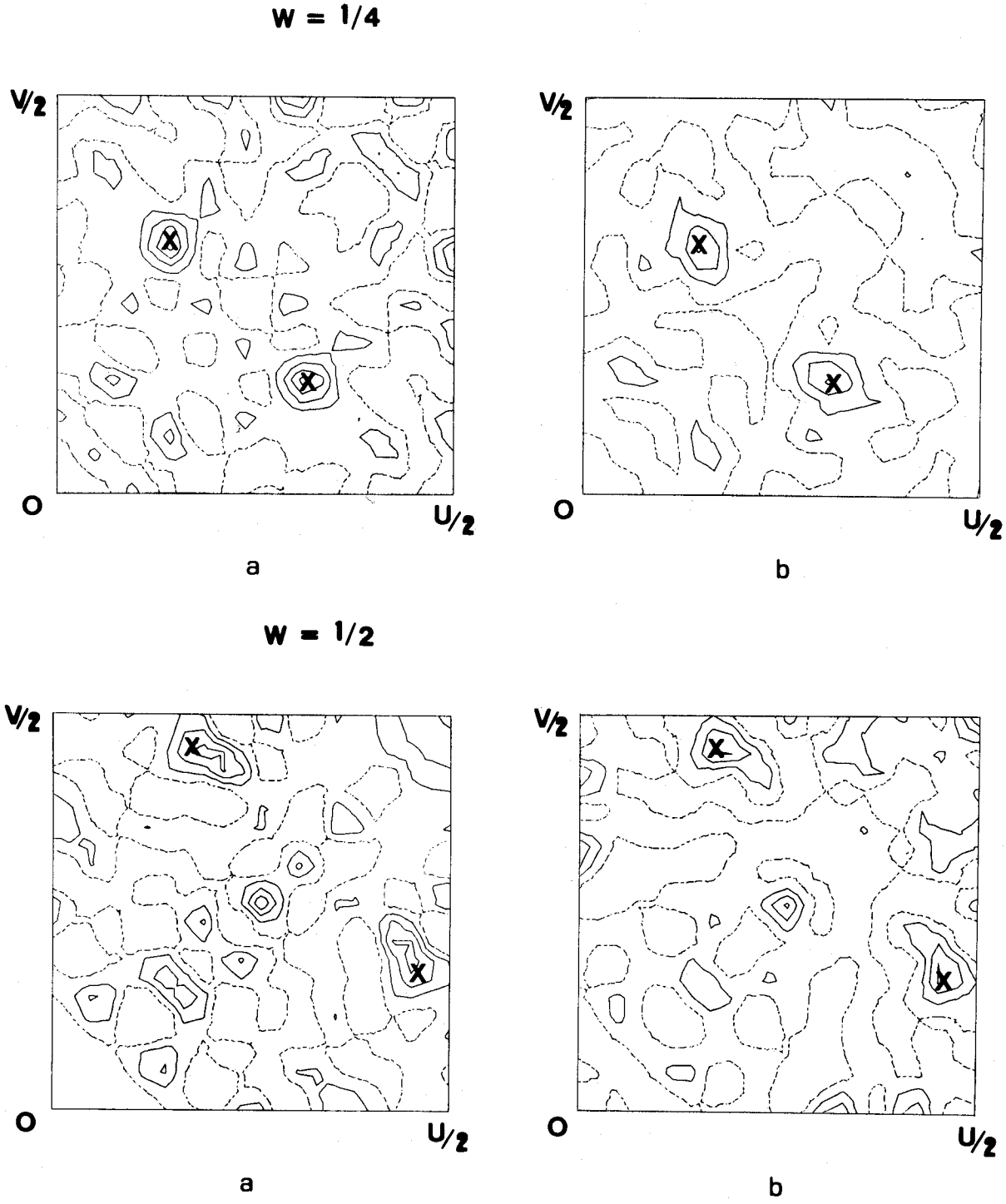

Figure 3-5

Native anomalous difference Patterson maps
using data without local scaling

(a) coefficient of $|F_P(1.743)-F_P(1.38)|^2$, corresponding to $\Delta f'$
(b) coefficient of $|F_P^+(1.743)-F_P^-(1.743)|^2$, corresponding to $\Delta f''$

Dashed line shows zero level and these maps are contouring
of equal intervals in arbitrary unit

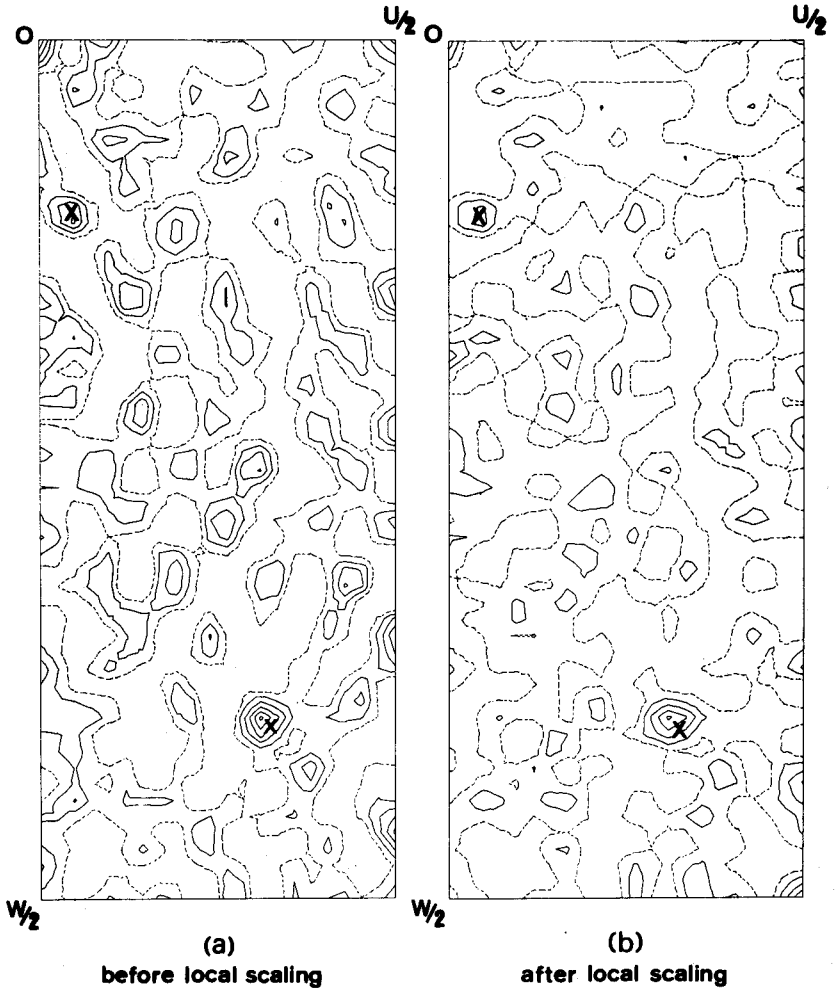

Figure 3-6

Effect of local scaling procedure

Showing native anomalous difference Patterson maps of which coefficient is $|F_P(1.743)-F_P(1.380)|^2$

(a) without local scaling, (b) after local scaling

Dashed line shows zero level and these maps are contouring of equal intervals in arbitrary unit

Film IDENT[2]	R_{merge}[1] (%) No Local Scaling	After Local Scaling[3]	No. of Reflection
601	7.2	6.4	6152
602	7.7	6.5	6544
603	8.7	6.5	6170
604	9.8	6.8	5710
605	11.4	7.1	4348
606	11.7	6.2	6098
607	10.2	6.2	5990
608	8.2	6.9	6424
609	7.2	6.1	6708
610	7.5	7.0	6768
Total		6.57	30954 (4726)[4]

Table 3-4

Effect of local scaling of data of cytochrome c_{553}

1) $R_{merge} = \dfrac{\sum_h \sum_i |I_{hi} - \langle I \rangle_h|}{\sum_h \sum_i \langle I \rangle_h}$

2) F_P (1.743Å) data

3) Local Scaling against F_P (1.040Å) data

4) No. of independent reflections

	Wave Length(Å)	R_{merge}[1] (%)	Resol.(Å)	No. of refln.[2]
λ_1	1.040	5.89	1.6	8101
λ_2	1.380	6.21	1.6	12378(1942)[3]
λ_3	1.743	6.57	2.0	4725(1549)
λ_4	1.746	6.50	1.8	4561

Table 3-5
Summary of F-data for each wavelength

1) $$R_{merge} = \frac{\sum_h \sum_j |I_{hj} - \langle I \rangle_h|}{\sum_h \sum_j \langle I \rangle_h}$$

2) Number of Bijvoet's pair-related reflections count as one

3) Number of Bijvoet's pair data

phase determination.

3-2-2. Native Anomalous Difference Patterson Maps

Figure (3-7(a)) to Figure (3-7(d)) showed native anomalous difference Patterson maps of both $\Delta f'$ and $\Delta f''$ term for phase determination. Figure (3-7(e)) did not show any significant peak, it indicated the wave length which was used for data collection of the data set at λ_4 was apparently longer than the wave length at K absorption edge of iron and $\Delta f''$ was negligible.

3-2-3. Absolute Scale

Figure (3-8) showed a Wilson's plot (Wilson, 1949) of data collected at 1.380 Å. Considering of this plot, scale factor and temperature factor were determined as 1.727 and 19.0, respectively.

Scale factors for other data sets were calculated from relative scale factors to the data at 1.380 Å and summarized in Table (3-6).

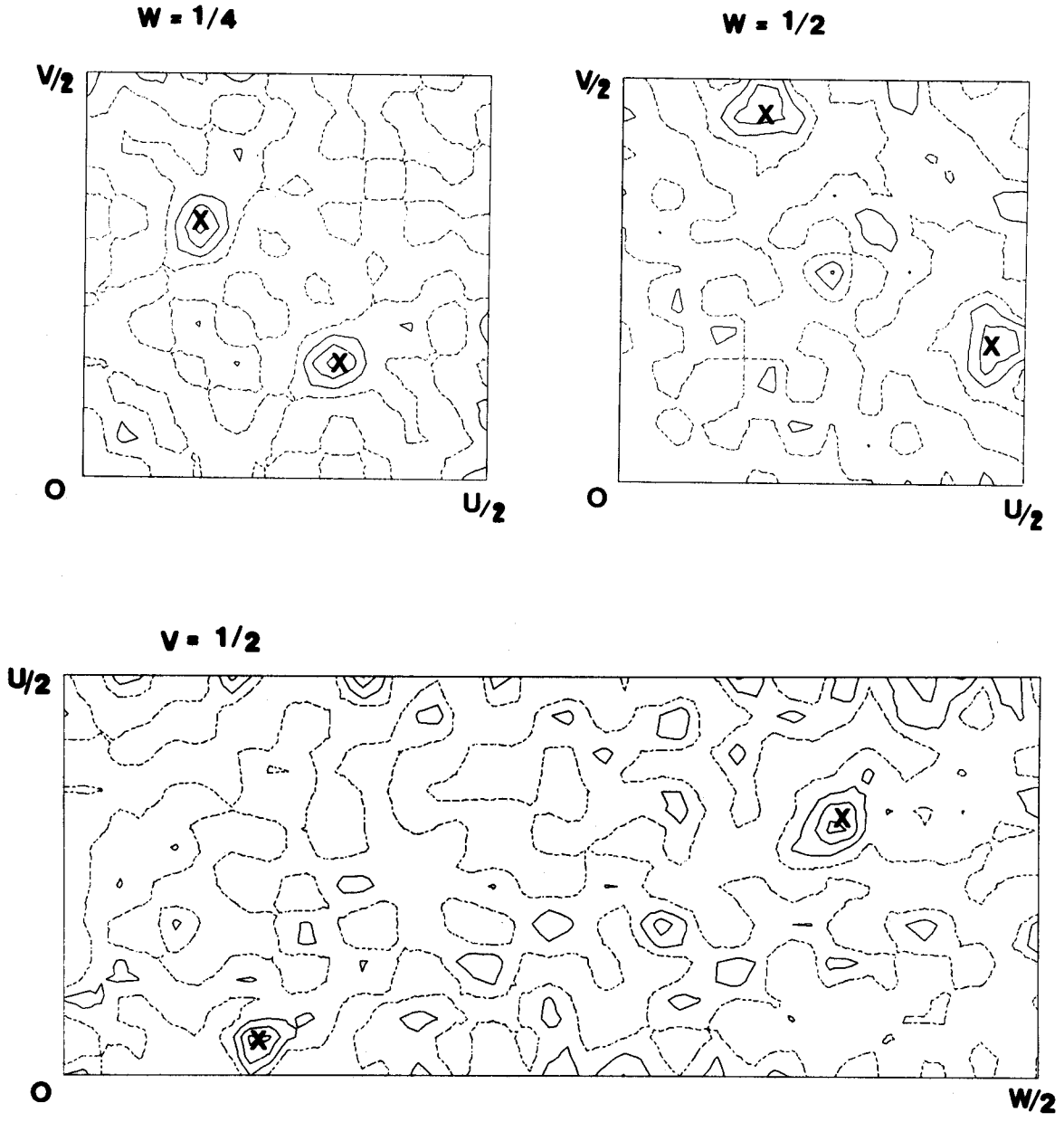

(a) $|F_P(1.743)-F_P(1.040)|^2$

Figure 3-7

Native anomalous difference Patterson maps

Dashed line shows zero level and these maps are contouring of equal intervals in arbitrary unit

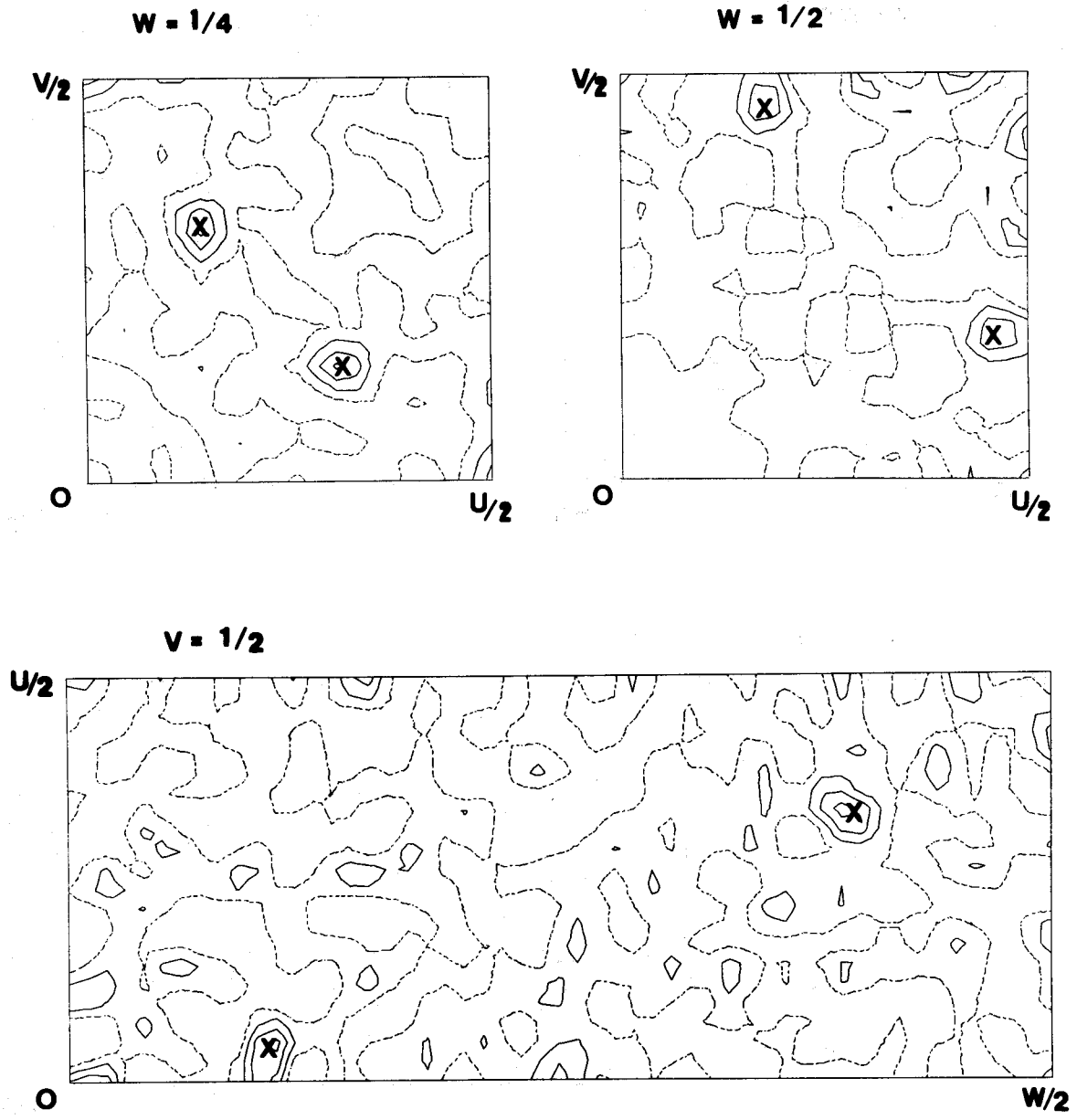

(b) $|F_P(1.746)-F_P(1.040)|^2$

Figure 3-7
(*continued*)

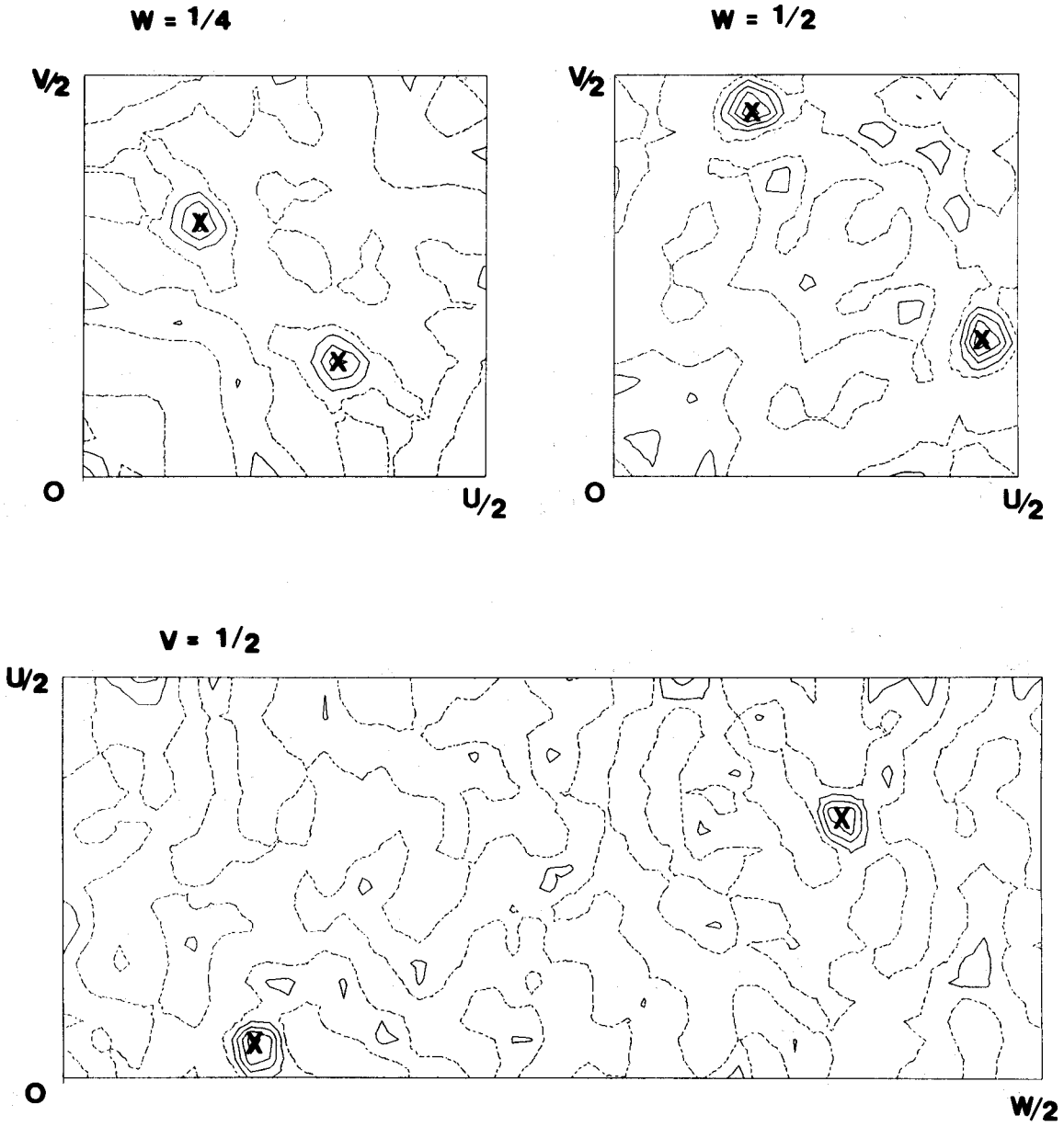

(c) $|F_P^+(1.380)-F_P^-(1.380)|^2$

Figure 3-7
(*continued*)

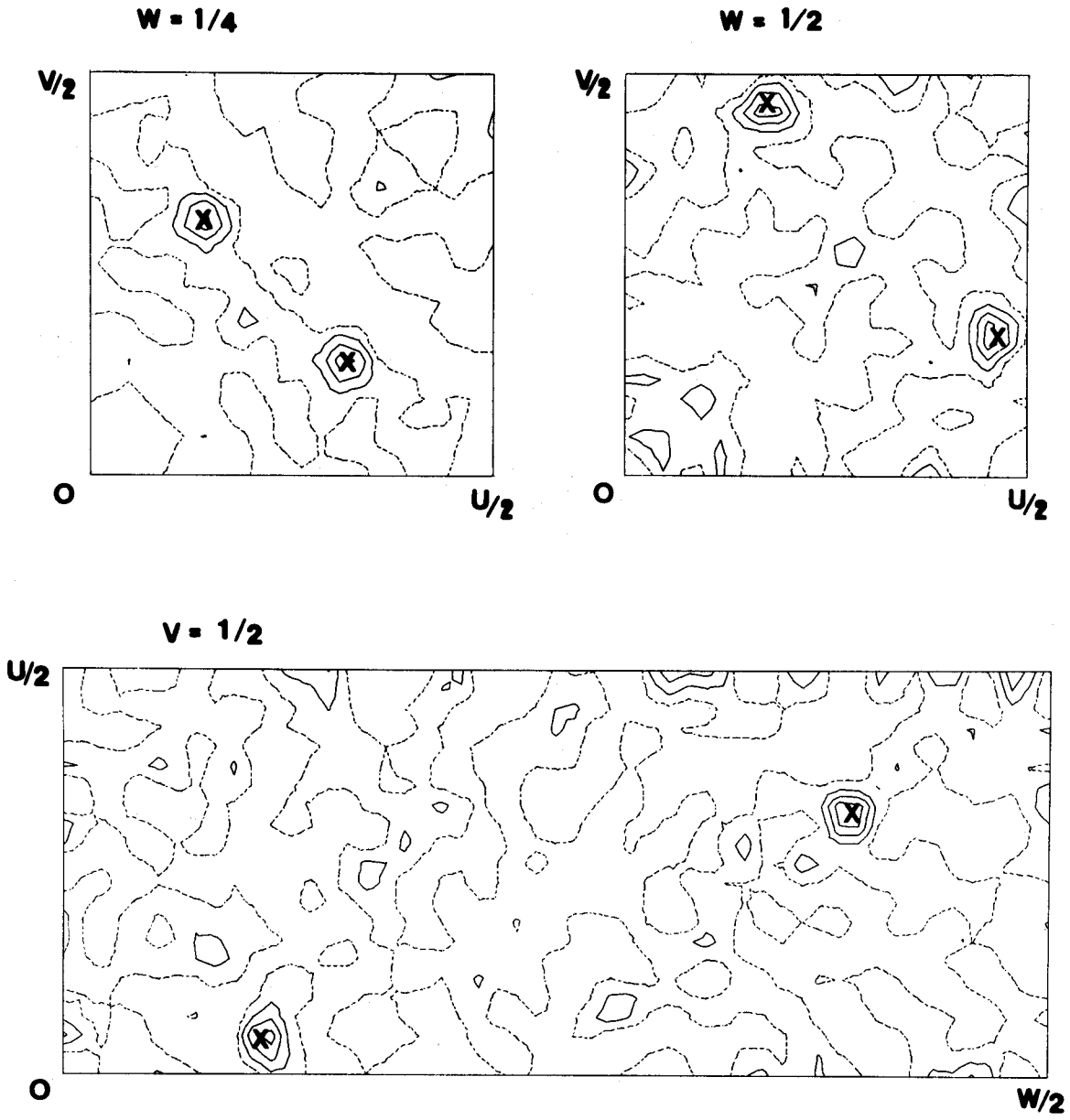

(d) $|F_P^+(1.743)-F_P^-(1.743)|^2$

Figure 3-7
(*continued*)

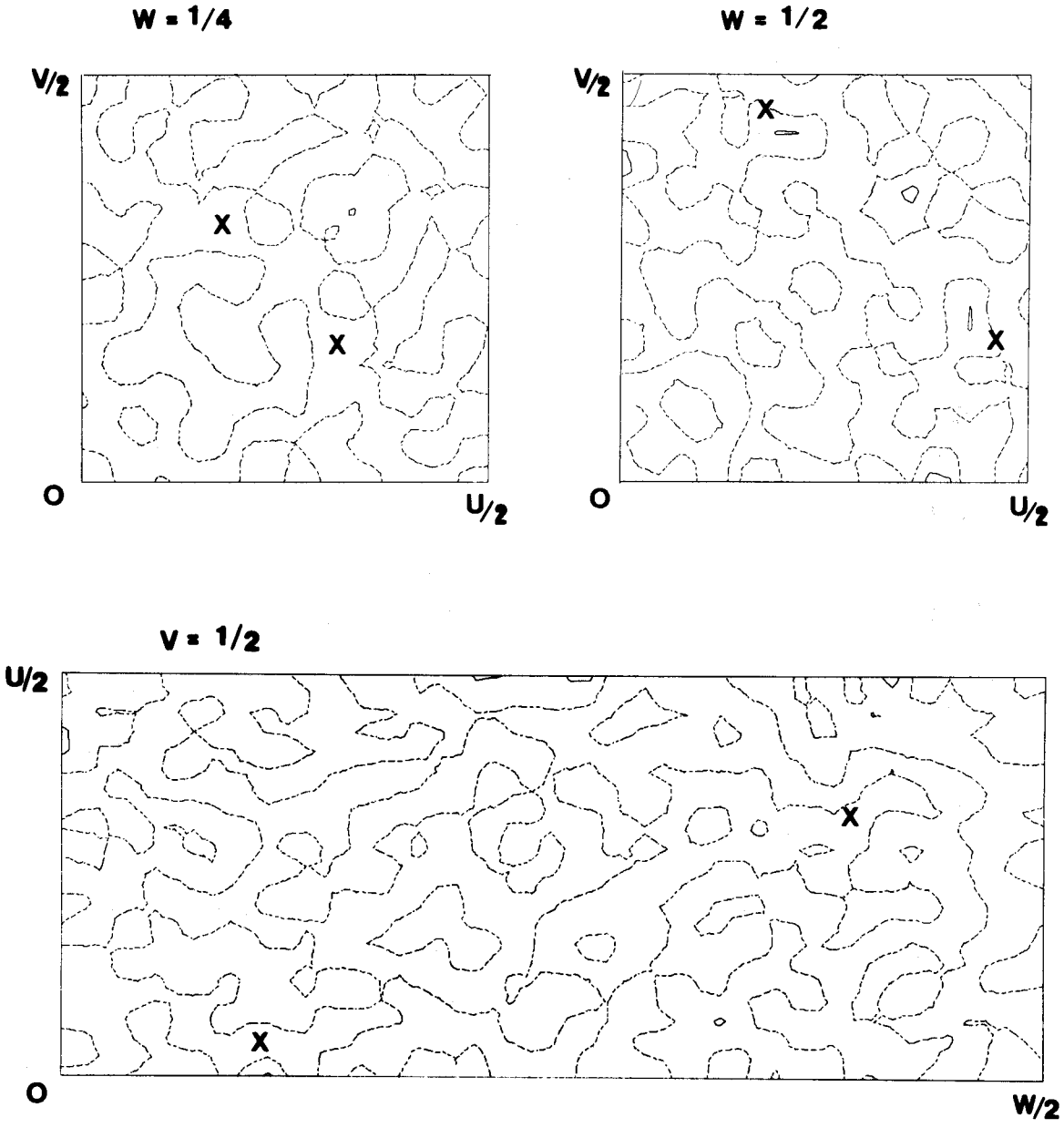

(e) $|F_P^+(1.746)-F_P^-(1.746)|^2$

Figure 3-7
(*continued*)

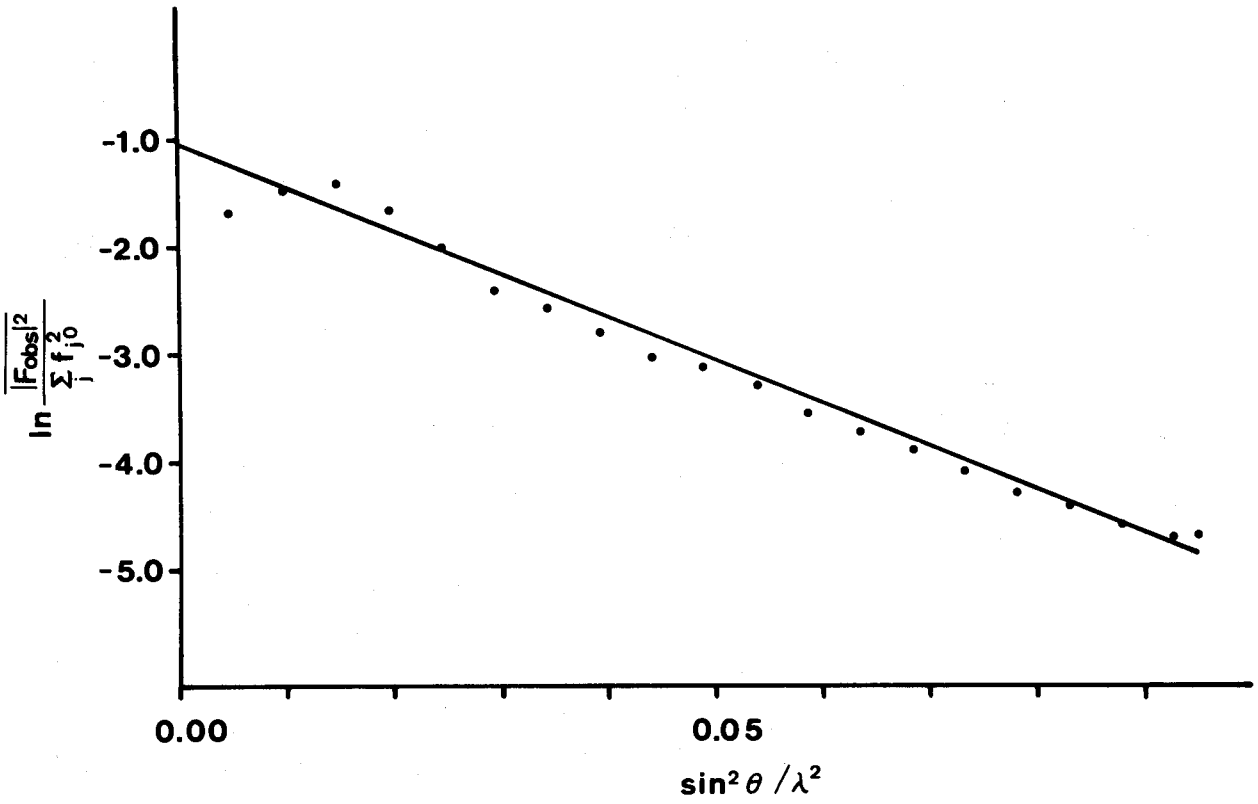

Figure 3-8

Wilson's plot (Wilson, 1949) of data
of cytochrome c_{553} at 1.380 Å

K = 1.727
B = 19.0

Wave length (Å)	Scale factor	$R^{*)}$
1.040	1.723	0.031
1.380	1.727	———
1.743	1.706	0.056
1.746	1.710	0.064

Table 3-6

Scale factors and *R*-factors for each data sets

$$^{*)}\ R = \frac{\Sigma\ |\,|F_P(1.380)| - |F_P(\lambda_A)|\,|}{\Sigma\ |F_P(1.380)|}$$

3-3. Phase Determination by Multi-Wavelength Anomalous Dispersion Method

3-3-1. Theoretical Background

a. Anomalous scattering effect

X-ray diffraction phenomenon from crystal is caused by the interface of scattering from each atoms in the crystal.

When X-ray is irradiated on a free electron, the influence of the fluctuating electromagnetic field of the incident wave forces the electron into oscillations of the same frequency as the incident wave. All the scattered X-rays from a single electron have the same phase relation to the incident beam, differs by 180 degree, so that the scattering is coherent. Scattering from one atom can be expressed as follows,

$$f = \int_{atom} \rho(r) \cdot \exp(2\pi i \mathbf{r}\cdot\mathbf{k}) \cdot dv \qquad (3\text{-}4)$$

where

$$\mathbf{k} = \mathbf{s}/\lambda$$

and $\mathbf{s}$ shows a scattering vector, $\mathbf{s}=\mathbf{s}_s-\mathbf{s}_i$, difference of the direction from incident, $\mathbf{s}_i$, to scattered beam, $\mathbf{s}_s$. When the direction of scattered beam is same as that of incident beam, f_0 becomes as Z, where Z is the total number of electrons in the atom.

This assumption is correct for free electrons of atoms. But real electrons are bound quite tightly, particularly those in the inner K and L

shells and such a description is only adequate for the lightest of elements (*eg.* carbon, nitrogen and oxygen). Then atomic scattering factor must write are follows,

$$f = f_0 + \Delta f' + i\Delta f'' \qquad (3\text{-}5)$$

this means that atomic scattering factor has its real term, $f_0+\Delta f'$, and its imaginary term, $\Delta f''$. The phase of imaginary part of atomic scattering factor is always $\pi/2$ in front of that of the scattered X-rays. Figure (3-2) showed one example of both real and imaginary term of anomalous dispersion effect, $\Delta f'$ and $\Delta f''$. The real part of anomalous scattering term varies dramatically near its absorption edge, and the imaginary part of anomalous scattering term varies slightly at the wavelength which is shorter than absorption edge and is nearly equal to zero at wavelength which is longer than absorption edge.

Suppose that structure factor amplitudes of the reflection hkl and its inverse reflection $\bar{h}\bar{k}\bar{l}$.

$$F_P(+) = \sum_J f_j \cdot \exp(2\pi i \mathbf{h}\cdot\mathbf{r}_j) \qquad (3\text{-}6)$$

and

$$F_P(-) = \sum_J f_j \cdot \exp(-2\pi i \mathbf{h}\cdot\mathbf{r}_j) \qquad (3\text{-}7)$$

where summation is over all the atoms in the unit cell. Therefore

$$F_P(+) = F^*_P(-) \qquad (3\text{-}8)$$

and

$$|F_P(+)|^2 = |F_P(-)|^2 \qquad (3\text{-}9)$$

when imaginary part, $\Delta f''$, of atomic scattering factor is negligible.

As shown in Figure (3-9), if there are some anomalous scatterers in the crystal, $F_P(+)$ is no longer equal to $F_P(-)$ for the general case. And if the reflection is centric, $F_P(+)$ is equal to $F_P(-)$.

Magnitude of diffraction data collected at the wavelength close to absorption edge varies by the $\Delta f'$ term, and its structure factor is different from the corresponding data which is collected at the wavelength far from absorption edge.

These two kind of differences, both real and imaginary part of diffraction, due to anomalous dispersion effect, can be used for phase determination.

As an analogue of isomorphous replacement method, Figure (3-10) showed a Harker diagram that showed a multi-wavelength anomalous dispersion method.

At first, atomic parameters of anomalous scatterer are refined, then phases were determined.

As the multi-wavelength anomalous dispersion (MAD) technique has just been applied to structure determination of macromolecular crystals, there is no established procedure for this method on both refinement of parameters of anomalous scatterers and phasing procedure. In this study, the similar procedure of isomorphous replacement technique was applied.

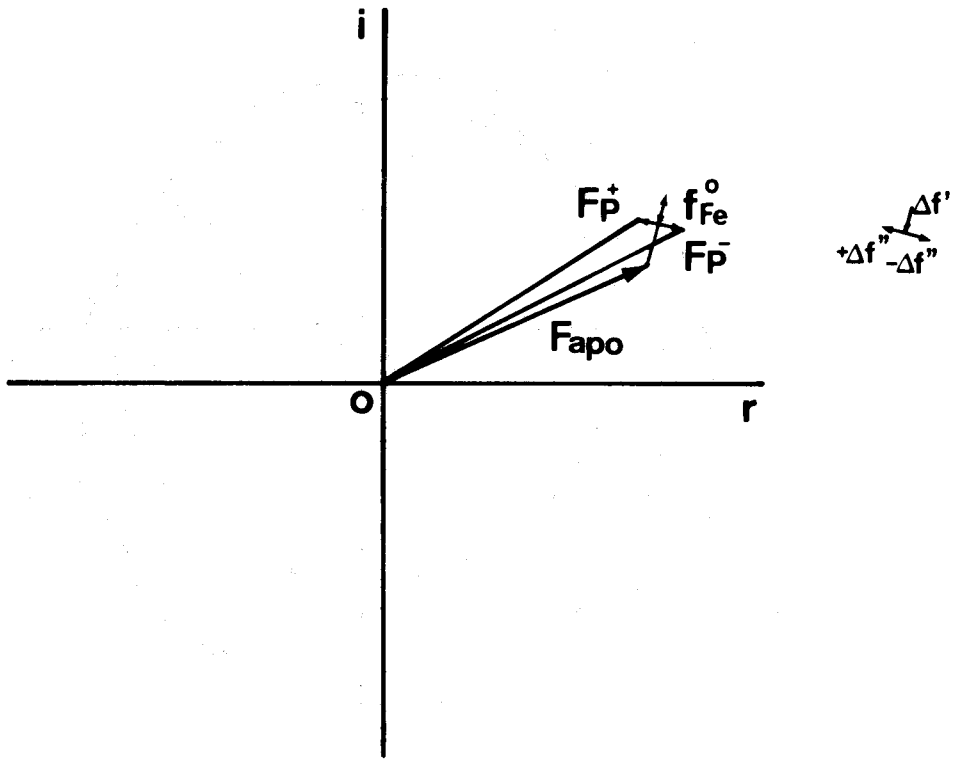

Figure 3-9

Vector diagram showing
native anomalous case

F_{apo} : Structure factor of protein without anomalous scatterer
F_P : Strucure factor of protein
f_{Fe} : Structure factor of iron atom (anomalous scatterer)

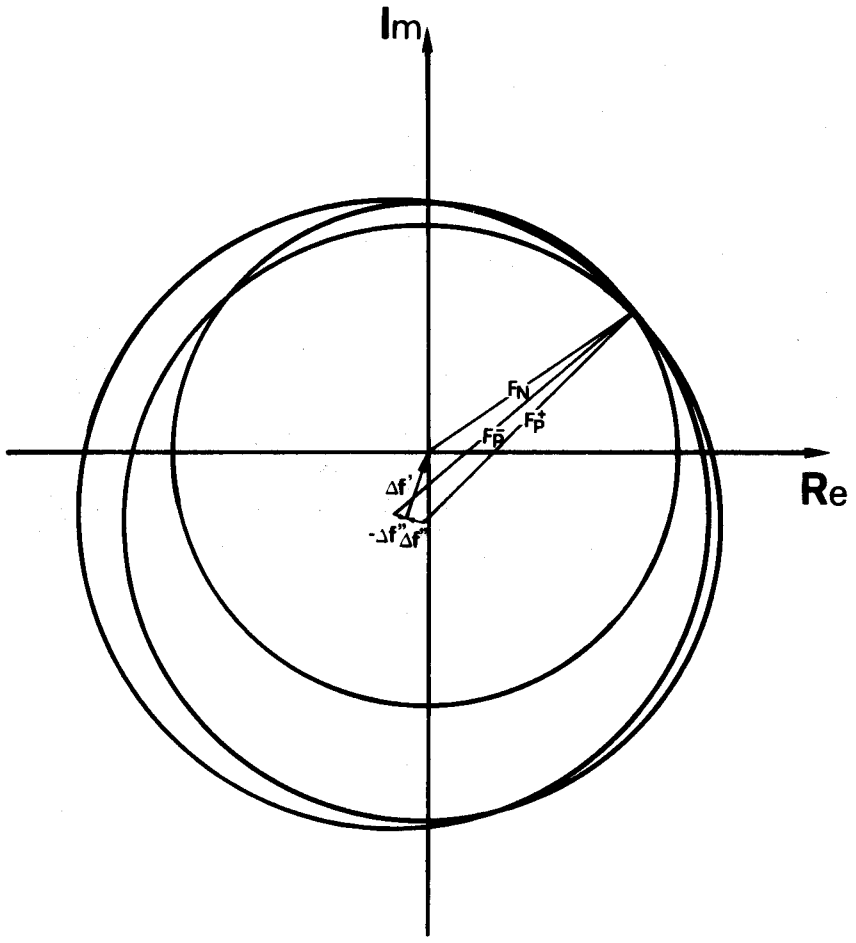

Figure 3-10

Harker diagram showing
MAD case

b. Refinement of atomic parameters of anomalous scatterer

The occupancy parameter of anomalous scatterer may be unity after scale factor is applied to each wavelength data. Thus the coordinates, (x,y,z), and the temperature factor will be refined.

In this study, centric refinement technique was applied to the refinement of atomic parameters. In this method, parameters were refined to minimize the following quantity using only centric reflections.

$$\varepsilon^2 = | | F_P{}^A - F_P{}^0 | - | \Sigma \Delta f'_j B_j \cos 2\pi i(hx_j + ky_j + lz_j) | |^2 \qquad (3\text{-}10)$$

where $F_P{}^A$ is an observed structure factor with anomalous effect, $F_P{}^0$ is an observed structure factor without anomalous scattering effect and $\Delta f_j'$, B_j, (x_j, y_j, z_j) are real part of anomalous scattering term, temperature factor, of anomalous scatterer and its coordinates, respectively. The least-squares refinement was applied to minimize the equation (3-10).

For the data which was only used its imaginary part of anomalous scattering effect, refinement of atomic parameters was proceeded described by Hendrickson (Hendrickson, 1981). This method minimize followings,

$$\varepsilon^2 = | \Delta F_P(\pm)(\mathrm{obs}) - (-2 \sum_J \Delta f''_j B_j \sin(hx_j + ky_j + lz_j)) |^2 \qquad (3\text{-}11)$$

for only large $\Delta F_P(\pm)(\mathrm{obs})$ reflections.

c. Phase Calculation

Phase determination procedure was according to Blow and Crick's best phase calculation (see 2-2-1).

Apparently, as shown in Figure (2-5), the unique correct phase can not be determined by the single isomorphous replacement method. Figure (3-11) showed an example of phase distribution of single isomorphous case. The dashed line showed a distribution of isomorphous term and dot-dashed line showed a distribution of anomalous term. In this case, if the root-mean squares error of isomorphous term, E_{iso}, and the root-mean squares error of anomalous term, E_{ano}, are same value, it could not possible to select correct phase from two possible phases of isomorphous term. North showed that a phase calculation with a phase calculation with an assumption of $E_{ano}=1/3E_{iso}$ could select the correct phase without ambiguity (North, 1965). On the other hand, in the multi-wavelength anomalous dispersion method, both magnitudes of real and imaginary differences are close to each other. As shown in Figure (3-12(b)), calculation with the assumption of $E_{ano}=1/3E_{iso}$ does not give correct phase, although the figure of merit is greater than that of with $E_{ano}=E_{iso}$. Using the assumption that E_{ano} is same as E_{iso} gives better result as shown in Figure (3-12(a)).

Phase probability of real part of anomalous difference is given as,

$$\varepsilon_{real}(\alpha) = |F_P{}^A| - (|F_P{}^0|^2+|\Delta f'|^2 - 2\cdot|F_P{}^0|\cdot|\Delta f'|\cdot\cos(\phi-\alpha)) \qquad (3\text{-}12)$$

$$P_{real}(\alpha) = \Pi \; N\cdot\exp(-\varepsilon^2{}_{real}(\alpha)/2E^2) \qquad (3\text{-}13)$$

and imaginary part was given as,

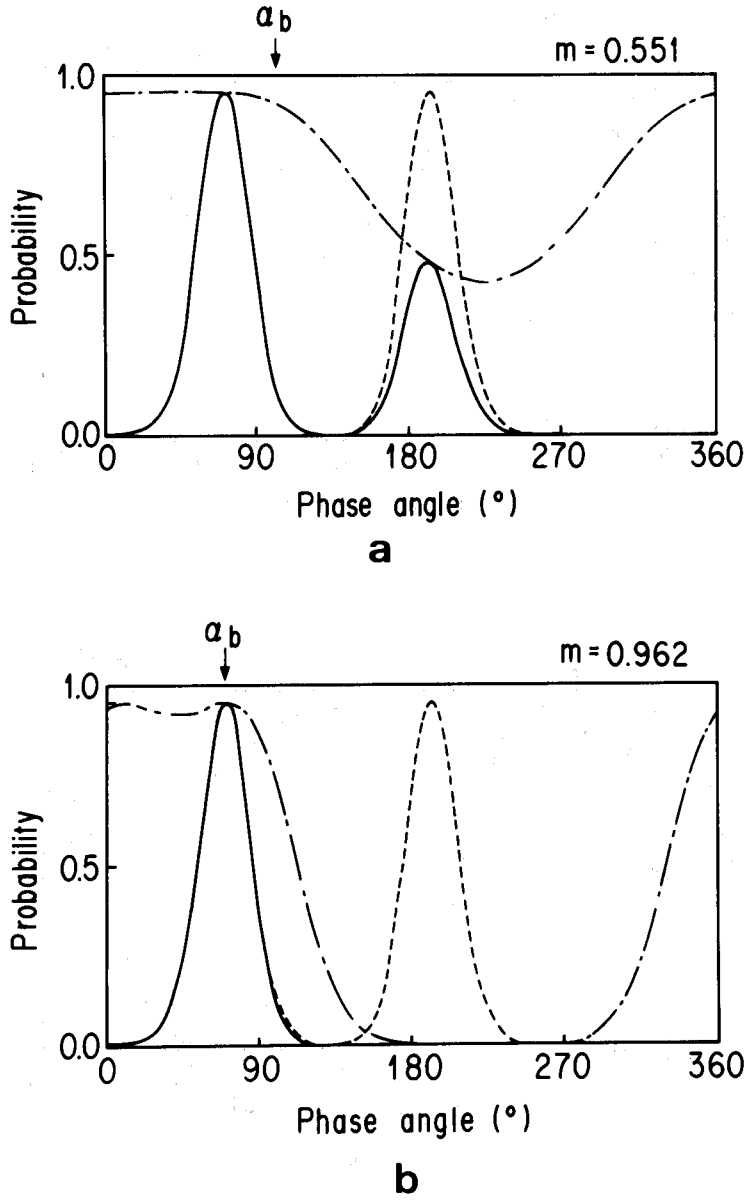

Figure 3-11

An example of phase distribution of SIRA case

(a) $E_{ano}=E_{iso}$
(b) $E_{ano}=1/3E_{iso}$

Assumption of $E_{ano}=1/3E_{iso}$ gives correct phase without ambiguity (North, 1965)

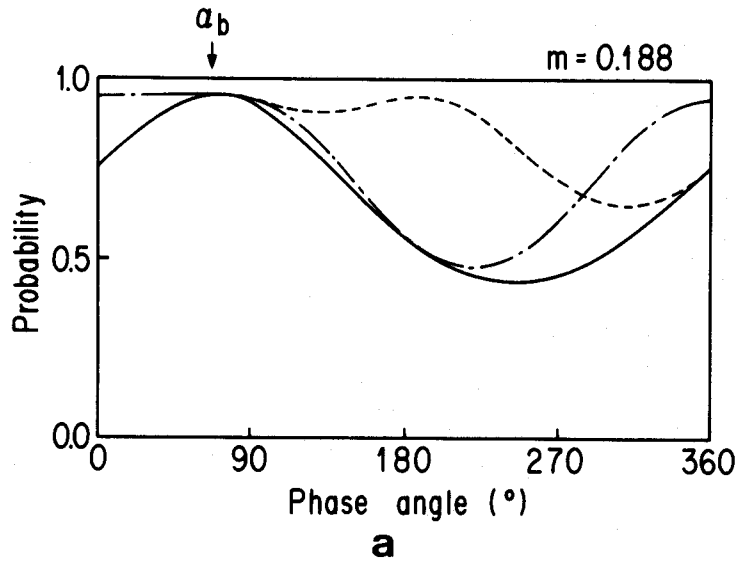

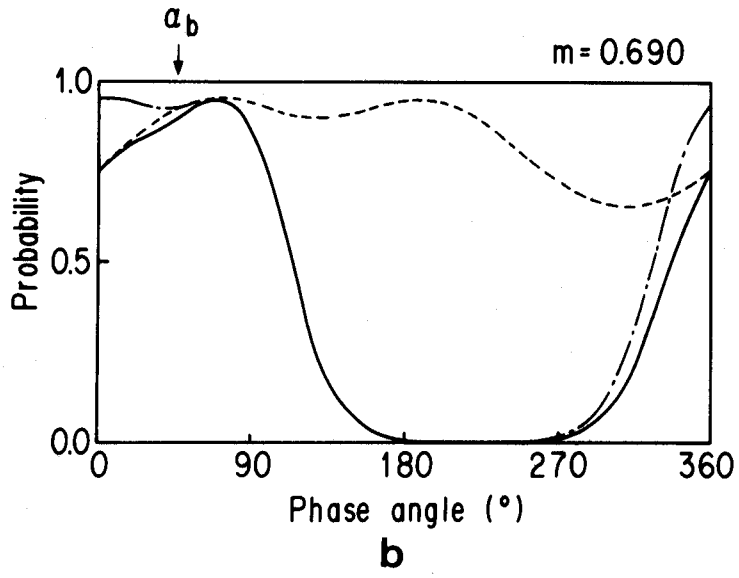

Figure 3-12

An example of phase distribution of MAD case

(a) $E_{ano}=E_{iso}$
(b) $E_{ano}=1/3E_{iso}$

Assumption of $E_{ano}=E_{iso}$ gives better result than assumption of $E_{ano}=1/3E_{iso}$

$$\varepsilon_{imag}(\alpha) = -\Delta F_P(\pm) - (2\cdot|F_P{}^0|\cdot|\Delta f''|/|F_P(\pm)\cdot|\Delta f'|)\cdot(b\cdot\cos\alpha - a\cdot\sin\alpha) \quad (3\text{-}14)$$

$$P_{imag}(\alpha) = \Pi\ N\cdot\exp(-\varepsilon^2{}_{imag}(\alpha)/2E^2) \quad (3\text{-}15)$$

$$\Delta F_P = |F_P{}^+| - |F_P{}^-|,\ a = \Delta f'\cdot\cos\psi,\ b = \Delta f'\cdot\sin\psi$$

Total phase probability distribution is given as the product of these terms as followings,

$$P(\alpha) = \Pi\ P_{j,real}(\alpha)\cdot\Pi\ P_{j,imag}(\alpha) \quad (3\text{-}16)$$

3-3-2. Refinement of Atomic Parameters

Scale factors for each data were determined from statistics between $F_P{}^A$ and $F_P{}^0$(1.380Å) (see Chapter 3-2-3).

Atomic parameters corresponded to data at 1.743 Å and 1.746 Å were refined by centric refinement technique. The real part of anomalous scattering term, $\Delta f'$, varies dramatically near the absorption edge, and it was very difficult to determine absolute wavelength and correct absorption edge using the instruments at BL-6A2. So in these refinement procedure, real part of anomalous scattering term, $\Delta f'$, was refined as one parameter of least-squares procedure. The least-squares procedure was used in the refinement program in the BOSS system (REFINE).

Atomic parameters corresponding to data at 1.380 Å were refined according to Hendrickson's procedure (Hendrickson *et al.*, 1981). Imaginary part, $\Delta f''$, does not vary dramatically, so it was not refined. The imaginary

part of anomalous scattering term was used the value calculated by Cromer and Liberman's method (Sasaki, 1984).

All atomic parameters are summarized in Table (3-7). These refined parameters for each data were treated as independent derivatives although these values should be same.

3-3-3. Phasing

The data sets collected at 1.380 Å, 1.743 Å and 1.746 Å were treated as three different derivatives, and best phases were calculated according to Blow and Crick's treatment (Blow and Crick, 1985) and the program PHASE in the BOSS system was used for phase calculation.

Phase probability distribution for the data set at 1.380 Å was calculated using only the imaginary part of anomalous difference term.

The data below 2.2 Å resolution were used for the best phase calculation because the phasing power, r.m.s.$|F_c|$/r.m.s.$|E|$, was greater than 1.0 below 2.2 Å resolution data. The mean value of the figure of merit at this resolution was 0.597 for 4995 independent reflections (93% of total reflections at 2.2 Å resolution). The result of phasing is summarized in Figure (3-13).

3-4. Model Building

The electron density map calculated using crystallographic phases

Wave length (Å)	x	y	z	B	Δf'
1.743	0.41311	0.76813	0.17569	9.33	-5.62
		R = 0.586		<E> = 10.01	
1.746	0.41576	0.76628	0.17594	8.01	6.15
		R = 0.599		<E> = 11.40	
1.380	0.41486	0.76709	0.17599	9.42	
				<E> = 7.15	

Table 3-7

Atomic parameters of MAD procedure

Three different wavelength data are treated as different derivatives

Parameters are refined against data from 10.0 to 2.2 Å resolution

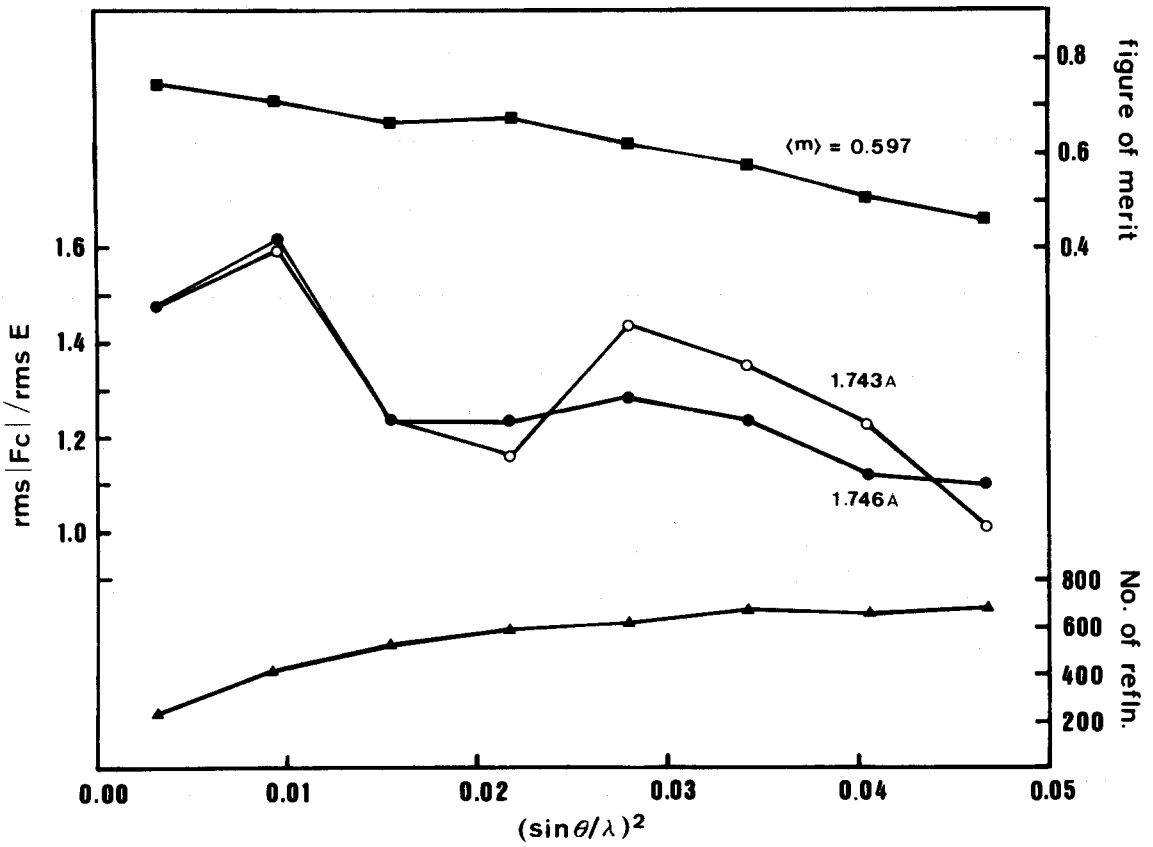

Figure 3-13

The radial distribution of the ratio of r.m.s.|Fc|/r.m.s.E, figure of merit and number of reflections

■ : Figure of merit
□ : r.m.s.|Fc|/r.m.s.|E| of 1.743 Å data
● : r.m.s.|Fc|/r.m.s.|E| of 1.746 Å data
▲ : Number of reflections

determined by the multiple-wavelength anomalous dispersion method at 2.2 Å resolution had good quality to interpret main chain folding on the mini-map.

The model building procedure was carried out using the model fitting program FRODO (Jones, 1978) on the three-dimensional graphics display PS340, Evans & Sutherland Co.LTD. The author used the Rice university version of FRODO, PS300 FRODO.

Interpretation of the electron density map and model building procedure was not so difficult as many part of side chains were found on the electron density map. Only a few part showed very weak electron density and these part were difficult to assign atomic models. These region were constructed considering geometries of backbone atoms. Interpretation of $2F_o-F_c$ map calculted using atomic coordinates of the model showed unambiguous electron density for interpretation.

Figure (3-14) shows MAD-map which was used for model building.

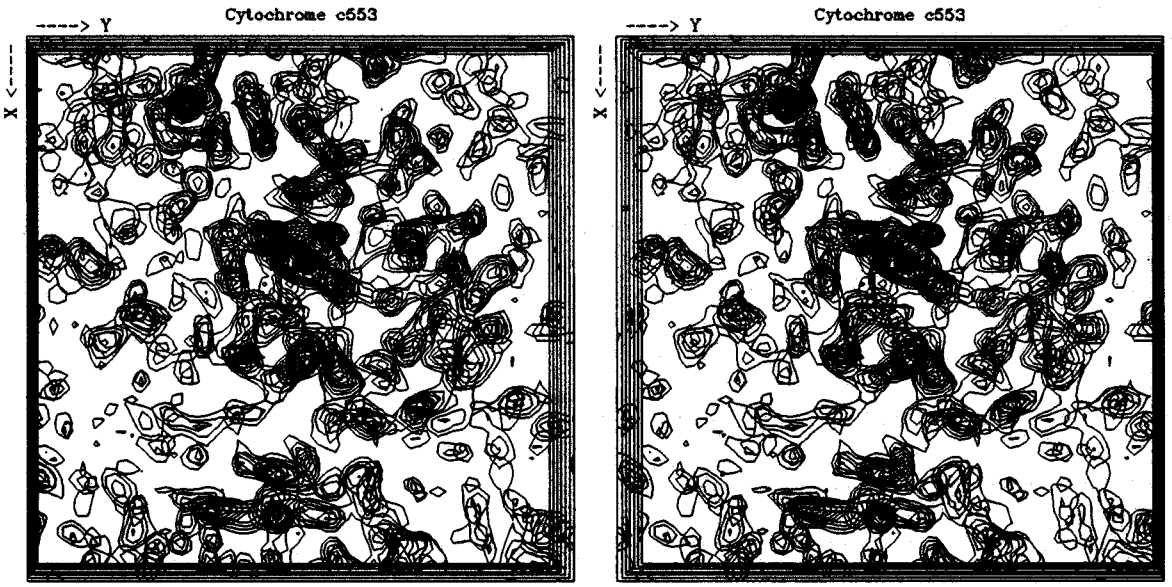

Figure 3-14

Electron density map using MAD phases

(a) Stacking map calculated by MAD method

The map was obtained from MAD phase information (m=0.60). This map is at 2.2 Å with contouring of levels at 20,30,40,... in arbitrary unit. Seven sections, taken at 0.99 Å intervals from section 15/104 to 21/104, are superimposed.

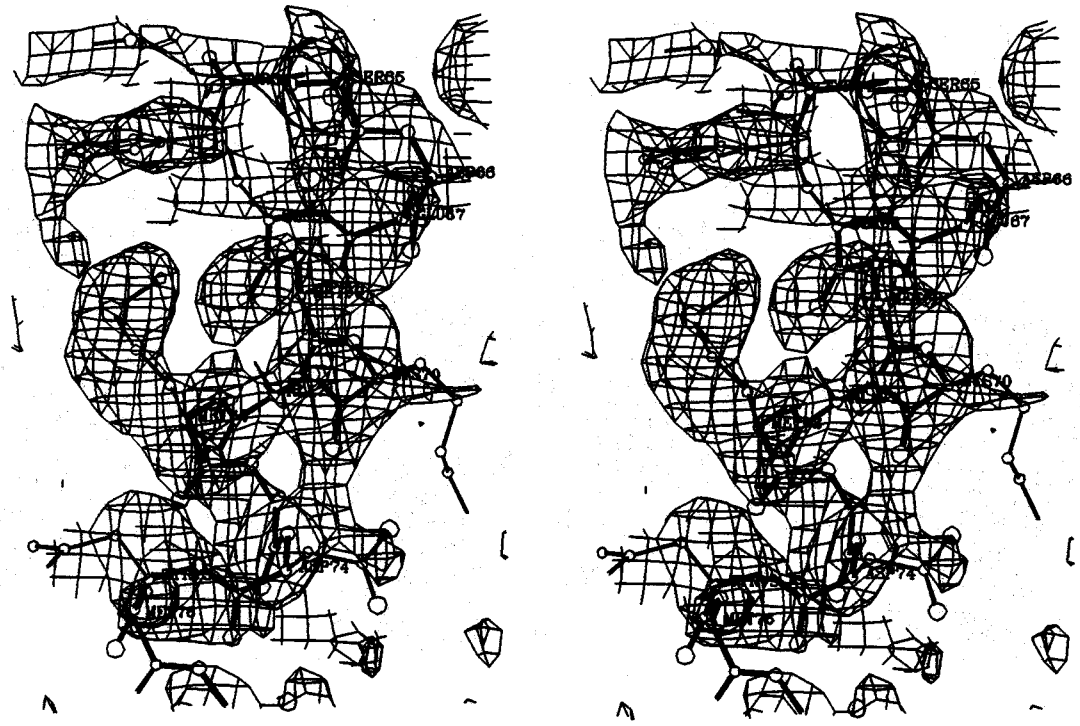

Figure 3-14
(continued)

(b) Electron density map around C-terminal helix

MAD map showing C-terminal helix, from Tyr64 to Tyr75, superimposed in MAD-map contoured at arbitrary level. Refined atomic coordinate (R=0.226) are superimposed. Intervals of contouring mesh is about 0.65 Å.

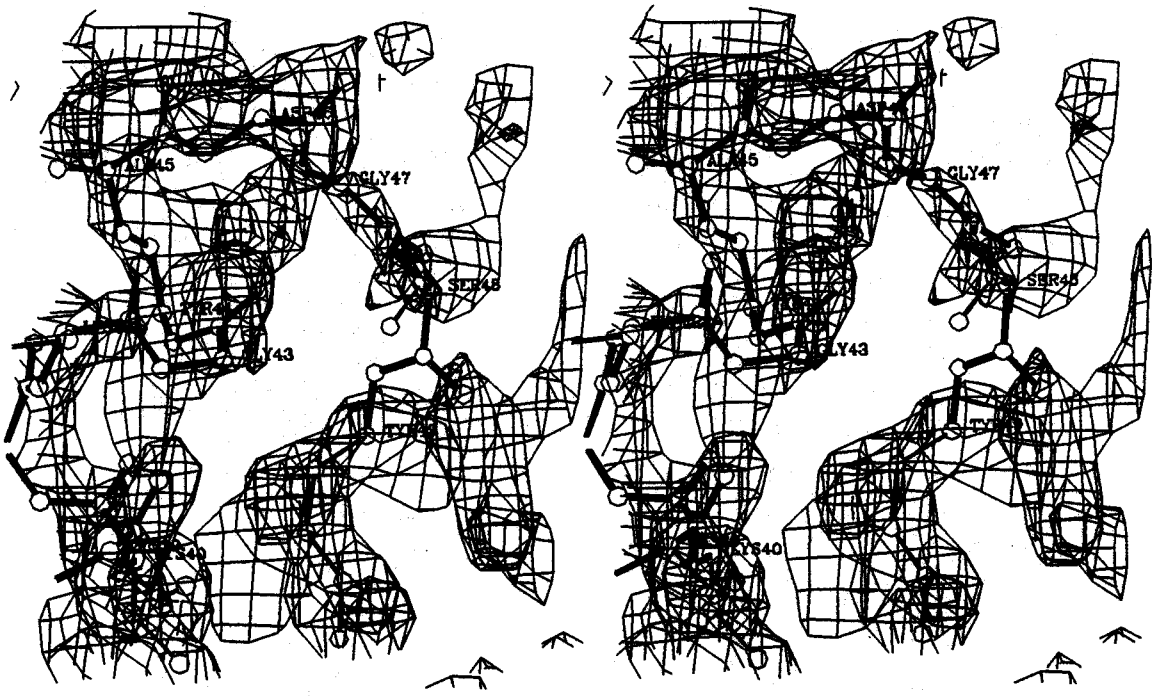

Figure 3-14
(continued)

(c) Electron density map shows the short loop which is in the bottom of the molecule

MAD map showing the region from Lys42 to Tyr49 superimposed in MAD-map contoured at arbitrary level. Refined atomic coordinate (R=0.226) are superimposed. Intervals of contouring mesh is about 0.65 Å. This region is the most difficult region to make an atomic model.

4. REFINEMENT STAGE OF STRUCTURE ANALYSIS

4-1. Refinement

4-1-1. Theoretical Background

An atomic structure model which is build by the interpretation of the electron density map has some errors, such as misinterpretation of the map, fitting error to the electron density map, structure distortion, lack of solvent structure, disorder of atoms. It must be neccesary to refine the atomic parameters of the model.

In the X-ray structure analysis, observed structure factor, F_{obs}, is the only observation. So it is necessary to minimize the difference between observed and calculated structure factors.

For usual structure analysis of small molecules, the refinement proceeds to minimize the following quantity,

$$\varepsilon^2 = \Sigma W_j \cdot |F_j(obs) - F_j(calc)| \qquad (4\text{-}1)$$

where W_j is a weight for each reflections that is often used as the inverse of the deviation of the observed structure factor, $1/\sigma_F$. Number of observation should exceed number of parameters those are to be refined by a factor of ten.

However macromolecular crystal does not diffract towards so high Bragg

angle, and the number of observations might not be enough for normal refinement unlike small molecular crystallography. The ratio of observation *via* parameters ratio is about two at 2.0 Å resolution data, and that means the structure is underdetermined for the refinement.

Hendrickson and Konnert proposed the restrained parameter least-squares refinement procedure for macromolecular crystal structure analysis (Hendrickson and Konnert, 1980). Their program, PROLSQ, is one of the most famous and the most useful technique for refinement of macromolecular structure, and this method was applied to the refinement of the structure analysis of cytochrome c_{553}.

This method minimize the following quantity,

$$\begin{aligned}
\Phi = & \sum_J W_j^F \cdot |F_j^O - F_j^C|^2 \\
& + \sum_J W_j^B \cdot |D_j^I - D_j^M|^2 \\
& + \sum_J W_j^A \cdot |D_j^I - D_j^M|^2 \\
& + \sum_J W_j^P \cdot |D_j^I - D_j^M|^2 \\
& + \sum_J W_j^C \cdot |V_j^I - V_j^M|^2 \\
& + \sum_J W_j^V \cdot |D_j^I - D_j^M|^2 \\
& + \sum_J W_j^T \cdot |B_j^I - B_j^M|^2 \qquad (4\text{-}2)
\end{aligned}$$

where the first term is the diffraction term which is the term to minimize in the refinement procedure for small molecular crystal, same function as the equation (4-1). The second term minimizes the deviation of bond distances from their ideal values. The third term minimizes the deviation of angle-related distances. The forth term minimizes the deviation of planarity. The fifth term minimizes the deviation of chiral center volumes.

The sixth term prevents the unreasonably short non-bonded contacts. The seventh term minimizes the unreasonably discrepancy between the thermal parameters of the neighboring atoms those are covalently bonded, and this is known as a "rigid motion".

All ideal values, those are shown as a superscript "I", are determined from small molecular crystal structures. The superscript "M" means the current value of the parameter of the present model. Superscripts "O" and "T" of the last term mean original and target temperature factors. And superscripts "O" and "C" of the first term means observed and calculated structure factors. The term "W" denotes the weighting factor for each terms.

The least-squares procedure is proceeded according to minimization of the summation of these parameters. It is obvious that minimization of Φ value is depends on the balance of weighting terms for these terms. It is necessary to reduce the discrepancy between observed and calculated structure factors, which is described as a crystallographic *R*-factor,

$$R = \frac{\Sigma \mid F_o - F_c \mid}{\Sigma \mid F_o \mid} \qquad (4\text{-}3)$$

with stereo chemically reasonable values of other parameters.

In the usual refinement procedure of protein structure analysis, the least-squares refinement procedure often falls to local minimum. Thus it is necessary to be jumped out from a local minimum. It is important to revise the atomic model according to the residual Fourier maps, ($2F_o$-F_c) or (F_o-F_c) maps.

4-1-2. Refinement Survey

The starting atomic coordinates used for the refinement were derived from the model which was built by the interpretation of 2.2 Å electron density map calculated using MAD phases. At the end of each refinement stage, the ($2F_o$-F_c)-map was calculated using the atomic coordinates those were derived at their stage, and misplaced fragments were manually corrected using the three-dimensional color graphics display and the model building program FRODO to be jumped out from the local minimum.

Sixty three water molecules are included in the last stage of the refinement. And finally, the crystallographic R value decreased to 0.226 using 10903 reflections between 6.0 and 1.6 Å resolution (83% of acceptable reflections) which have values grater than 3σ and also greater than 10. Disorder structure does not consider in this stage.

Weighting parameters at the final stage of the refinement were summarized in Table (4-1). Constrain for temperature factor variation does not applied at the final stage. Figure (4-1) shows the distribution of the final R factor against Bragg angle of reflections.

All atomic parameters are listed in Appendix B. Temperature factor of the carbonyl oxygen atom of Asp46 shows relatively high value, the omit-map of this region shows possibility of rotating movement of the peptide plane between Asp46 and Gly47.

Figure (4-2) shows a $2F_o$-F_c map using the atomic parameters at the final stage, it shows same region as shown in Figure (3-15).

Restraints		σ	r.m.s deviation	No. of parameters
Distances (total)				1748
Bond distance	Å	0.015	0.025	643
Angle distance	Å	0.030	0.042	859
Planer distance	Å	0.040	0.058	244
Heme coordination	Å	0.020	0.128	2
Planar group	Å	0.020	0.019	553
Chiral group	$Å^3$	0.150	0.212	79
Non-bonded contacts (total)				470(2218)
Single-torsion	Å	0.500	0.170	204
Multiple-torsion	Å	0.500	0.256	205
Possible H-bond	Å	0.500	0.209	61
Torsion angles (total)				204(374)
Planar (ϕ)	°	3.0	2.9	79
Staggered ($\pm$ 60,180)	°	15.0	20.3	117
Orthonormal ($\pm$ 90)	°	20.0	17.3	8
Isotropic thermal factors (No restrain) (Total)				1504
Main-chain bond	$Å^2$	-	8.985	365
Main-chain angle	$Å^2$	-	8.928	468
Side-chain bond	$Å^2$	-	15.319	278
Side-chain angle	$Å^2$	-	17.150	393

R = 0.226 (10903 refln.) 6.0 Å - 1.6 Å
(F_{min}=10.0, F≧ 3σ)

Table 4-1

Weighting parameters for refinement of
cytochrome c_{553} at the final stage of refinement

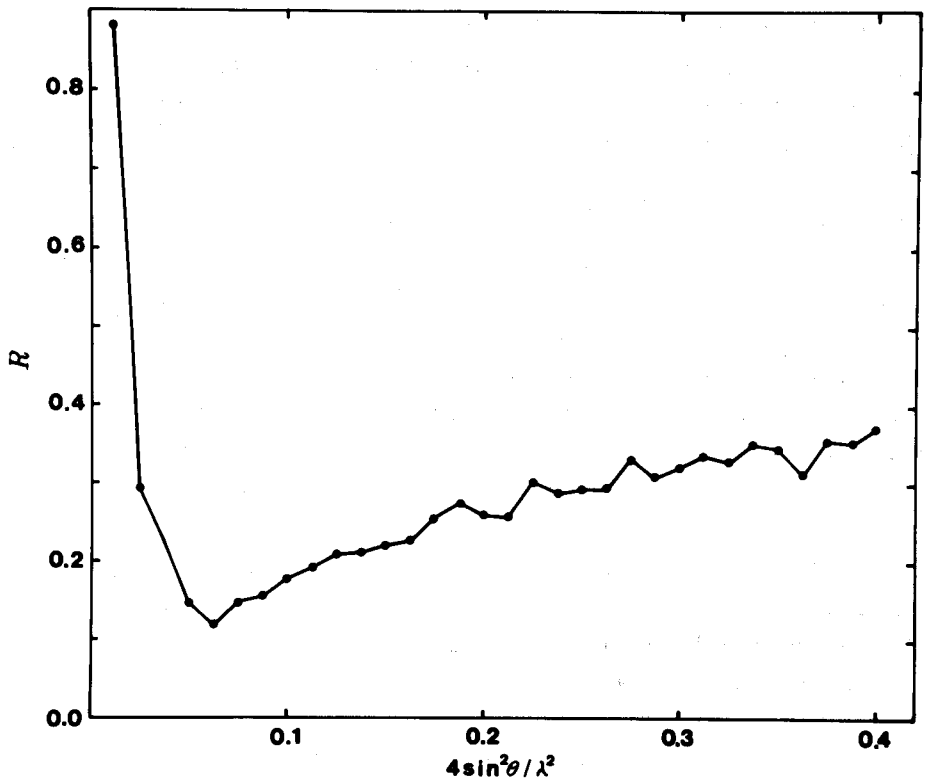

Figure 4-1

The final R factor *versus* $4(\sin\theta/\lambda)^2$

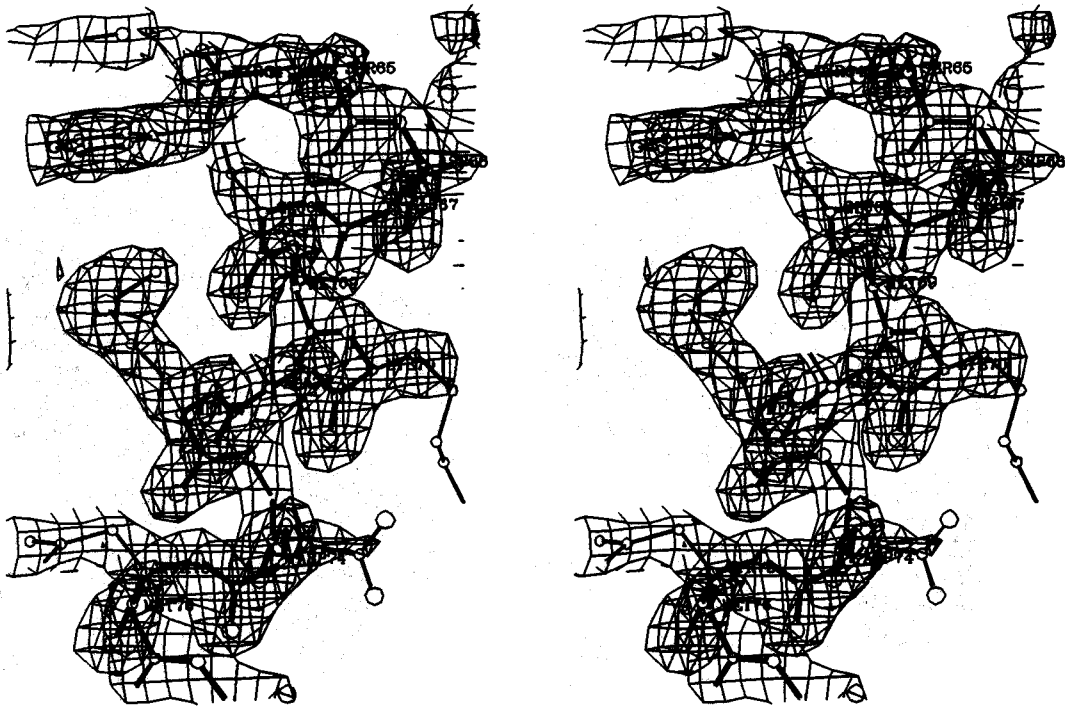

Figure 4-2

$2F_o-F_c$ map at the final stage
using 1.6 Å resolution data

(a) Electron density map around C-terminal helix

The map was obtained from calculated phase information (R=0.226) with coefficient of $2F_o-F_c$. Contouring level is arbitrary, and interval of contouring mesh is about 0.65 Å. (see, Fig(3-14(b)))

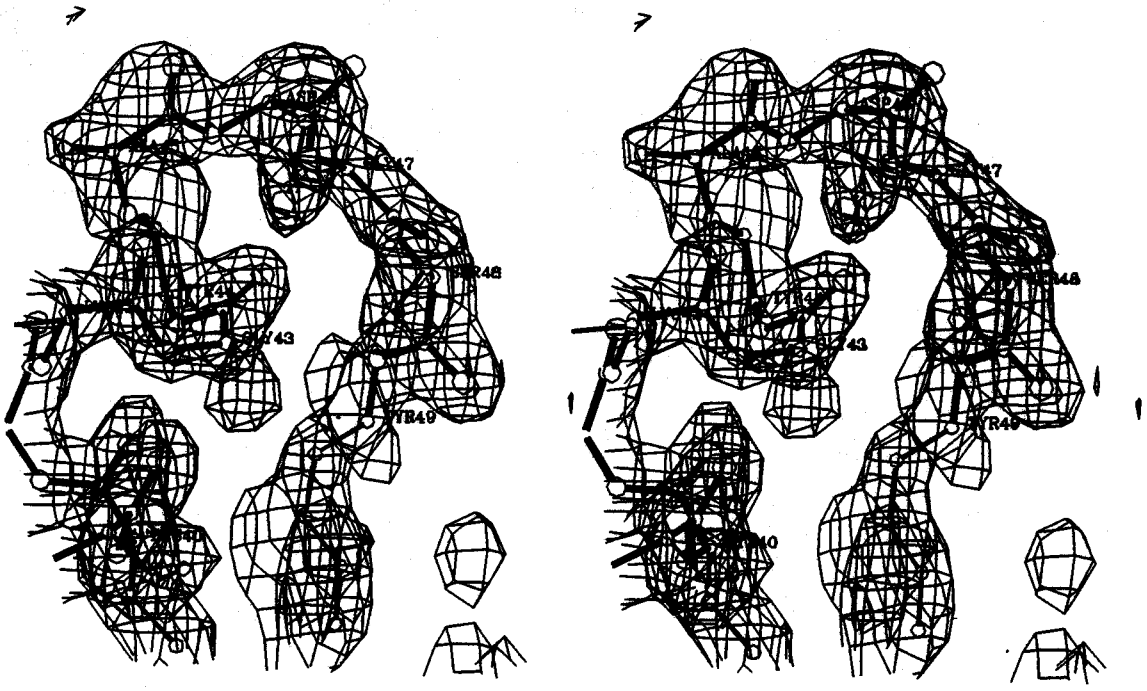

Figure 4-2
(*continued*)

(b) Electron density map shows the short loop which is in the bottom of the molecule

The map was obtained from calculated phase information (R=0.226) with coefficient of $2F_o-F_c$. Contouring level is arbitrary, and interval of contouring mesh is about 0.65 Å. (see, Fig(3-14(c)))

5. RESULT AND DISCUSSION

5-1. Refined structure

5-1-1. Molecular Packing

Packing of molecules contacted to a molecule (MOL1) are shown in Figure (5-1). There are one molecule in an asymmetric unit, and it was supported by the calculated V_M value (see Chapter 2-1-2). The MOL1 is contacted to the other symmetry-related molecules by hydrogen bonds. Intermolecular contacts are listed in Table (5-1).

The closest intermolecular iron-iron distance is 18.9 Å (MOL1 to MOL3) and other intermolecular iron-iron distances which are shorter than 30.0 Å are 23.9 Å (MOL1 to MOL4) and 29.8 Å (MOL1 to MOL2, MOL1 to MOL5). The closest intermolecular iron-iron distances in ferricytochrome *c* and ferrocytochrome *c* from albacore, ferrocytochrome *c* from bonito and cytochrome c_5 from *Azotobacter vinelandii* are 24.2, 21.7, 22.2 and 16.4 Å, respectively (Higuchi *et al.*, 1984, Carter *et al.*, 1985). The closest iron-iron interaction of cytochrome c_5 is corresponding to dimer interaction of these molecules (Carter *et al.*, 1985). A cytochrome c_{553} molecule, therefore, has relatively close heme-heme interactions within neighboring molecules.

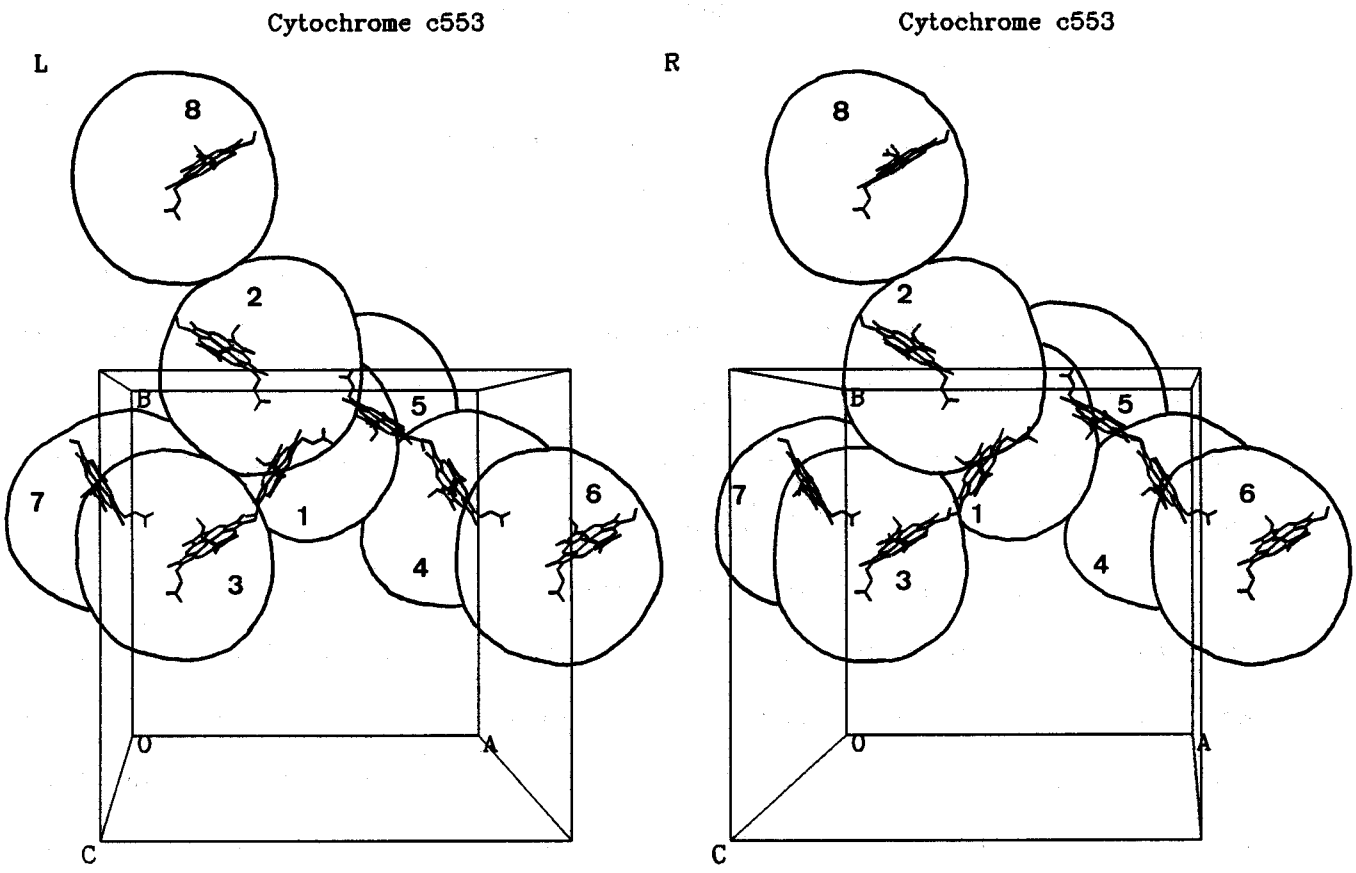

Figure 5-1

A schematic drawing of the crystal structure of cytochrome c_{553}

The envelopes show boundaries of molecules

Source atoms			symmetry operation	target atoms			distance (Å)
Asp	2	Oδ1	SYM2	Lys	40	Nζ	2.72
Lys	8	O	SYM3	Wat	99	O	2.80
Ser	9	O	SYM3	Ser	9	O	3.10
Ser	9	O	SYM3	Wat	108	O	2.52
Gln	21	Nε2	SYM4	Lys	62	Nζ	2.84
Gln	21	Oε1	SYM4	Wat	87	O	3.07
Gly	24	O	SYM4	Lys	62	Nζ	2.72
Gly	26	O	SYM4	Asn	59	Nδ2	2.83
Gly	26	N	SYM5	Wat	105	O	3.07
His	27	Nε2	SYM5	Wat	83	O	3.02
Lys	30	Nζ	SYM6	Glu	67	Oε2	2.50
Lys	40	Nζ	SYM5	Asp	2	Oδ1	2.72
Gly	50	N	SYM5	Wat	96	O	2.94
Gly	51	O	SYM7	Wat	90	O	2.77
Asn	59	Nδ2	SYM7	Gly	26	O	2.83
Asn	59	Nδ2	SYM3	Wat	83	O	3.02
Asn	59	Oδ1	SYM3	Wat	124	O	2.59
Leu	60	Cδ2	SYM3	Wat	124	O	2.95
Lys	62	Nζ	SYM7	Gln	21	Nε2	2.84
Lys	62	Nζ	SYM7	Gly	24	O	2.72
Arg	63	O	SYM3	Arg	63	Nη1	3.01
Arg	63	Nη1	SYM3	Arg	63	O	3.01
Arg	63	Nη1	SYM3	Glu	68	Oε2	2.84
Arg	63	Nη2	SYM3	Glu	68	Oε1	2.67
Ser	65	Oγ	SYM2	Wat	85	O	2.84

Table 5-1

Intermolecular contacts

SYM1 x,y,z ; SYM2 1/2+y,1/2-x,1/4+z ; SYM3 -y,-x,1/2-z ;
SYM4 1/2+x,-1/2-y,1/4-z ; SYM5 1/2-y,-1/2+x,-1/4+z ;
SYM6 1-y,-x,1/2-z ; SYM7 -1/2+x,-1/2-y,1/4-z ;
SYM8 -y,1-x,1/2-z

These symmetry operations above are correspoding to Figure (5-1)

Source atoms			symmetry operation	target atoms			distance (Å)
Glu	67	$O\varepsilon_2$	SYM8	Lys	30	$N\zeta$	2.50
Glu	68	$O\varepsilon_1$	SYM3	Arg	63	$N\eta_2$	2.67
Glu	68	$O\varepsilon_2$	SYM3	Arg	63	$N\eta_1$	2.84
Hem	80	O2D	SYM5	Wat	82	O	2.89
Wat	82	O	SYM2	Hem	80	O2D	2.89
Wat	82	O	SYM2	Wat	93	O	2.91
Wat	83	O	SYM2	His	27	$N\varepsilon_2$	3.02
Wat	83	O	SYM3	Asn	59	$N\delta_2$	3.02
Wat	85	O	SYM5	Ser	65	Oc	2.84
Wat	85	O	SYM5	Wat	103	O	2.73
Wat	86	O	SYM3	Wat	104	O	3.19
Wat	87	O	SYM7	Gln	21	$O\varepsilon_1$	3.07
Wat	87	O	SYM3	Wat	105	O	3.11
Wat	89	O	SYM5	Wat	113	O	2.96
Wat	90	O	SYM4	Gly	51	O	2.77
Wat	93	O	SYM5	Wat	82	O	2.91
Wat	96	O	SYM2	Gly	50	N	2.94
Wat	98	O	SYM3	Wat	94	O	3.04
Wat	99	O	SYM3	Lys	8	O	2.80
Wat	99	O	SYM3	Wat	99	O	2.74
Wat	103	O	SYM2	Wat	85	O	2.73
Wat	104	O	SYM3	Wat	86	O	3.19
Wat	105	O	SYM2	Gly	26	N	3.07
Wat	105	O	SYM3	Wat	87	O	3.11
Wat	108	O	SYM3	Ser	9	$O\eta$	2.52
Wat	113	O	SYM2	Wat	89	O	2.96
Wat	113	O	SYM2	Wat	141	O	3.09
Wat	115	O	SYM3	Wat	115	O	2.54
Wat	118	O	SYM2	Wat	123	O	2.99
Wat	123	O	SYM5	Wat	118	O	2.99
Wat	124	O	SYM3	Asn	59	$O\delta_1$	2.59
Wat	124	O	SYM3	Leu	60	$C\delta_2$	2.95
Wat	124	O	SYM3	Wat	94	O	3.02
Wat	132	O	SYM3	Wat	92	O	3.08
Wat	141	O	SYM5	Wat	113	O	3.09

Table 5-1
(*continued*)

5-1-2. Secondary structure, Main chain folding and Heme packing

Figure (5-2(a)) shows main chain atoms(C,N,O,Cα,OXT), heme group atoms and side chain atoms bonded to heme group (Cys10, Cys13, His14, Met57) viewed along z-axis of crystallographic unit cell. N-terminus is located at the top of the molecule, and heme group is nearly perpendicular to the paper.

Figure (5-2(b)) shows same atoms as Figure (5-2(a)), but the view point is different from that in Figure (5-2(a)). This direction of view is always used to show a molecular structure of cytochromes *c*. The heme group is located perpendicular to the paper. N-terminus is located at the top of the molecule on this drawing and N-terminal six residues keep α-helical conformations. C-terminal region is located behind the molecule. C-terminal thirteen residues also have α-helical conformations, and C-terminus terminates at the right-side of the molecule in this figure.

Figure (5-3) shows all atoms except for solvent molecules from the same view point of Figure (5-2(b)). All side chain atoms are colored according to the kind of residues. Magenta shows acidic and hydrophilic residues,*eg.* aspartic acid and glutamic acid. Cyan shows basic and hydrophilic residues, *eg.* histidine, lysine and arginine. Red shows aromatic and hydrophobic residues, *eg.* phenylalanine and tyrosine. And red also shows heme group. Yellow shows aliphatic and hydrophobic residues, *eg.* leucine, methionine and valine. Green shows neutral residues, *eg.* asparagine, glutamine, cystein, threonine, serine, alanine and glycine.

As shown in Figure (5-4), this cytochrome c_{553} has many residues those conformations are α-helix type.

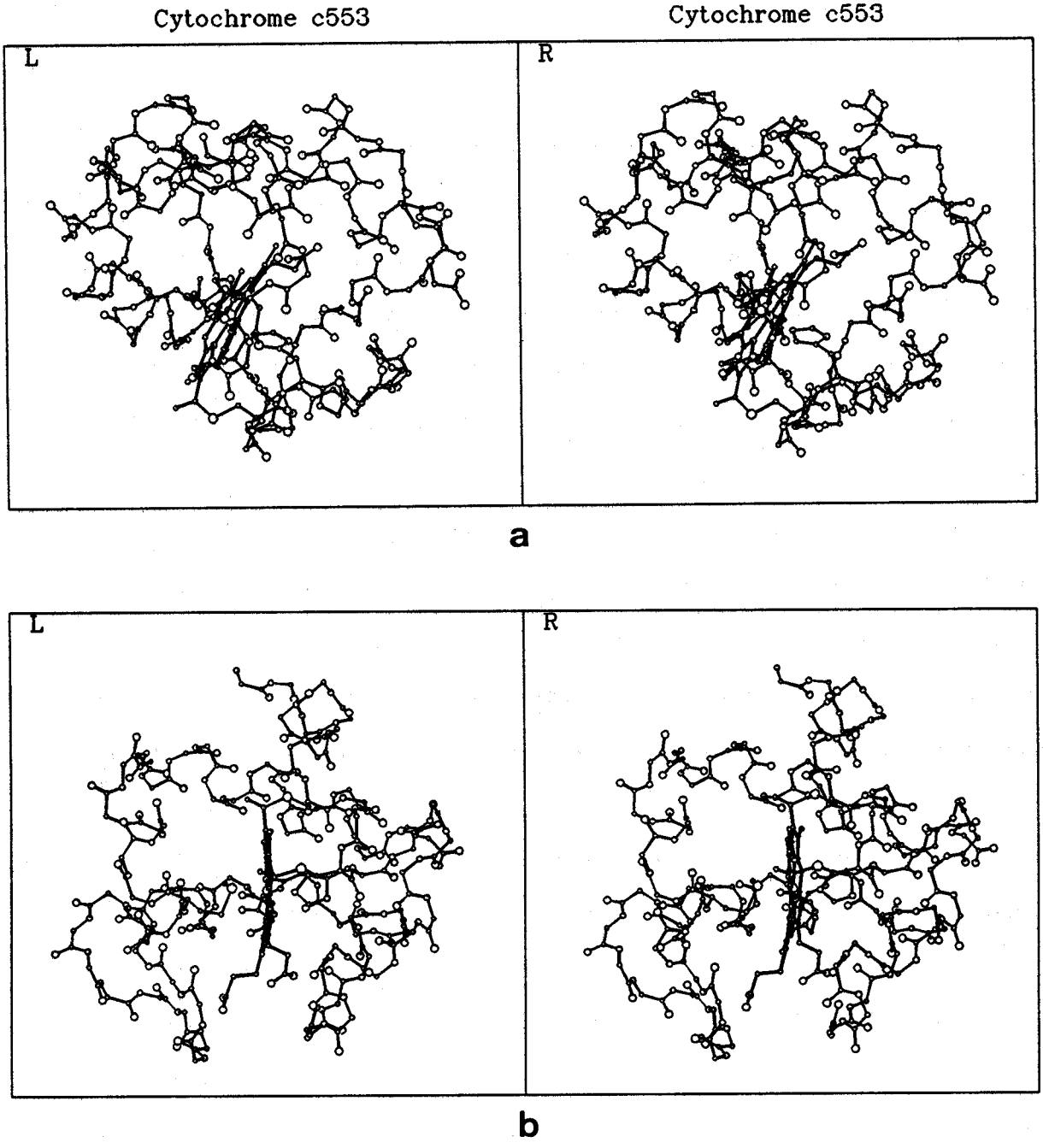

Figure 5-2

Folding pattern of cytochrome c_{553}

Showing main chain, heme group and side chain atoms which bond to heme group (Cys10, Cys13, His14, Met57)

(a) Viewing along crystallographic z-axis
(b) Viewing from the heme cleavage

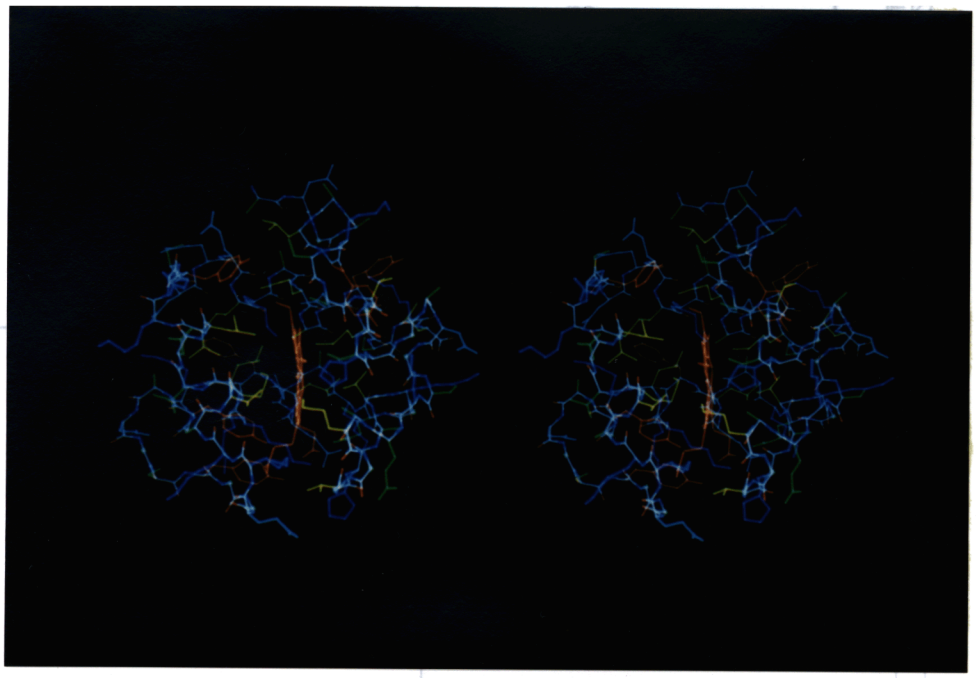

Figure 5-3

Wire-model of cytochrome c_{553} showing all atoms except for water molecules

Blue : Lys, Arg, His ; Cyan : Asp, Glu
Red : Phe, Tyr, Hem ; Yellow : Leu, Met, Val
Green : Asn, Gln, Cys, Thr, Ser, Ala, Gly

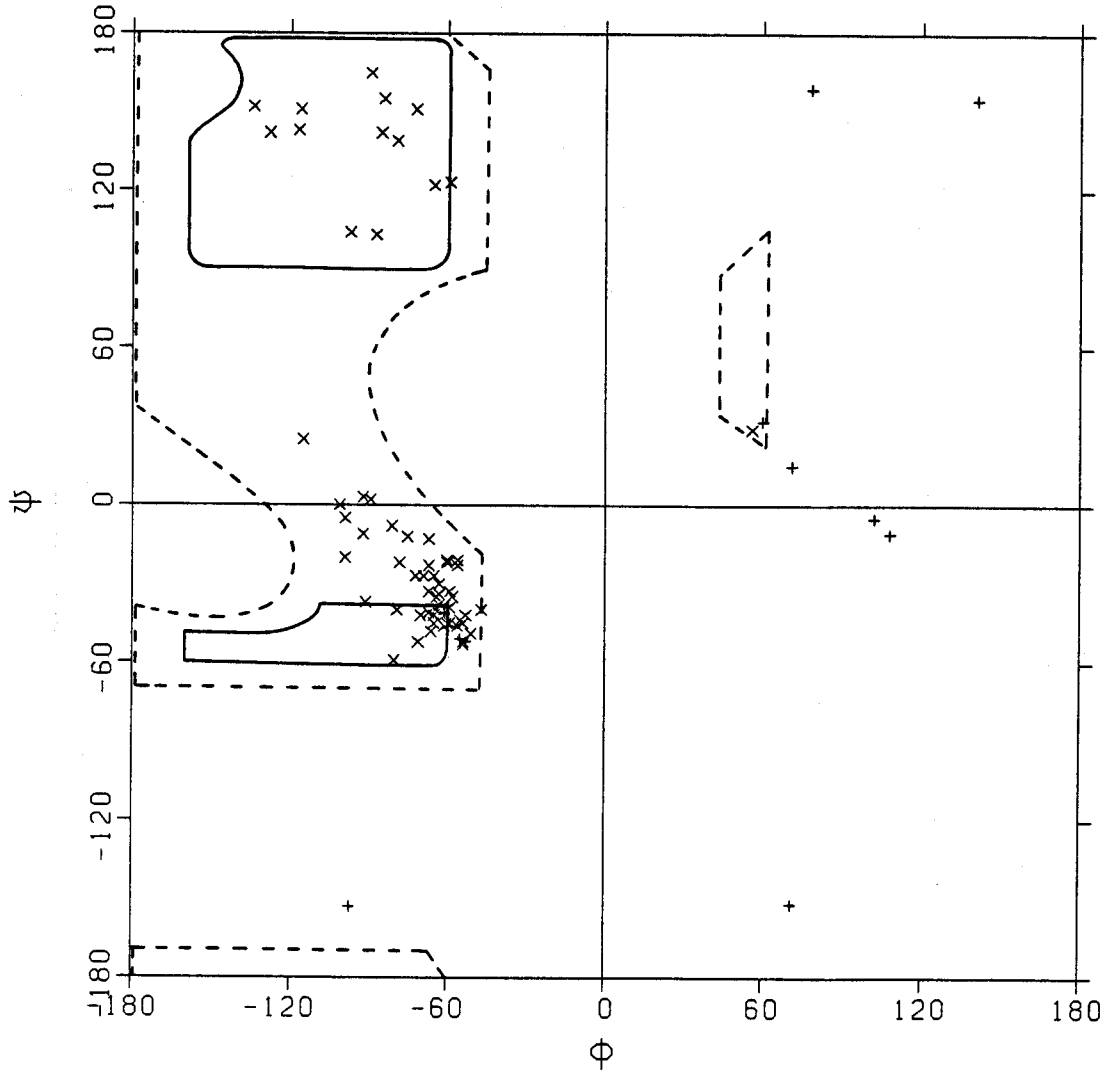

Figure 5-4

Ramachandran's plot of cytochrome c_{553}
(Ramakrishnan and Ramachandran, 1965)

+ Glysine residue
X Other residue

Considering hydrogen bonds and conformational torsion angles of main chain atoms, following nine secondary structures were identified.

·Asp2 - Tyr7	α-helix
·Ala5 - Cys10	3.10-helix
·Val11 - His14	α-helix
·Gly15 - Gly18	β-turn(type I)
·Gln21 - Val25	left-handed 3.10-helix (β-turn(type III))
·Lys33 - Gly47	α-helix
·Lys54 - Asn59	α-helix
·Ser65 - Ser77	α-helix
·Met76 - Leu79	β-turn(type I)

Above secondary structures with showing hydrogen bonds are shown in Figure (5-5(a)) to Figure (5-5(g)).

The classification of β-turns above is according to the classification proposed by Chou and Fasmann (Chou and Fasmann, 1977). Two β-turns are identified in cytochrome c_{553} molecule, and they keep type I conformation.

There are five α-helices and two 3.10-helices, one is right-handed and the other is left-handed, in cytochrome c_{553} molecule as shown above. Forty five of seventy nine residues have at least one hydrogen bond of a carbonyl or amido group in an α-helix conformation. There are no β-sheet conformation in this molecule.

Two α-helices of N- and C-terminal residues, large cleavage at the center of the molecule where heme group is located and overall main chain folding pattern shows "cytochrome c folding".

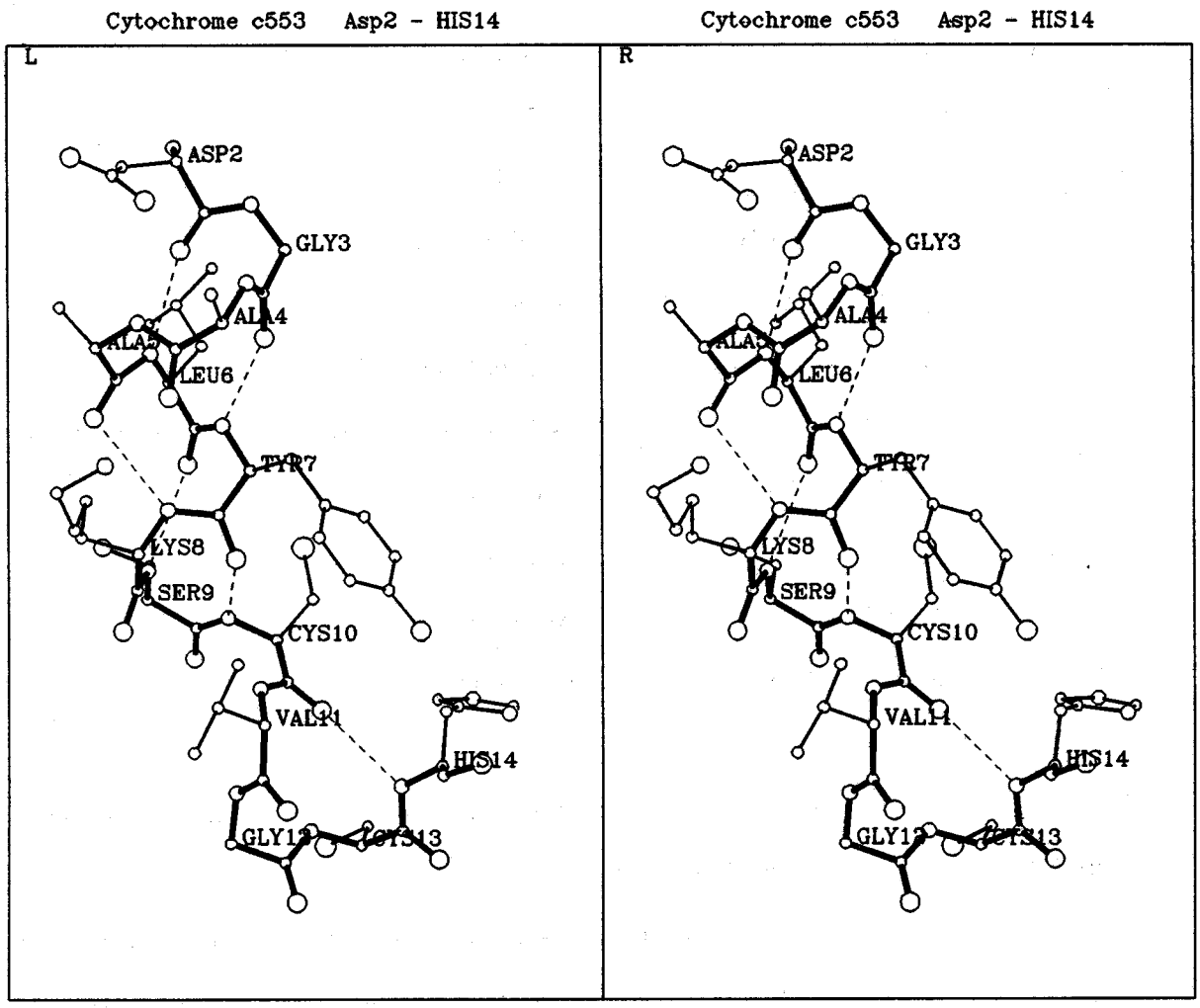

(a) Asp2 - His14

Figure 5-5

Identified secondary structures of cytochrome c_{553}

Dashed lines show hydrogen bonds

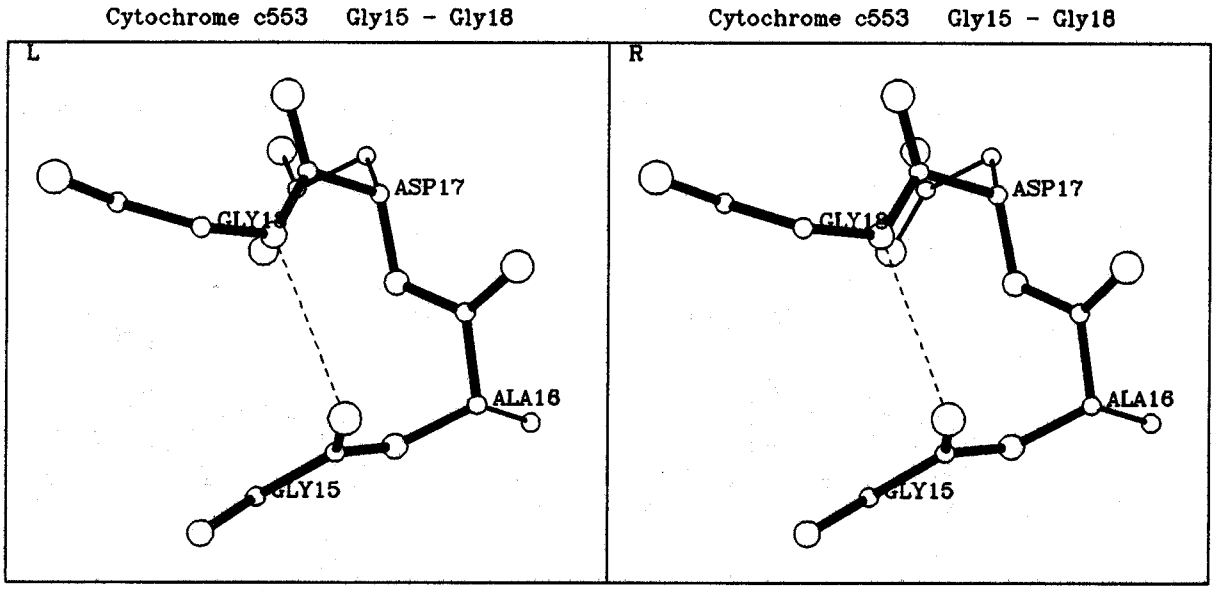

(b) Gly15 - Gly18

Figure 5-5
(*continued*)

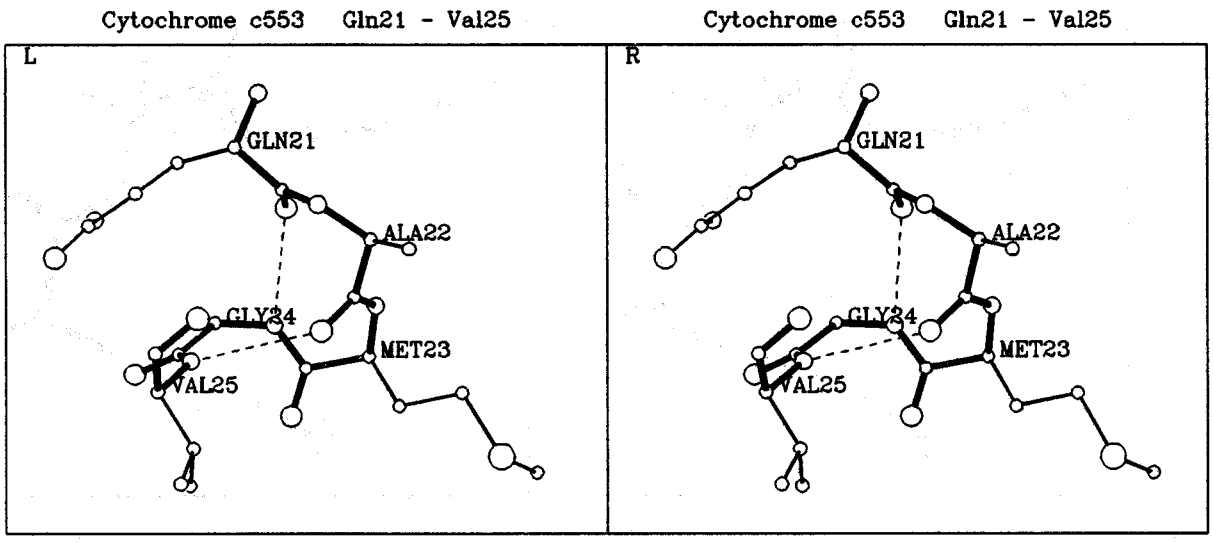

(c) Gln21 - Val25

Figure 5-5
(*continue*)

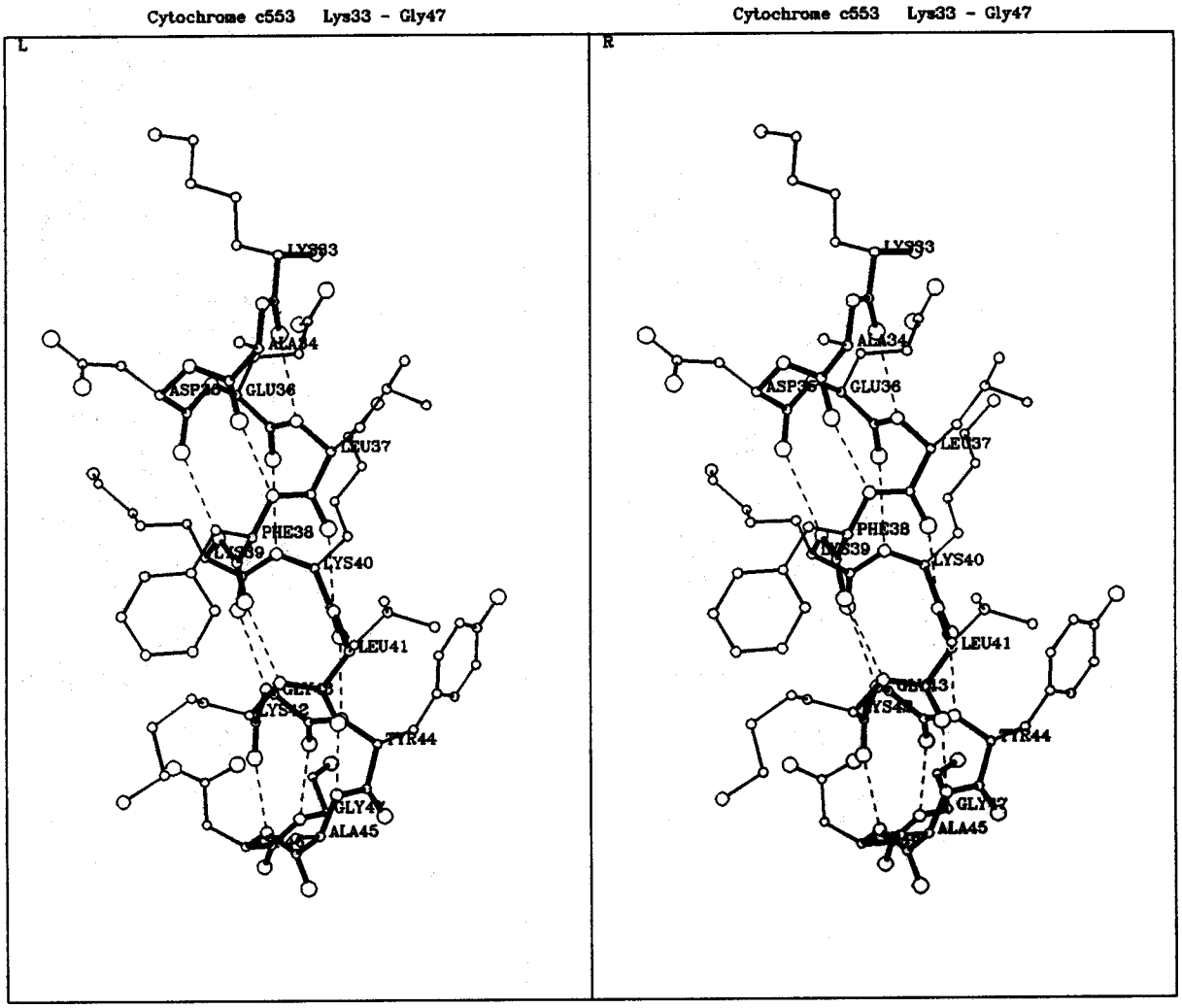

(d) Lys33 - Gly47

Figure 5-5
(*continued*)

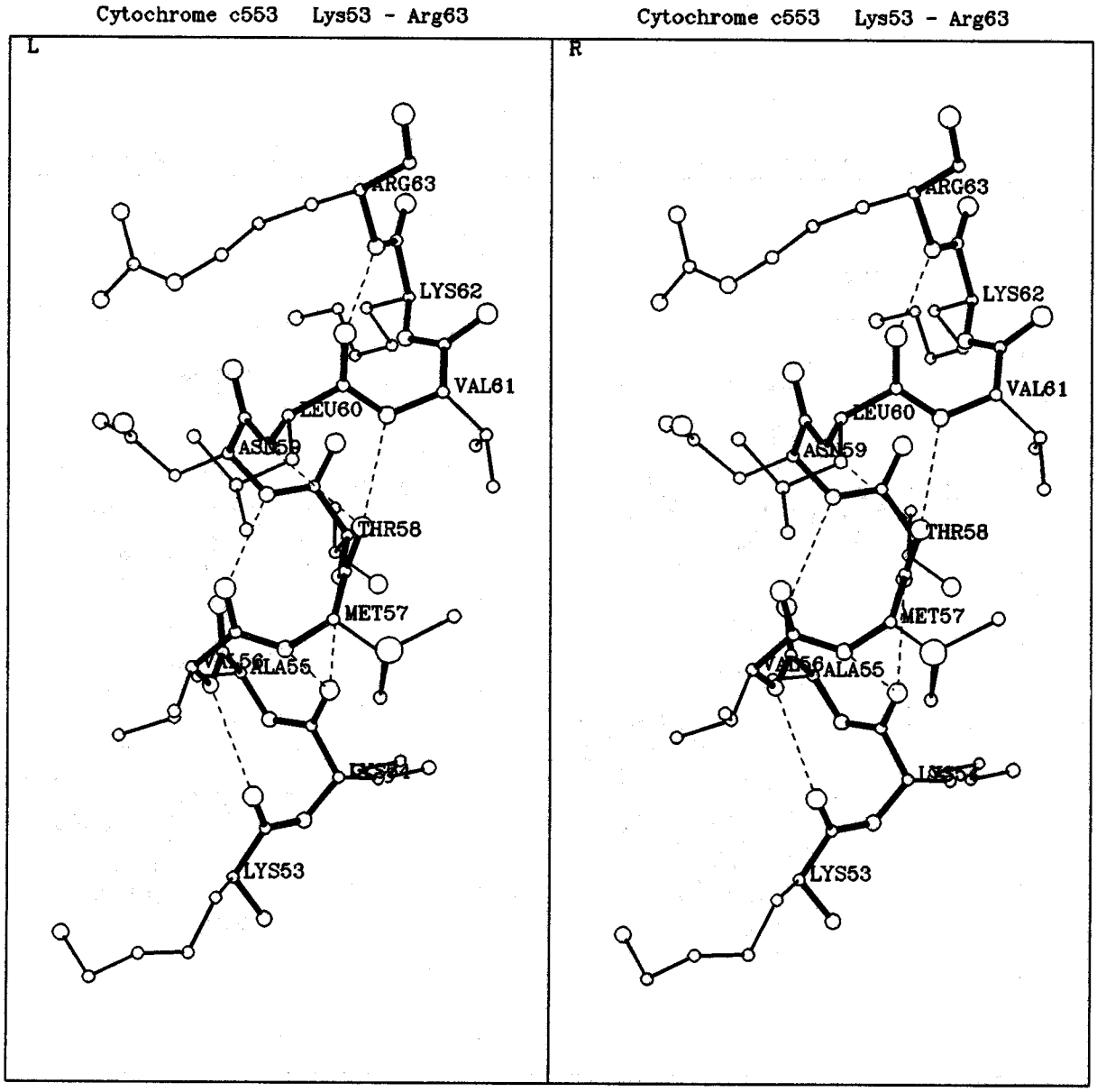

(e) Lys53 - Arg63

Figure 5-5
(*continued*)

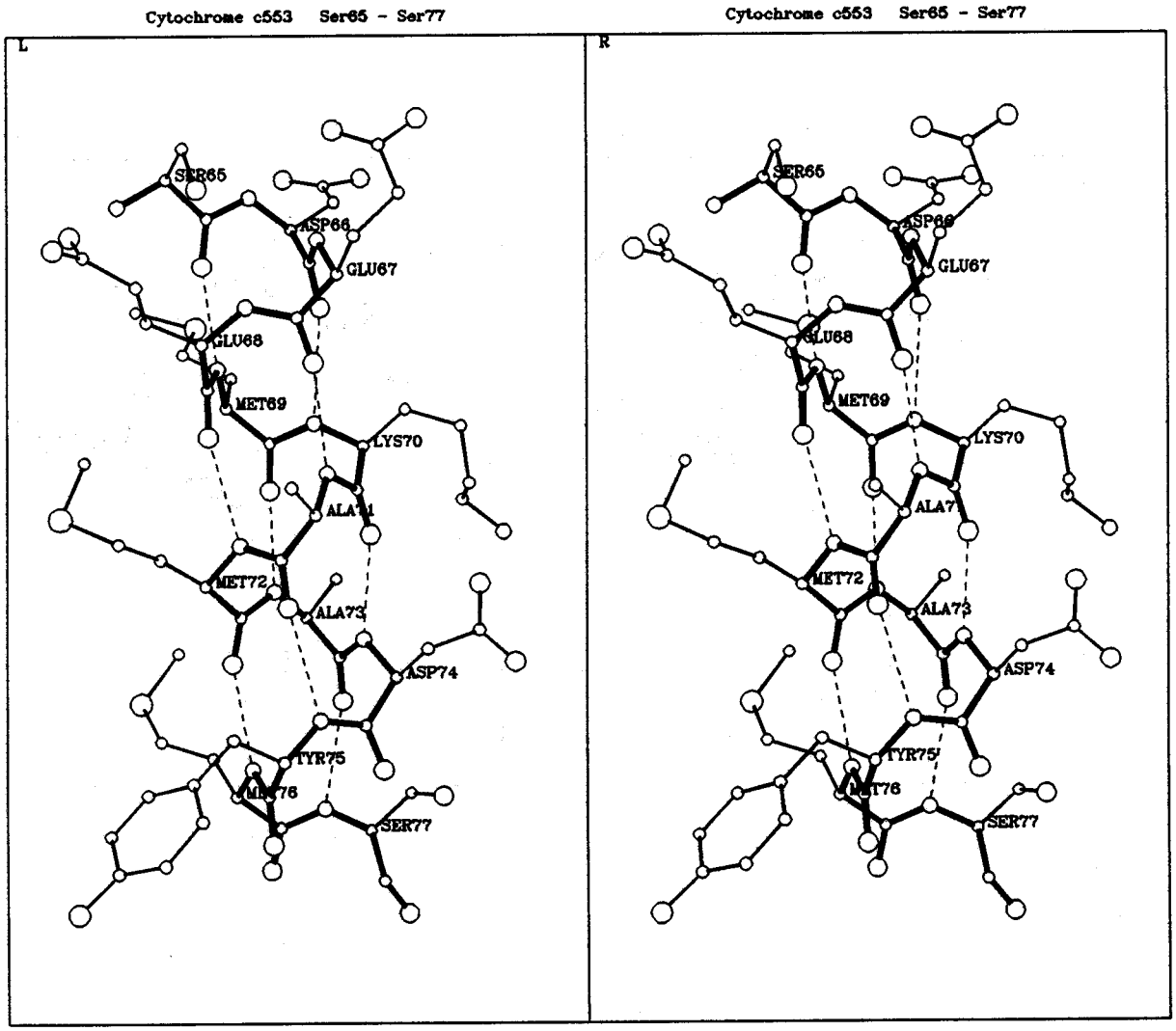

(f) Ser65 - Ser77

Figure 5-5
(*continued*)

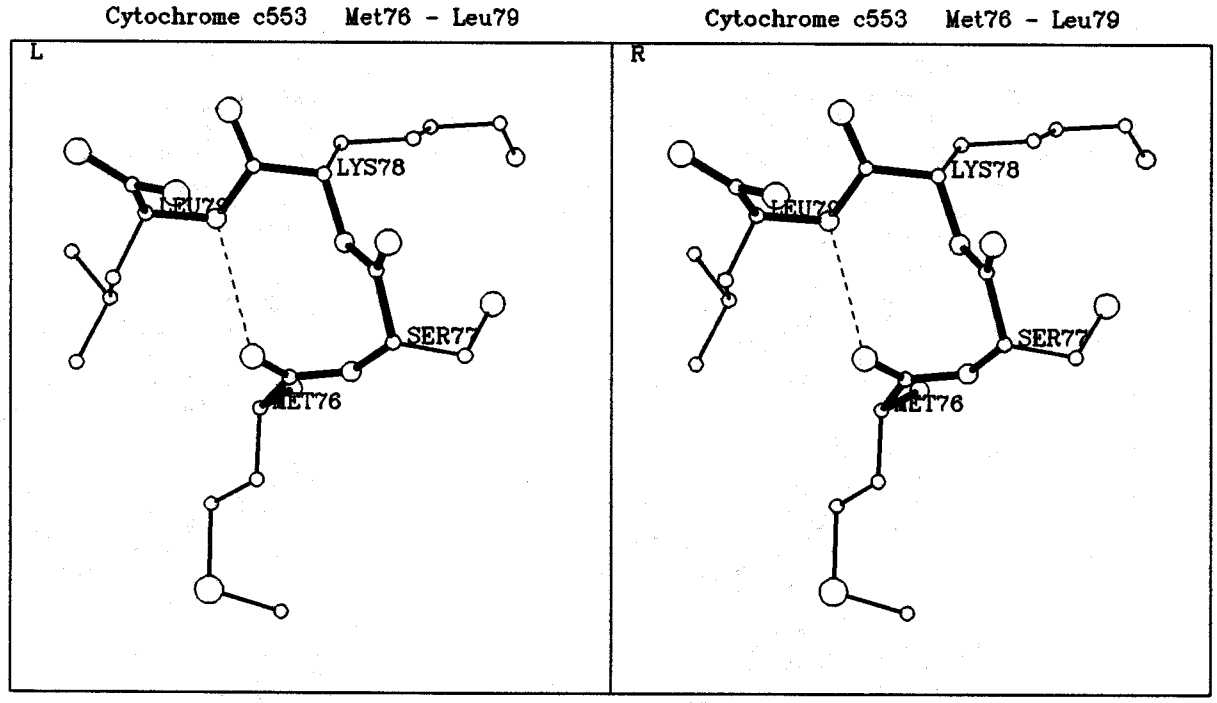

(g) Met76 - Leu79

Figure 5-5
(*continued*)

The heme group is covalently bonded to amino acid chain with two residues and coordinated with two residues, just same as other cytochromes *c*. Two reduced vinyl groups of the heme group are bonded to Cys10(Sγ to CAB) and Cys13(Sγ to CAC). The fifth coordinate of iron of heme is His14(Nε_2) and the sixth coordinate is Met57(Sδ). The propionate side-chains of the heme group make hydrogen bond to polypeptide chain and are fixed.

Main chain folding pattern was summarized as follows,

1. N-terminal α-helix which goes down from the top of the molecule
   (Ala1 to Tyr7)
2. Covalently bonds to reduced vinyl groups of the heme group by Sγ atoms of cysteins
   (Cys10 and Cys13)
3. Coordinates to heme iron by Nζ atom of histidine as the fifth coordinate
   (His14)
4. Small loop at the right side of the molecule
   (Gly15 to Gly18)
5. Goes down to the right bottom, and makes loop, covering right bottom of the molecule
   (Lys20 to Val29)
6. Goes across the behind of the molecule
   (Lys30 to Gln32)
7. α-helix at the left-back side of the molecule, covering the back of the molecule

(Lys33 to Gly47)

8. The loop covering left-bottom side of the molecule

(Ser48 to Lys53)

9. Short distorted α-helix covering left side of the molecule, and coordinates to heme iron by Sδ of methionine 57

(Cys54 to Asn59)

10. Short extended conformation

(Val61 to Tyr64)

11. C-terminal α-helix from left side to right side of the behind of the molecule

(Ser65 to Leu79)

5-1-3. Heme Environment

The heme group is covalently bonded to the polypeptide chain with four residues same as other cytochromes *c*. The heme group is displaces at the center of the molecule and some part of the heme group is expressed to the molecular surface. Figure (5-6) showed contact and re-entrant surface area of heme group (Conolly, 1983). There are three regions of heme group those are exposed to molecular surface. Two propionates are both exposed, the side chain of pyrrole D is more exposed than that of pyrrole A. Both propionates are fixed by hydrogen bonds. These hydrogen bonds are summarized in Table (5-2).

Senn *et al.* suggested the conformation of the side chain of Met57 of reduced form of cytochrome c_{553} from *Desulfovibrio vulgaris* using NMR tech-

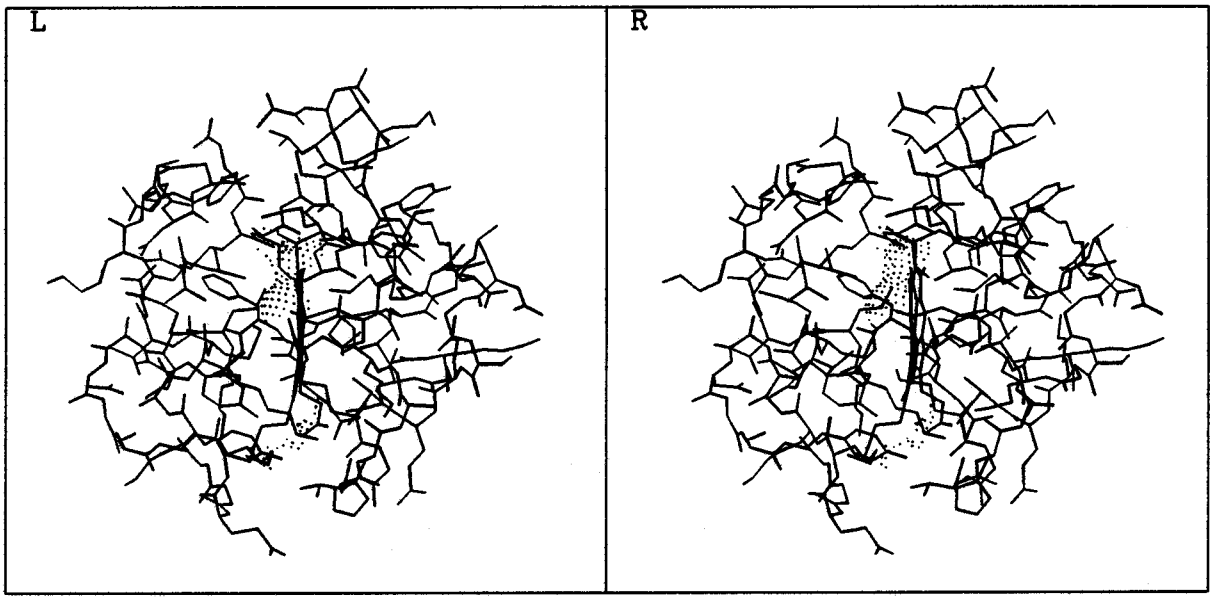

a

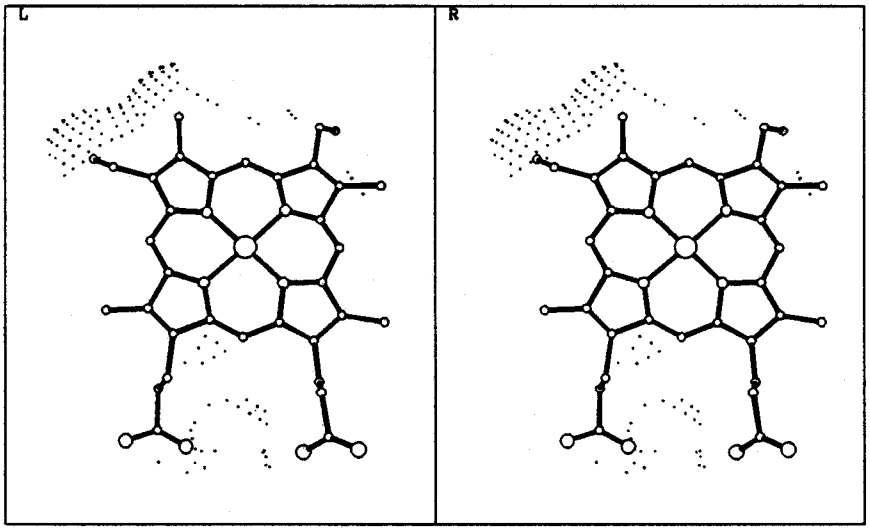

b

Figure 5-6

Contact and reentrant surface area
of heme group

Propionate A			
	O1A	Gln32 $N\varepsilon_2$	2.72 Å
		Lys40 $N\zeta$	2.66
	O2A	Tyr49 $O\eta$	2.69
		Wat93 O	2.65
Propionate D			
	O1D	Lys53 N	2.86
		Lys54 N	3.08
	O2D	Tyr49 $O\eta$	2.69
		Gly51 N	2.75

Table 5-2

Possible hydrogen bonds to heme propionates

nique (Senn *et al.*, 1983). Figure (5-7(a)) and (5-7(b)) showed predicted and determined conformations of the side chain atoms of Met57. Althogh over all conformations of both model are similar to each other, positions of $C\beta$ and $C\gamma$ of Met57 are relatively different.

5-1-4. Hydrogen Bonds

Intramolecular hydrogen bonds, excluding water molecules, are listed in Table (5-3). There are ninety five hydrogen bonds within the range from 2.3 Å to 3.2 Å. The bonds are categorized into four groups : main chain - main chain, main cain - side chain, side chain - side chain, heme - other residue.

In Table (5-3(a)), hydrogen bonds in α-helices and β-turns are marked by (α), (T), respectively. There are threesalt-bridges, marked by (S) in Table (5-3(c)) between the lysine Nζ moiety and the carboxyl groups of aspartic or glutamic acids on the molecular surface.

5-1-5. Water Molecules

Sixty three peaks showed on both MAD-map and D-Fourier map were assigned to water molecules. These waters are incorporated in the refinement procedure. The temperature factors of water molecules are in the range from 19.2 to 77.2 Å^2. Twelve water molecules have temperature factors greater than 50 Å^2. All of these water molecules are assumed as fully occupied sol-

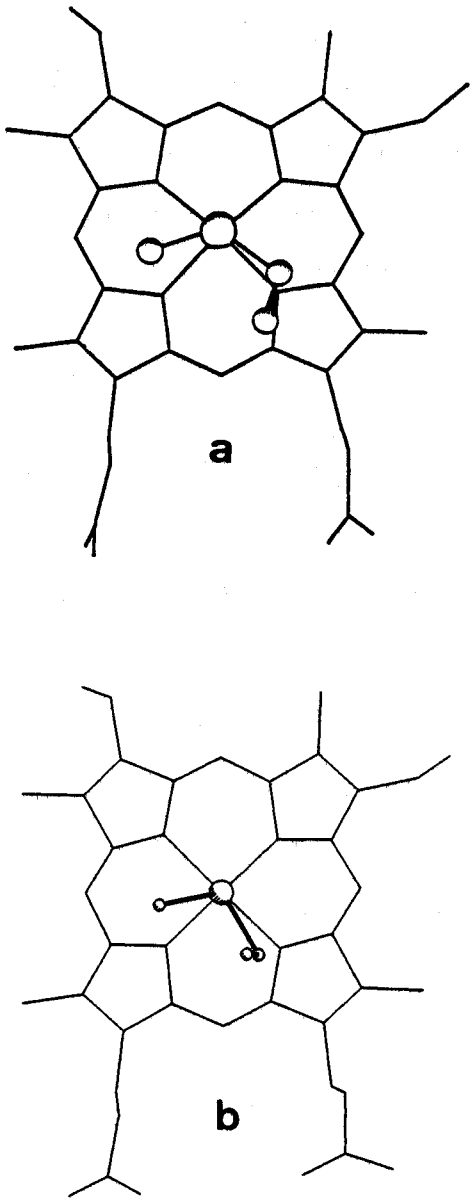

Figure 5-7

Heme group and axial methionine of cytochrome c_{553}

(a) predicted conformations
(Senn *et al.*, 1983)

(b) determined conformations

(a) Main chain - main chain interactions

D 2 O	A 5 N	3.15		D 2 O	L 6 N	2.95	(α)
G 3 O	Y 7 N	2.89	(α)	L 6 O	K 8 N	3.08	
L 6 O	S 9 N	3.22	(α)	Y 7 O	S 9 N	3.05	
Y 7 O	C 10 N	2.85	(α)	C 10 O	H 14 N	3.06	
V 11 O	G 15 N	3.02		G 15 O	G 18 N	3.10	
G 18 O	V 29 N	3.18		G 18 O	K 30 N	3.12	
K 20 O	A 22 N	3.20		Q 21 O	M 23 N	3.17	
Q 21 O	G 24 N	3.03		A 22 O	G 24 N	3.01	
A 22 O	V 25 N	3.20		K 33 O	D 35 N	3.18	
K 33 O	E 36 N	2.84		K 33 O	L 37 N	2.93	(α)
A 34 O	E 36 N	3.24		A 34 O	F 38 N	2.83	(α)
D 35 O	K 39 N	2.99	(α)	E 36 O	K 40 N	3.12	(α)
L 37 O	L 41 N	3.02	(α)	F 38 O	L 41 N	3.19	
F 38 O	K 42 N	3.04	(α)	K 39 O	G 43 N	2.79	(α)
K 40 O	G 43 N	2.96		K 40 O	Y 44 N	2.97	(α)
L 41 O	Y 44 N	3.19		K 42 O	A 45 N	2.94	
K 42 O	D 46 N	3.11	(α)	G 43 O	G 47 N	2.85	(α)
G 43 O	S 48 N	3.00		G 43 O	Y 49 N	3.14	
K 53 O	A 55 N	3.10		K 53 O	V 56 N	3.03	
K 54 O	V 56 N	3.18		K 54 O	M 57 N	2.99	
K 54 O	T 58 N	3.06	(α)	A 55 O	N 59 N	3.18	(α)
M 57 O	L 60 N	3.08		M 57 O	V 61 N	2.94	(α)
L 60 O	K 62 N	3.08		L 60 O	R 63 N	2.87	
V 61 O	R 63 N	3.14		S 65 O	E 68 N	3.09	
S 65 O	M 69 N	2.76	(α)	D 66 O	M 69 N	3.19	
D 66 O	K 70 N	3.05	(α)	E 67 O	A 71 N	2.88	(α)
E 68 O	M 71 N	3.17		E 68 O	M 72 N	2.89	(α)
M 69 O	M 72 N	3.08		M 69 O	A 73 N	2.72	(α)
K 70 O	A 73 N	3.24		K 70 O	D 74 N	2.80	(α)
A 71 O	Y 75 N	3.11	(α)	M 72 O	M 76 N	2.79	(α)
A 73 O	S 77 N	2.95	(α)	Y 75 O	S 77 N	3.22	
Y 75 O	K 78 N	2.95		M 76 O	K 78 N	3.10	
M 76 O	L 79 N	2.93					

Table 5-3

Intramolecular hydrogen bonds

(b) Main chain - side chain interaction

G 12 O	K 20 Nζ	3.01	A 5 N	D 2 Oγ2	3.17
G 15 O	Y 7 Oζ	2.60	G 26 O	Q 21 Oε1	2.84
A 28 O	Q 32 Nε2	3.06	K 42 O	D 46 Oδ2	3.05
G 43 O	D 46 Oδ2	2.53	Y 44 O	T 58 Oγ1	2.52
G 47 N	D 46 Oδ2	3.14	G 47 O	K 54 Nζ	3.23
S 48 N	D 46 Oδ2	3.23	N 59 O	R 63 Nε	3.02
E 68 N	S 65 Oγ	3.18	S 65 N	E 68 Oε2	2.95
K 70 O	D 74 Oδ2	3.06	D 74 O	S 77 Oγ	2.69

(c) Side chain - side chain interaction

D 17 Oδ1	S 19 Oγ	2.90		Q 32 Oε1	E 36 Oε2	3.06	
Q 32 Oε1	K 40 Nζ	2.74	(S)	K 42 Nη	D 66 Oδ1	3.23	(S)
K 42 Nη	D 66 Oδ2	3.02	(S)	D 46 Oδ2	S 48 Oγ	3.10	
N 59 Oδ1	R 63 Nζ2	3.12					

(d) heme - other residue interaction

X 80 O1A	Q 32 Nε2	2.72	X 80 O1A	K 40 Nζ	2.66
X 80 O2D	Y 44 Oη	2.51	X 80 O2A	Y 49 Oη	2.69
X 80 O2D	G 51 N	2.75	X 80 O1D	G 53 N	2.86
X 80 O1D	K 54 N	3.08			

Table 5-3
(continued)

vent molecules, and disordered water molecules are not included in this model. Table (5-4) shows hydrogen bonds which are bonded to water molecules. Sixty four hydrogen bonds between water molecule and protein molecule are identified.

5-2. Comparion of the Sturucture of Cytochrome *c* families

5-2-1. Folding Pattern and Charge Distribution

Figure (5-8(a)) to Figure (5-8(f)) show folding patterns of six different[2] cytochromes *c*. They are cytochrome c_2 (2C2C; Salemme *et al.*, 1973), as an example of L-class cytochrome *c*, cytochrome *c* from albacore (3CYT; Takano and Dickerson, 1980), as an example of M-class mitochondrial cytochrome *c*, cytochrome *c* from rice (1CCR; Ochi *et al.*, 1983), as an example of plant cytochrome *c*, cytochrome c_{551} from *Pseudomonas aeruginosa* (351C; Matsuura *et al.*, 1982), as an example of S-class cytochrome *c*, cytochrome c_5 from *Azotobacter vinelandii* (1CC5; Carter *et al.*, 1985) and cytochrome c_{553} from *Desulfovibrio vulgaris* Miyazaki.

All these cytochromes *c* have similar folding pattern called "cytochrome *c* folding". All of them have identical two α-helices at C-terminal and N-terminal and they cross right angle at the top of the

---

2. All coordinates are supplied by the Brookheaven Protein Data Bank (Bernstein *et al.*, 1977)

(a) Main chain - water molecule interactions

A 1 N	Wat 82	2.56	A 1 O	Wat 81	2.91
A 1 O	Wat 96	2.73	G 3 N	Wat 81	2.82
A 4 O	Wat 102	2.71	A 5 O	Wat 98	2.59
A 5 O	Wat 132	2.90	L 6 O	Wat 88	2.90
K 8 O	Wat 129	2.75	S 9 O	Wat 99	2.79
S 9 O	Wat 108	3.10	G 12 N	Wat 99	2.86
A 16 O	Wat 120	2.80	G 18 O	Wat 97	2.90
K 20 O	Wat 97	2.69	Q 21 N	Wat 140	3.15
A 22 N	Wat 111	3.17	M 23 N	Wat 95	2.97
V 25 O	Wat 114	2.84	H 27 N	Wat 93	3.05
H 27 O	Wat 111	2.97	A 28 O	Wat 141	2.61
V 29 N	Wat 97	3.05	G 31 N	Wat 110	2.77
A 34 N	Wat 109	3.13	D 35 N	Wat 91	3.04
K 39 O	Wat 125	2.82	G 50 O	Wat 123	2.36
E 52 N	Wat 85	3.01	A 55 N	Wat 84	2.91
V 56 O	Wat 94	2.94	N 59 O	Wat 87	2.77
K 62 O	Wat 130	2.74	R 63 o	Wat 104	2.95
Y 64 O	Wat 119	2.77	D 66 N	Wat 100	3.10
E 67 O	Wat 92	2.86	A 71 O	Wat 133	2.93
Y 75 O	Wat 122	2.94	M 76 O	Wat 110	2.70
L 79 OXT	Wat 110	2.81	L 79 OXT	Wat 127	2.66

Table 5-4

Hydrogen bonds with water molecules

(b) Side chain - water molecule interaction

D 2	$O\delta_1$	Wat 126	2.82	K 8	$N\eta$	Wat 102	2.71
S 9	$O\gamma$	Wat 88	2.83	H 14	$N\delta_1$	Wat 97	2.87
H 14	$N\delta_1$	Wat 111	3.15	D 17	$O\delta_2$	Wat 128	2.99
H 27	$N\delta_1$	Wat 89	2.31	K 30	$N\zeta$	Wat 90	2.94
K 30	$N\zeta$	Wat 128	2.57	E 52	$O\varepsilon_2$	Wat 85	2.66
K 54	$N\zeta$	Wat 123	3.04	Y 64	$O\eta$	Wat 88	2.60
Y 64	$O\eta$	Wat 115	2.79	D 66	$O\delta_1$	Wat 119	3.04
E 67	$O\varepsilon_1$	Wat 116	2.10	E 67	$O\varepsilon_2$	Wat 116	2.85
E 68	$O\varepsilon_1$	Wat 83	2.77	E 68	$O\varepsilon_1$	Wat 105	2.85
E 68	$O\varepsilon_2$	Wat 101	3.09	Y 75	$O\eta$	Wat 102	2.97
Y 75	$O\eta$	Wat 120	2.59				

(c) Heme - water molecule chain interaction

X 80	O2A	Wat 93	2.65

Table 5-4
(*continued*)

(d) Water molecule - water molecule chain interaction

Wat	81	Wat 133	2.65	Wat	82	Wat 103	2.80
Wat	86	Wat 87	3.16	Wat	88	Wat 124	2.90
Wat	90	Wat 128	2.39	Wat	92	Wat 96	2.98
Wat	92	Wat 106	2.82	Wat	98	Wat 132	2.81
Wat	98	Wat 142	3.03	Wat	100	Wat 116	3.11
Wat	102	Wat 121	2.97	Wat	101	Wat 117	2.56
Wat	101	Wat 135	2.54	Wat	105	Wat 135	2.78
Wat	105	Wat 135	2.78	Wat	108	Wat 115	2.60
Wat	111	Wat 114	2.63	Wat	113	Wat 126	3.11
Wat	120	Wat 121	2.58	Wat	124	Wat 132	2.77
Wat	130	Wat 134	2.70				

Table 5-4
(*continued*)

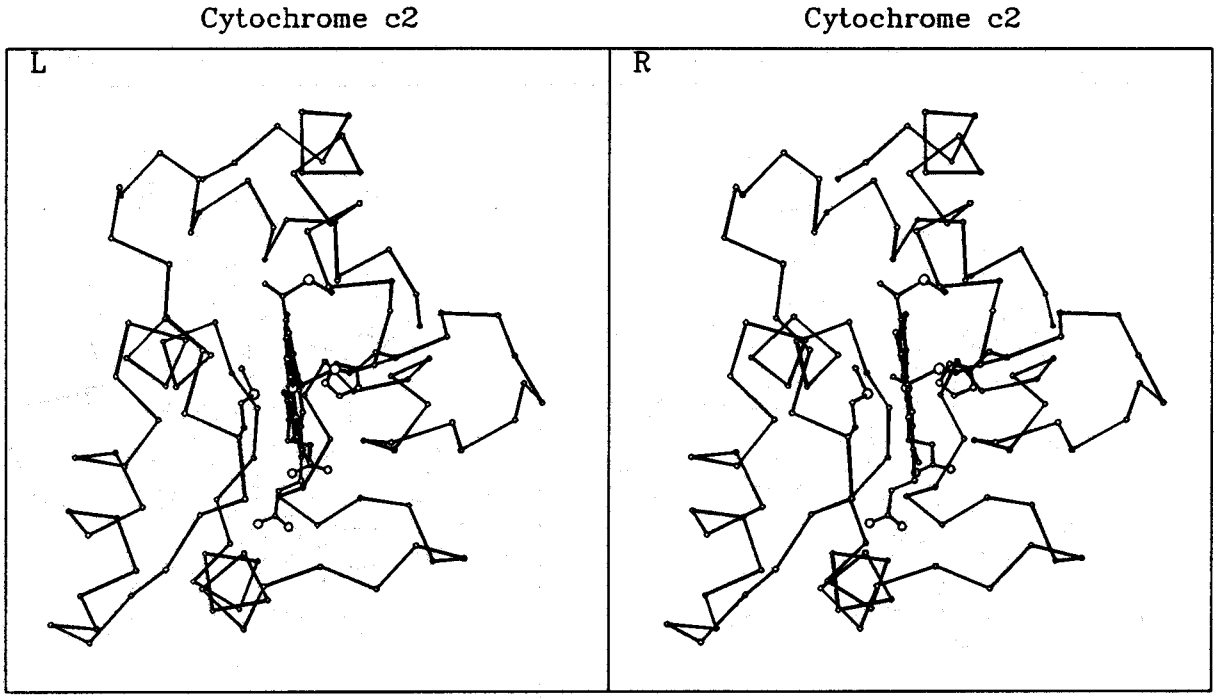

(a) cytochrome c_2

Figure 5-8

Folding patterns of different cytochromes *c*

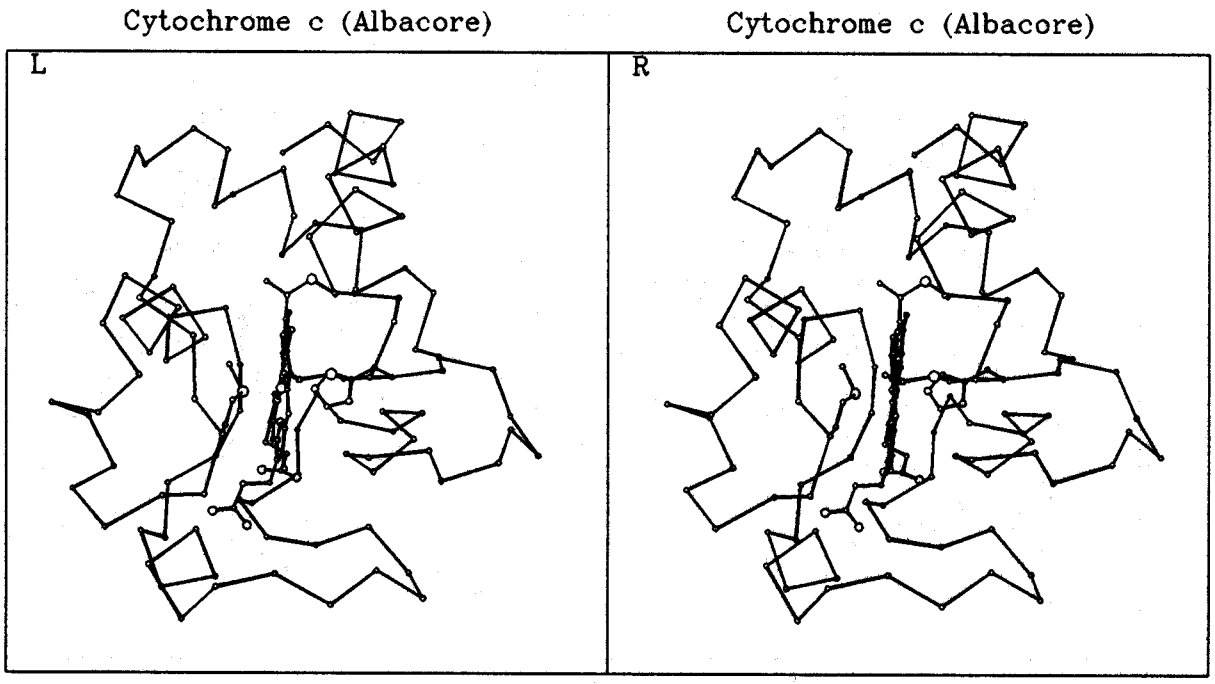

(b) cytochrome *c* from albacore

Figure 5-8
(*continued*)

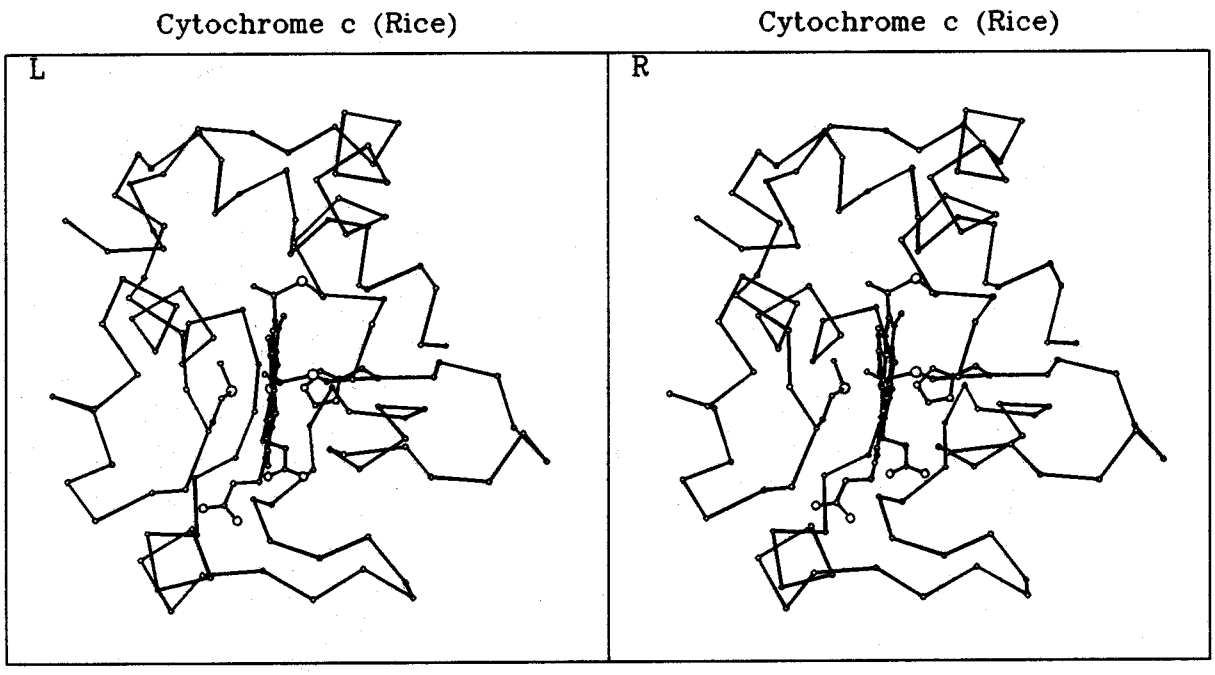

(c) cytochrome *c* from rice

Figure 5-8
(*continued*)

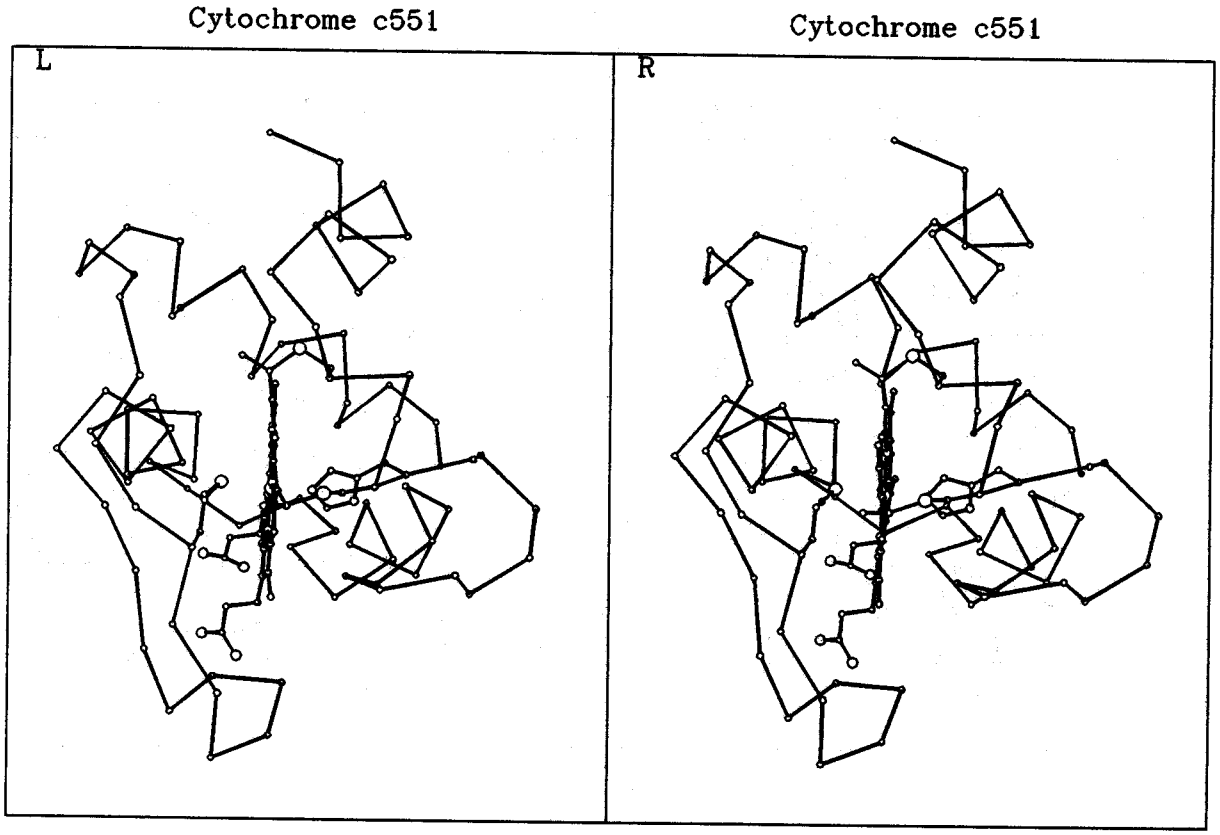

(d) cytochrome c_{551}

Figure 5-8
(*continued*)

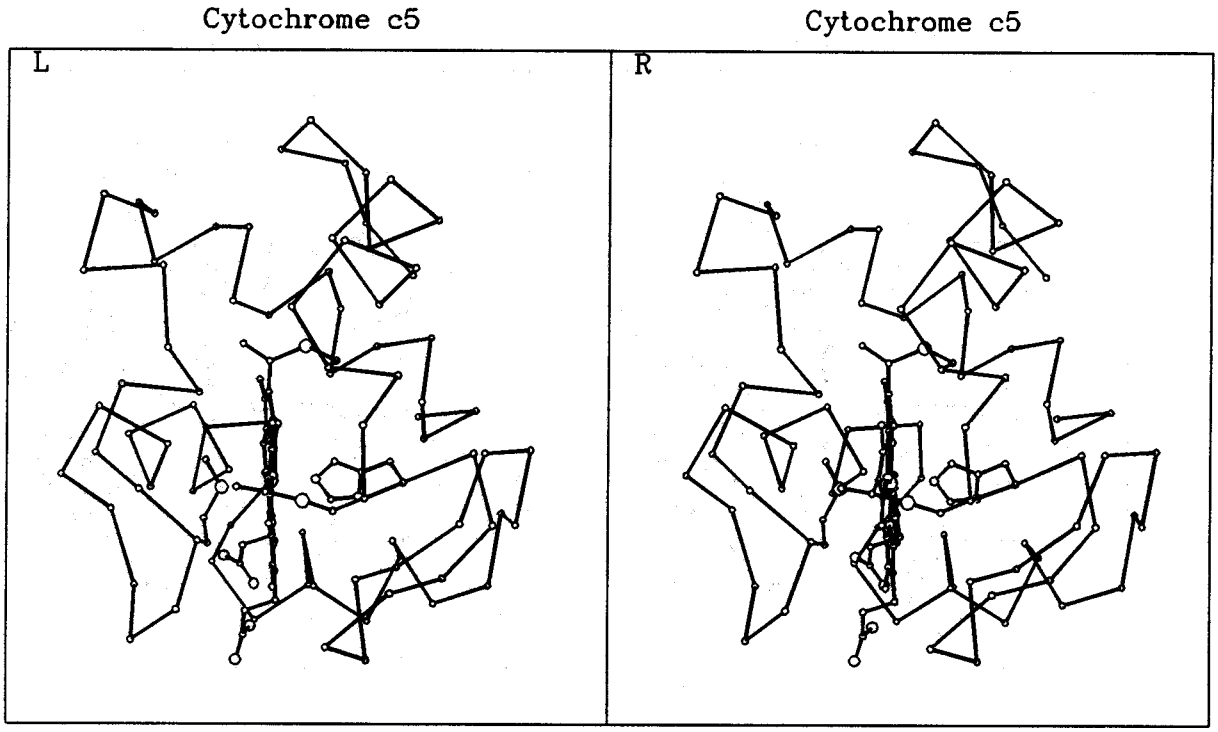

(e) cytochrome c_5

Figure 5-8
(*continued*)

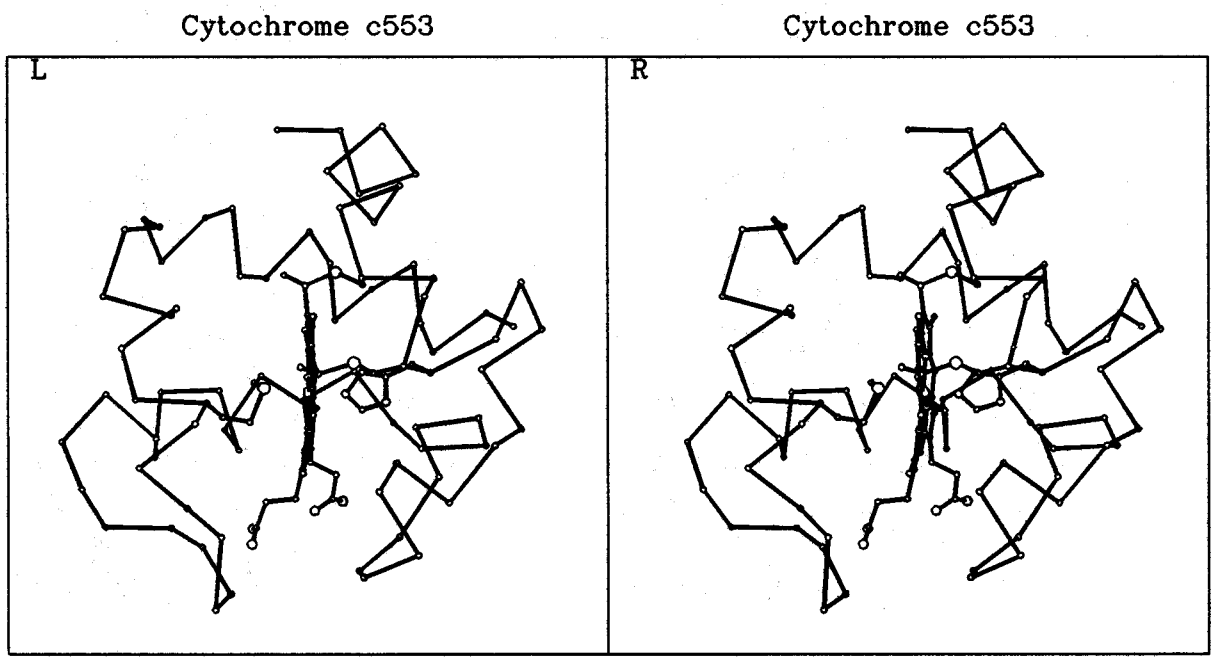

(f) cytochrome c_{553}

Figure 5-8
(*continued*)

molecule. The upper part of the molecules highly conserved in cytochrome *c* superfamily. And covalently bonded and coordinated residues to heme group, Cys, Cys, His, Met, are also highly conserved.

In the contrast, the lower part of the molecule is quite different from each other, the lower part of L- and M-class cytochrome *c* is covered by the middle part of the amino acid chain and propionates of heme group are buried from the molecular surface. Cytochrome c_{551}, one kind of S-class cytochrome *c*, lost the long middle part of amino acid chain corresponding to L- and M-class cytochromes *c* and its folding pattern, especially the lower part of the molecule, is quite different from other L- and M-class cytochromes *c*. But, although folding pattern is quite different from other classes of cytochromes *c*, two propionates of heme group is covered by polypeptide chain as shown in Figure (5-8(d)). In the contrast, as shown in Figure (5-8(e)), two propionates of heme group of cytochrome c_5 are not covered by polypeptide main chain. Folding pattern of cytochrome c_{553} is similar to that of cytochrome c_5. The main difference between cytochrome c_{553} and cytochrome c_5 is the lack of the back right side α-helix for cytochrome c_{553}. This part of cytochrome c_{553} has an extended random conformations, and this helical conformation is conserved in cytochrome c_{551} molecule.

Assuming that cytochrome c_{553} has the primitive folding pattern of cytochromes *c* superfamily, the following hypothesis can be built up.

1. Cytochrome c_5 : Insertion of the short helix at the right bottom of cytochrome c_{553}
2. Cytochrome c_{551} : Insertion of the short loop at the left bottom of cytochrome c_{553} and cover the bottom cleaves of the molecule

3. Cytochrome *c* : Insertion of the long loop at the bottom to cytochrome c_{553} and covers the bottom of the molecule

4. Cytochrome c_2 : Insertion of the left loop to M-class cytochrome *c*

The hypothesis of the evolution of cytochrome *c* superfamily considering amino acid sequences and folding patterns will be discussed in chapter 5-2-3.

Folding patterns of cytochrome *c* is not same among cytochrome *c* superfamily, but overall folding patterns are similar and the bottom are relatively different from each other.

Figure (5-9) shows the space-filling model of cytochrome c_{553} and it is colored according to kinds of residues. Blue color shows positively charged residues, such as lysine, arginine and histidine. Cyan color shows negatively charged residues, such as aspartic acid and glutamic acid.

Six lysine residues are surrounded the exposed edge of the heme group and positively charged residues are relatively rich in this side. In the other hand, there are many negatively charged residues in the opposite side. This charge distribution is also found in the other cytochromes *c* (Dickerson, 1972).

5-2-2. Interactions of Cytochrome c_{553}

Cytochromes *c* have many lysine residues and they are basic proteins. For example, cytochrome *c* from tuna has sixteen lysine residues of 103 amino acid polypeptide chain. Cytochrome c_{553} has also thirteen lysine residues

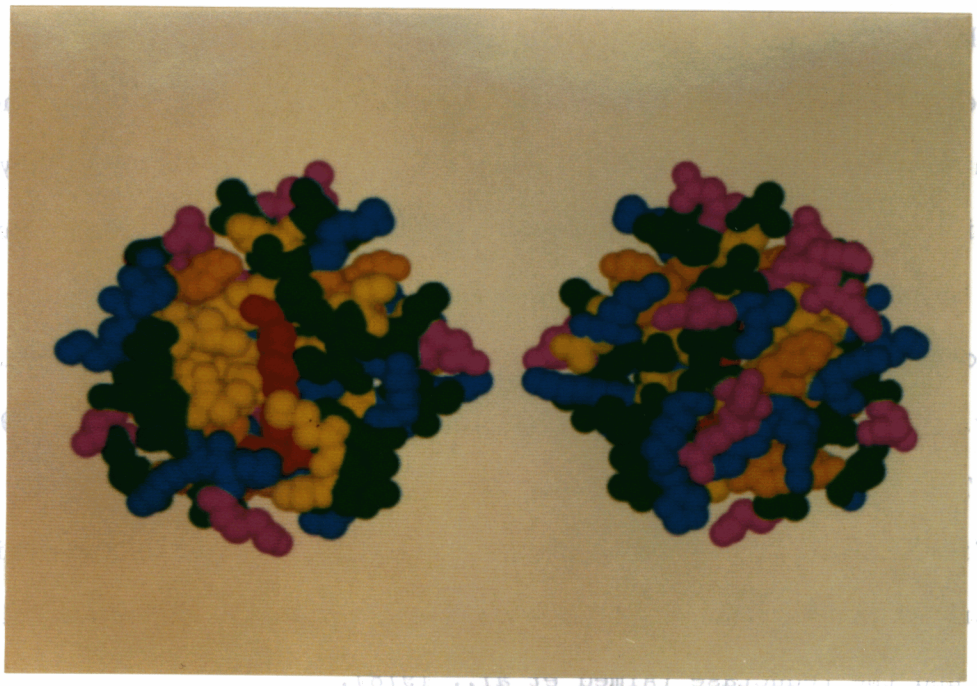

Figure 5-9

Space-filling models of cytochrome c_{553}

These two models show opposite side of molecule each other
The left one shows heme cleaves

Blue : Lys, Arg, His ; Cyan : Asp, Glu
Orange : Phe, Tyr ; Yellow : Leu, Met, Val
Green : Asn, Gln, Cys, Thr, Ser, Ala, Gly
Red : Hem

in 79 amino acid polypeptide chain, and isoelectric point of cytochrome c_{553} is 10.5.

Many lysine residues of cytochromes *c* are conserved in many different species. The reactions of naturally occurring variants of eukaryotic cytochrome *c* with its oxidase or reductase have implicated the positively charged lysine residues around the exposed edge of the heme in the mechanism of interaction (Ferguson-Miller *et al.*, 1979). Horse heart cytochrome *c* contains nineteen lysine residues. Millett and his colleague have prepared nine cytochrome *c* derivatives singly-modified at lysines with trifluoroacetate (TFA) and six singly-modified at lysines with trifluoromethylphenyl carbamate (TFC) (Ahmed *et al.*, 1978 ; Smith *et al.*, 1977, 1980). Both TFA and TFC neutralized the positively charged amino group of lysine. Modification of Lys13 produces a four to seven-fold reduction in the electron transfer rates of cytochrome *c* with the oxidase (Smith *et al.*, 1977) and the reductase (Almed *et al.*, 1978).

Margoliash and his colleagues have prepared ten cytochrome *c* derivatives singly-modified at lysine by 4-carboxyl-2,6-dinitrophenol (CDNP) (Ferguson-Miller *et al.*, 1978 ; Osheroff *et al.*, 1980). CDNP replaces the positively charge of lysine by a negatively charge. The effects of CDNP are qualitatively similar to those of TFA and TFC but much more pronounced. The lysine residue with greatest effect on the reaction rates or binding constants are at positions 13, 72, 86, 87 and 8 for the oxidase and 13, 86, 87, 27 for the reductase.

Reider and Bosshord have used differential chemical modification to identify the lysine residues of horse heart cytochrome *c* involved in interactions with the oxidase or the reductase (Reider and Bosshard, 1980). The lysine

residues afforded the greatest protection by cytochrome *c* oxidase are numbers 13, 86, 87, 8, 72, 73 and by purified cytochrome *c* reductase are numbers 86, 87, 13, 8, 79, 5.

All three studies of the cytochrome *c* interaction surface implicate lysine residues surrounding the exposed edge of the heme group. Lysines 13, 86 and 87 interact strongly with both the oxidase and the reductase as shown by all of the studies. Lysine 72 appears to interact strongly with the oxidase but less strongly with the reductase.

Cytochrome *c* transfer electrons from the pyrrole C region and lysine residues act as important residues to contact to electron acceptor. As shown in Figure (5-10(b)), cytochrome c_{553} also has lysine residues surrounding pyrrole C region. But Lys8 of cytochrome c_{553}, which occupied the near position of the Lys13 of cytochrome *c* from horse heart, does not locate at the same position in the molecule. Ser9 of cytochrome c_{553} is locates at that place, and water molecule bonded to Oγ of Ser9 was found on the MAD electron density map. Lys8 in cytochrome c_{553} is located very near part of the molecule. Lysine residue in this position is not conserved on primary structures in all cytochromes *c* superfamily. But lysine residues are very important for activity of cytochrome *c* in the electron transfer system and overall location of lysine residues in cytochromes *c* molecules are similar to each other.

5-2-3. Structure and Redox Potential

As described in chapter 5-1-3, heme group of cytochrome c_{553} is ex-

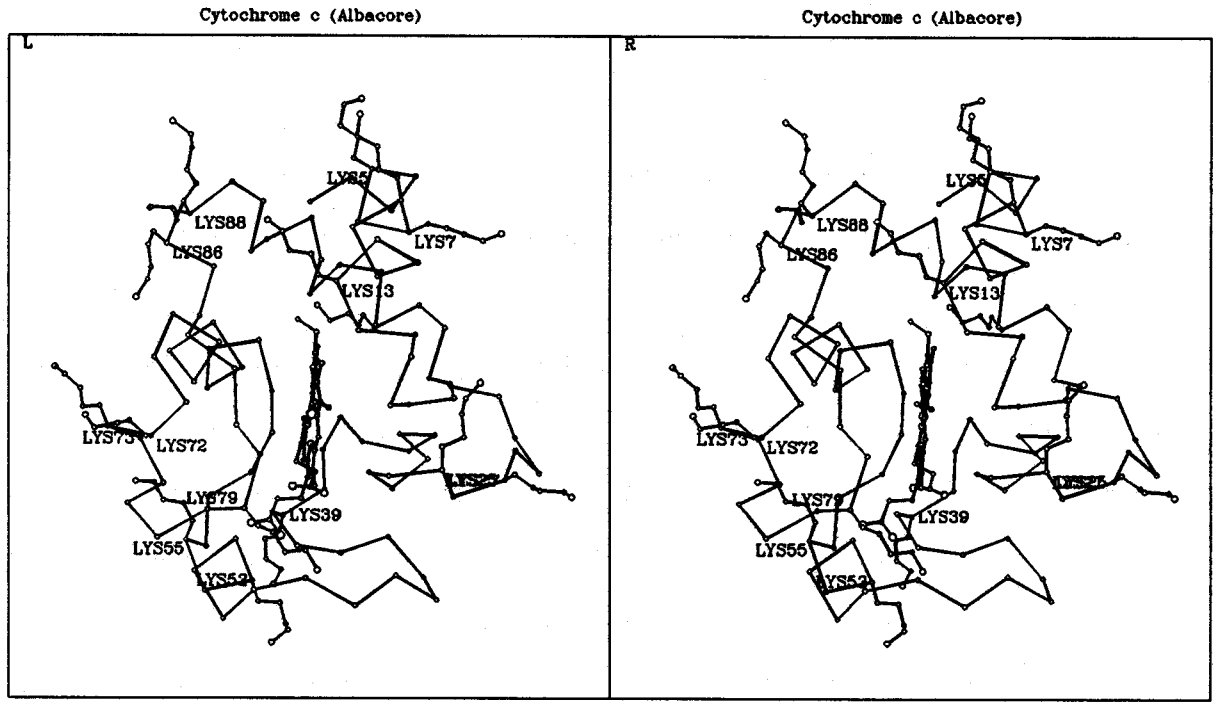

a

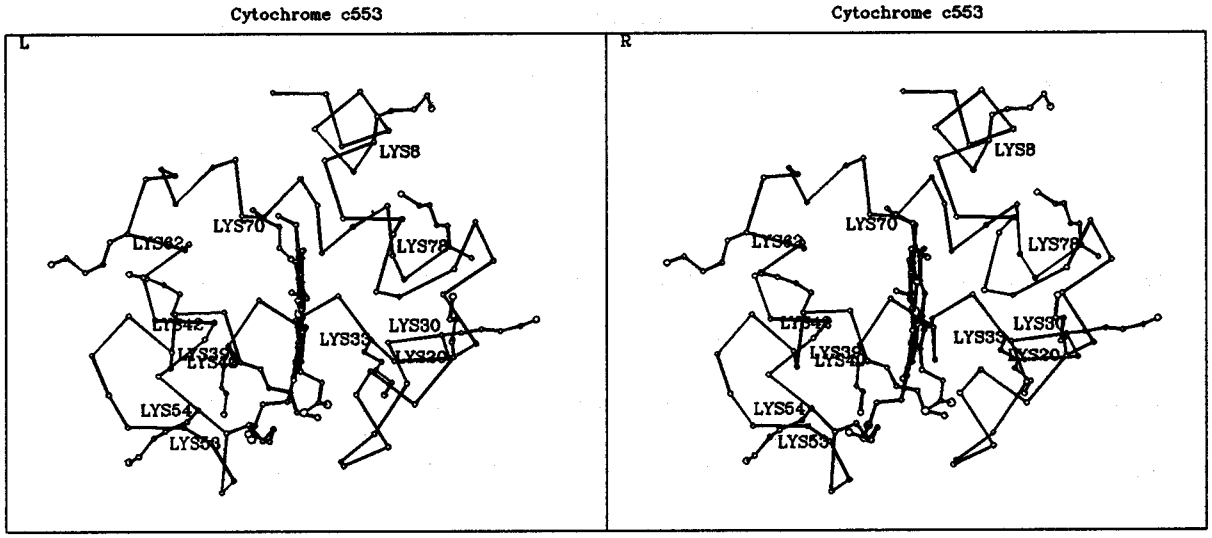

b

Figure 5-10

Lysine residues in cytochromes *c*

(a) cytochrome *c* from albacore
(b) cytochrome c_{553}

posed to its molecular surface at three region. These three solvent accessible surface areas of heme are summarized in Table (5-5). These areas and their size were calculated using the program ACCESS in the CCP4 computer program package. Radius of solvent probe was used 1.4 Å, which was assumed a water molecule. The heme group is mainly exposed to molecular surface at pyrrole C region(CMC and CBC of heme group). Stellwagen suggested the relationship between redox potential and exposed area of heme group (Stellwagen,1978). He tested six heme proteins[3], and showed that reduction potential, E_0', was inversely dependent on the exposure if the heme to an aqueous solvent. Figure (5-11) shows the dependence of reduction potential, E_0' , and the fraction of heme surface exposed and the fraction of apolarity of heme crevice. The fraction of heme surface exposed could be expressed as the following equation

$$E_0'(mV) = -15 \cdot A + 345,$$

where A is a percentage of exposure area of heme group. Using this relationship, calculated E_0' value for cytochrome c_{553}, of which A is 7 %, becomes 240mV, although observed redox potential was about 0mV (Niki *et al.*, *unpublished result*). Cytochrome c_{553} has extremely low redox potential compare to other heme proteins. This result suggested that the exposure of heme moiety is not the only determinant for the magnitude of its redox

---

3. Stellwagen tested following six heme proteins,

   Cytochrome c_2, Cytochrome c, Cytochrome c_{550}, Heamoglobin α-chain,

   Heamoglobin β-chain, Myoglobin, Cytochrome b_5

   with their coordinates in the Protein Data Bank. (Bernstein *et al.*, 1977)

Heme+protein	Total accessible surface	4490.3
	Accessible apolar surface	2567.8
	Accessible heme surface	60.1
Heme	Total accessible surface	843.3
Heme crevice of apoprotein		
	Total accessible surface	639.9
	Accessible apolar surface	491.3
Tabulations		
	% Heme exposed in heme protein	7
	% Heme crevice apolar	76
	% Heme environment apolar	58

Accessible surface area of heme group

CHA	0.4
O2A	2.7
CMB	0.9
CAB	0.5
CBB	2.9
CMC	18.1
CBC	29.3
C3D	0.4
C4D	0.2
CAD	1.4
CGD	1.0
O2D	3.1

Table 5-5

Solvent accessible surface area
of cytochrome c_{553}

The heme group is mainly exposed to
molecular surface at pyroll C region

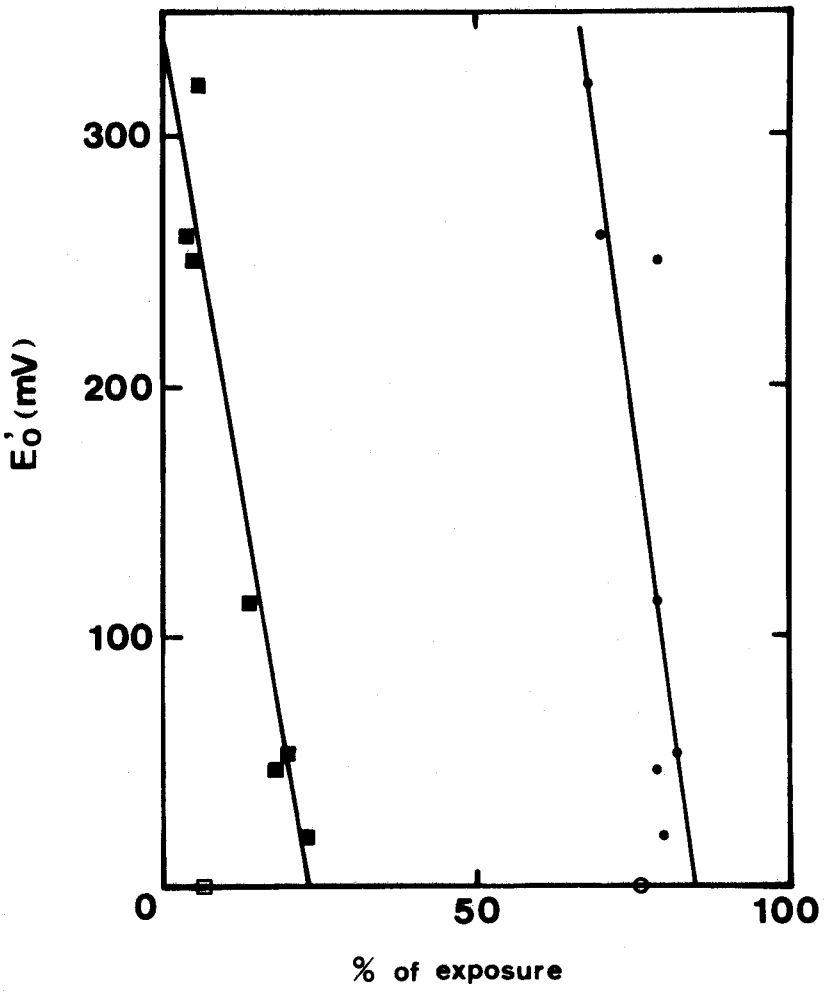

Figure 5-11

The dependense of reduction potential, E_0',
to the fraction of exposed surface of heme(● ○)
and the fraction of apolarity of the heme crevice(■ □)

The marks ○ and □ indicate the values of cytochrome c_{553}

potential.

This irregular behavior on low redox potential of cytochrome c_{553} must be depend on its structure. Considering hydrogen bonds to carbonyl oxygens of the two propionates. The O1A is bonded with Nε_2 of Gln32 and Nζ of Lys40, and the O2A is bonded to Oη of Tyr49 and Wat93 molecule. The O1D is bonded with N of Lys53 and N of Lys54 and the O2D is bonded to Oη of Tyr49 and N of Gly51 by hydrogen bonds (Table (5-2) and Figure (5-12)). Two propionates of heme group bond to many basic atom by hydrogen bonds. Further more, two side chains of tyrosine residues, Tyr44 and Tyr49, are closed together. The closest inter-residue distance is 3.65 Å, between Oη of Tyr44 and Cε_2 of Tyr49, that is comparable to their van der Waals distance, and it means that these two aromatic rings are contact each other. And dihedral angle between the best plane (Blow, 1960) of the aromatic ring of Tyr44 and that of Tyr49 is 89.8 degree. It seems that these residues are important on the electron transfer properties, but it must be necessary to study further to find the relationship between its structure and redox potential.

5-2-4. Alignment of Amino Acid Sequence

Alignment of amino acid sequence of cytochrome c_{553} from sulfate-reducing bacterium was proposed by Dickerson *et al.* (Dickerson *et al.*, 1976), considering the amino acid sequence of cytochrome c_{553} from *Desulfovibrio vulgaris* Hildenborough (Bruschi and Le Gall, 1972). Amino acid sequence of cytochrome c_{553} from *Desulfovibrio vulgaris* Miyazaki was determined by Yagi and colleagues (Nakano *et al.*, 1983) and they proposed new

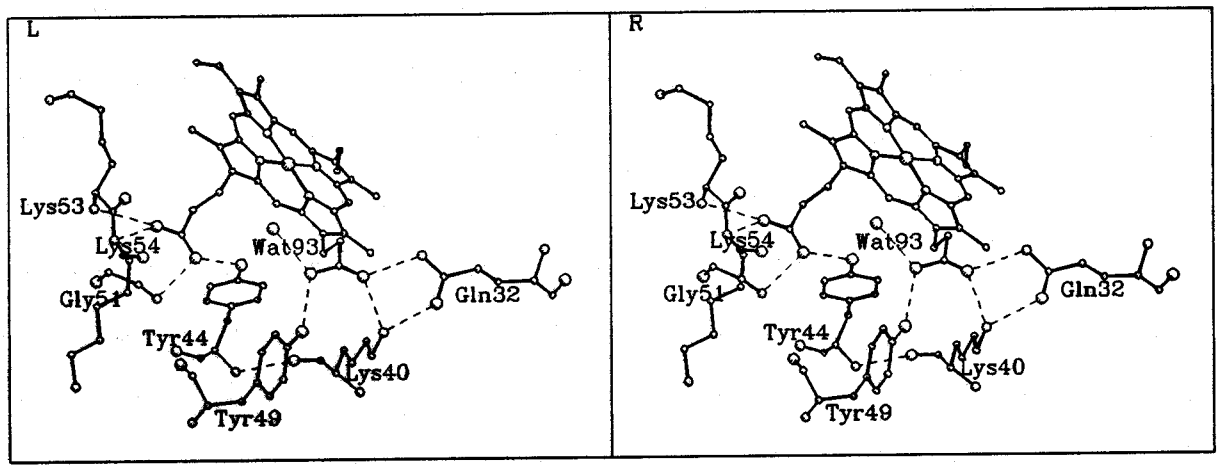

Figure 5-12

Heme group and its neighbor residues
which bond to heme by hydrogen bonds

alignment of amino acid sequence of cytochrome c_{553} to that of other S-class cytochrome *c*, such as cytochrome c_{551} from *Pseudomonas aeruginosa* and that from *Pseudomonas fluorescence*. Amino acid sequence of cytochrome c_{553} of *Desulfovibrio vulgaris* Miyazaki is quite different from that of *Desulfovibrio vulgaris* Hildenborough, although amino acid sequences of cytochromes c_3 from both species are quite similar to each other. As shown in Figure (5-13), assuming that there was a mistake on the alignment of amino acid fragment during the determination of amino acid sequence, both amino acid sequences of cytochrome c_{553} are quite similar to each other. The author propose new alignment of amino acid sequence based on the three-dimensional structure of cytochrome c_{553} from *Desulfovibrio vulgaris* Miyazaki in Figure (5-14(a)). This alignment is essentially same as that proposed by Yagi *et al.* (Nakano *et al.*, 1983). There are two region where the three dimensional structure of cytochrome c_{553} differs greatly from that of cytochrome c_{551} from *Pseudomonas aeruginosa* as discussed in chapter 5-2-1. Alignment of amino acid sequence support this result. Although three dimensional structure of cytochrome c_{553} is more similar to cytochrome c_5 from *Azotobacter vinelandii* than that of cytochrome c_{551} from *Pseudomonas aeruginosa*, it seems that amino acid sequence of cytochrome c_{553} is more similar to that of cytochrome c_{551} than that of cytochrome c_5. And as shown in Figure (5-8(f)), in chapter 5-2-1, tertiary structure of cytochrome c_{553} has "cytochrome *c* folding" and the upper part of its structure is similar to that of other cytochromes *c*, alignment of amino acid sequence of cytochrome c_{553} to that of cytochrome *c* from albacore does not shows any similarity on its primary structure, see Figure (5-14(b)).

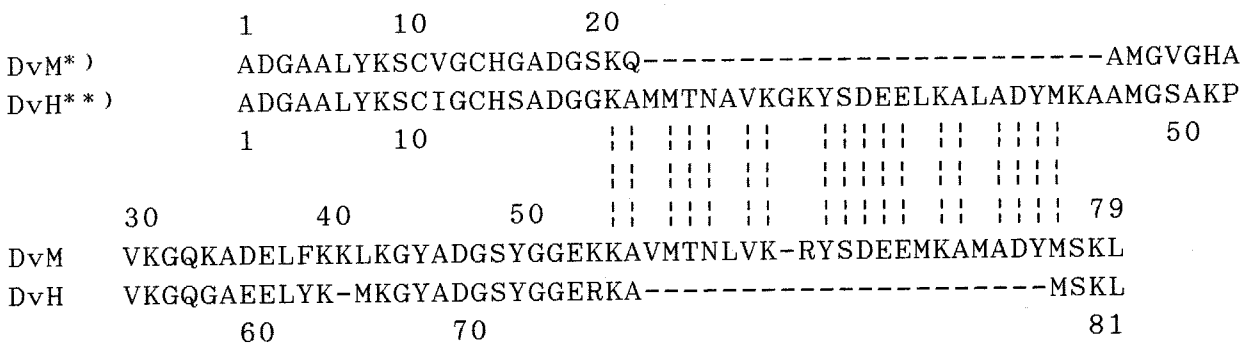

*) *Desulfovibrio vulgaris* Miyazaki
**) *Desulfovibrio vulgaris* Hildenborough

Figure 5-13

Alignement of amino acid sequence of cytochrome c_{553} from *Desulfovibrio vulgaris* Miyazaki and from *Desulfovibrio vulgaris* Hildenborough

Assuming that there was a mistake on the alignment of amino acid fragments during the determination of each one of its sequence, both sequences become quite similar to each other

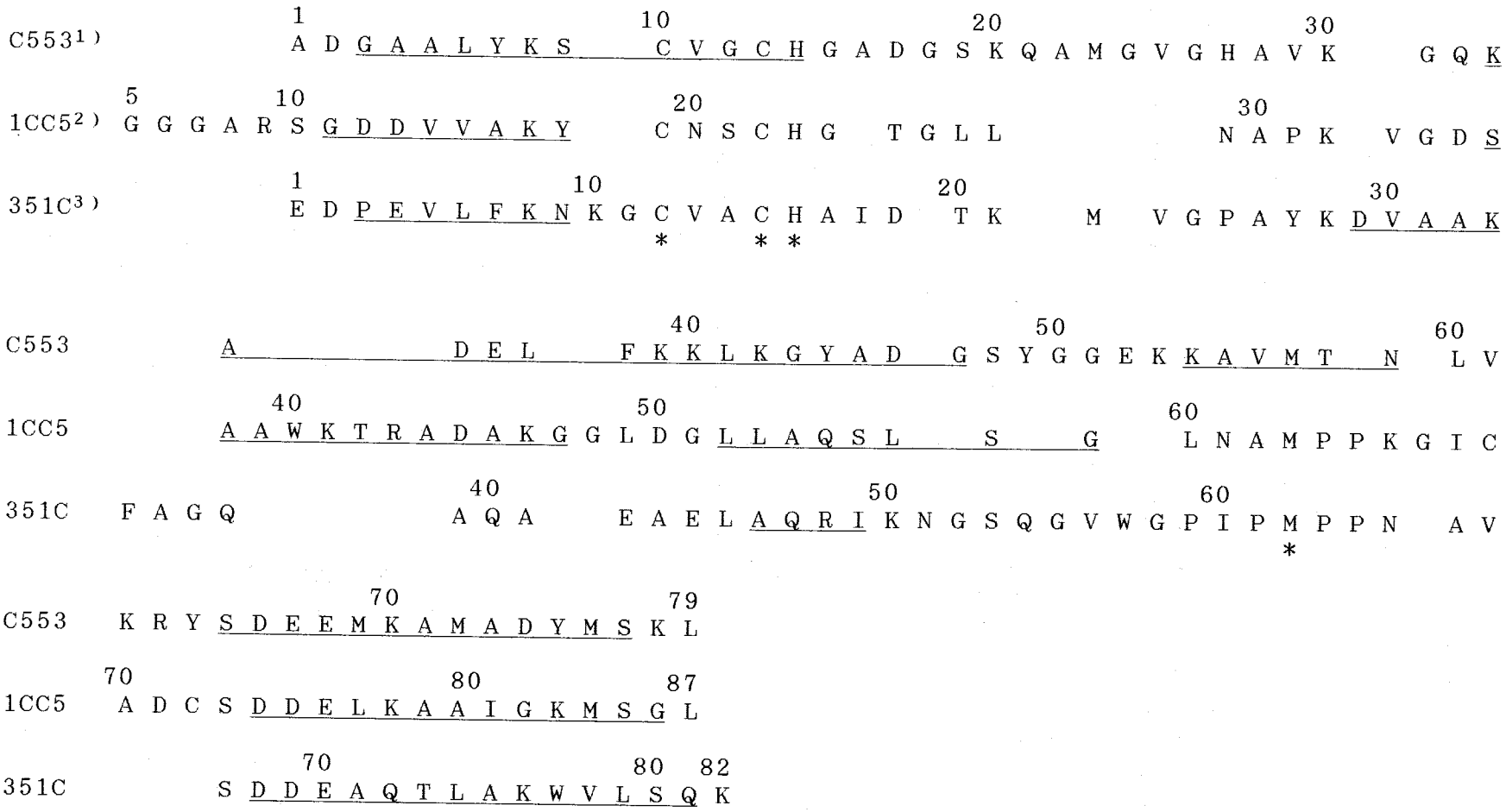

Figure 5-14

Alignment of amino acid sequence of cytochrome *c*

(a) S-type cytochrome *c* and cytochrome c_{553}

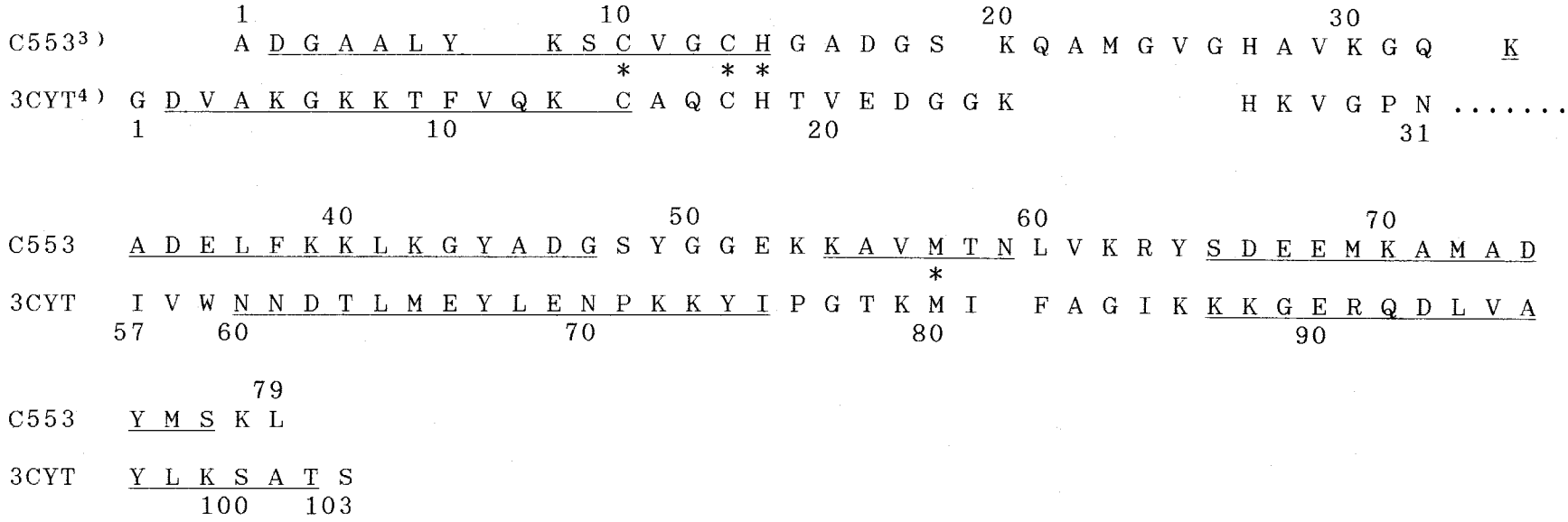

*) Underline shows helical conformations
**) The mark * shows heme binding residues

Figure 5-14
(*continued*)

(b) cytochrome c_{553} and cytochrome *c* from albacore

1) cytochrome c_{553} from *Desulfovibrio vulgaris* Miyazaki
2) cytochrome c_5 from *Azotobacter vinelandii*
3) cytochrome c_{551} from *Pseudomonas aeruginosa*
4) cytochrome *c* from albacore

5-2-5. Evolution of Cytochrome *c* Superfamily

As discussed in chapter 5-2-1, although three-dimensional structure of cytochrome c_{553} looks like "cytochrome *c* folding", it is quite different from that of mitochondrial cytochrome *c*. Dickerson classified cytochrome c_{553} into S-class cytochrome *c* (Dickerson, 1980), but its three-dimensional structure is not so similar to that of cytochrome c_{551} from *Pseudomonas aeruginosa* which is classified into S-class cytochrome *c*. Mathews classified cytochrome c_{553} from *Desulfovibrio* into S_4-class as spectral behavior of cytochrome c_{553} is quite different from other S-class cytochromes *c*(S_1-S_3) (Mathews,1985). Three-dimensional structure of cytochrome c_{553} determined by this thesis supported Mathews' classification. Folding pattern of cytochrome c_{553} does not so similar to that of cytochrome c_{551} from *Pseudomonas*, and it looks that folding pattern of cytochrome c_{553} is more similar to that of cytochrome c_5 from *Azotobacter*. But primary structure of cytochrome c_{553} is more similar to that of cytochrome c_{551} form *Pseudomonas aeruginosa* than that of cytochrome c_5 from *Azotobacter vinelandii*. Considering these result, although *Desulfovibrio* is one of the ancient-type bacterium, *Desulfovibrio* is not so far from both *Pseudomonas* and *Azotobacter* in the phylogenetic tree of cytochrome *c* superfamily. Thus it is necessary to considering the position of *Desulfovibrio* on the phylogenetic tree of cytochrome *c* (Figure (5-15)). When Dickerson proposed his phylogenetic tree of cytochromes *c*, amino acid sequence of *Desulfovibrio*, although he used amino acid sequence of cytochrome c_{553} from *Desulfovibrio vulgaris* Hildenborough (Bruschi and Le Gall, 1972), was quite different from other cytochromes *c*, and he proposed the branch of *Desulfovibrio* separated at the

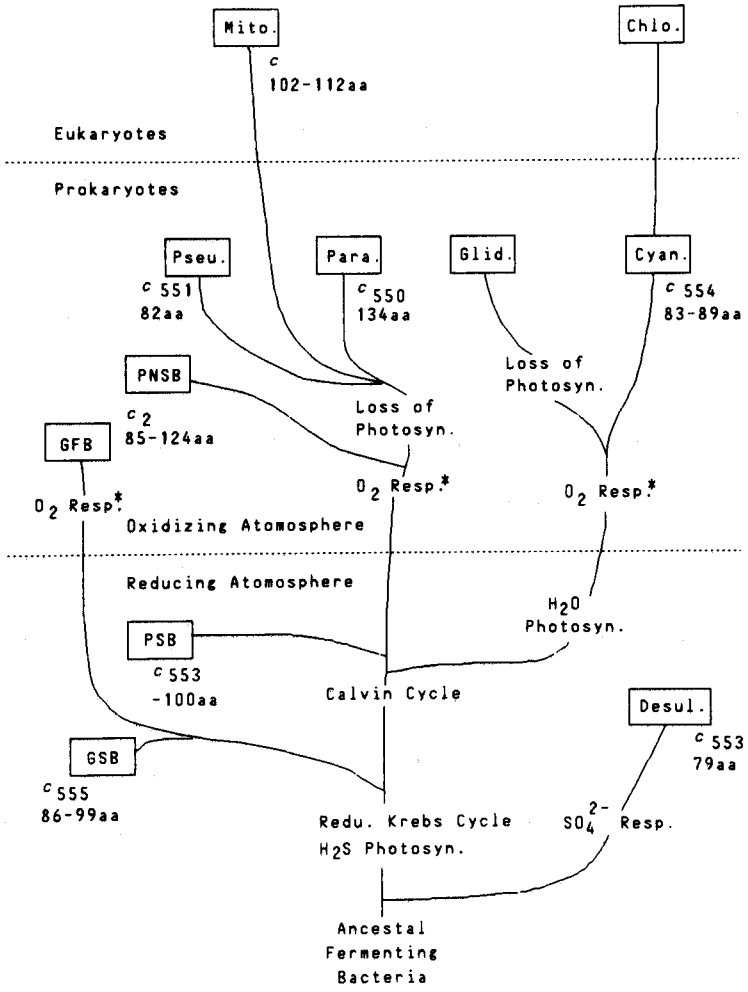

Figure 5-15

Phylogenetic tree of cytochrome *c* superfamily
(Dickerson, 1980)

Sulfate respiration is assumed to have arisen as a response to sulfate-releasing photosynthesis early on the primitive Earth, just as oxygen respiration arose as a consequence of oxygen-releasing photo synthesis at a later era. Oxygen respiration has involved independently from photosynthesis at least three times: in the green, purple and blue-green photosynthetic bacteria.

GSB=green sulfur bacteria (Chlotobiacea); GFB=green filamentous bacteria (Chloroflexaceae); PSB=purple sulfur bacteria (Chromatiaceae); PNSB=purple nonsulfur bacteria (Rhodospirillaceae); Pseu.=*Pseudomonas*; Mito.=eukaryotic mitochondria; Para.=*Paracoccus*; Glid.=gliding bacteria related to cyanobacteria; Cyan.=cyanobacteria or blue-green algae; Chlo.=eukaryotic chloroplasts; Desul.=*Desulfovibrio*

early stage of the evolution of cytochromes *c* superfamily.

Folding pattern of many cytochromes *c*, including L-,M- and S-class cytochromes *c*, seem that these have some insertion part into folding of cytochrome c_{553}. In this sense, it looks that cytochrome c_{553} has one of the most primitive "cytochrome *c* folding" and other cytochrome *c* has some insertions into primitive folding. This result supports the hypothesis that the branch of *Desulfovibrio* had separated at the early stage of the evolution in the phylogenetic tree of cytochrome *c* superfamily proposed by Dickerson (Dickerson,1980). But folding pattern of cytochrome c_{553} is similar to that of cytochrome c_5 from *Azotobacter vinelandii*, and it seems that the location of *Desulfovibrio* is quite closed to that of *Azotobacter*. Comparison of primary structure of flavodoxin from *Desulfovibrio* and *Azotobacter* supported this result (Kobayashi and Fox, 1978).

5-3. Usage of Multi-wavelength Anomalous Phase determination for Protein Crystallography

Multi-wavelength anomalous phase determination technique is a novel method to apply protein crystallography. Only two unknown protein crystal structure has been determined by this method, one is blue-copper protein (Guss *et al.*, 1988) and the other is streptavidin (Hendrickson *et al.*, 1989). The former has an intrinsic heavy atom, copper, in native protein and the latter was use extrinsic anomalous scatterer, selenium atom was used in that case, as a part of coenzyme. Although the theory of multi-wavelength anomalous phase determination can be expressed by analogue of

isomorphous replacement method, there are many difficulty to apply to the determination of unknown structure of proteins. The most difficult problem is how high precision data can be obtained. Although isomorphous difference is usually greater than several ten electrons, anomalous difference is always less than ten electrons. Success of structure determination of cytochrome c_{553} crystal should be depend following points;

1) Very fast data measurement using synchrotron radiation, Weissenberg camera and imaging plate reduces radiation damage of protein crystal
2) Bijvoet pair data are diffract at a same time by Weissenberg geometry and fluctuation of incident beam does not affect to measure Bijvoet difference
3) High precision data can be detected by imaging plate system
4) Averaging of many symmetry-related reflections reduced non-systematic errors
5) Local scaling method could be succeeded to reduce systematic errors

Si(111) monochromator was used in this experiment. Resolution of wavelength dispersion ($\Delta\lambda/\lambda$) of this crystal is order of 10^{-3} and it means that when real part of anomalous scattering effect, $\Delta f'$, varies dramatically at absorption edge, apparent value of $\Delta f'$ is not so large. It must be neccesary to use another monochromator of which wavelength dispersion is better than Si(111), such as Si(311) or double crystal monochromator, to get more useful data.

Many proteins in nature which have heavy atom(s) in native proteins and the multi-wavelength anomalous dispersion method will become powerful technique for protein crystallography. Absorption edges of elements of atomic

numbers in the range from 20(Ca) to 47(Ag) and from 50(Sn) to 92(U) are accessible in the range of 0.5 to 3.0 Å. As shown in Figure (5-16), although signal-to-noise ratio is not so good, native anomalous difference Patterson map showed iron-iron self vector even if $\Delta f''$ was 1.664 electrons at 1.04 Å. It means that it has an possibility to determine phases with proteins of which molecular weight is twice of that of cytochrome c_{553}, about 20000, with one heavy atom with X-ray at K absorption edge. But it must be very difficult to determine phases in such conditions, optics must be improved for this use. The author determined the real part of anomalous dispersion term, $\Delta f'$, as a parameter of refinement of heavy atom parameter, that was treated as occupancy, in this study. Strictly speaking, it should be better to determine wavelength of absorption edge and magnitude of real and imaginary part of anomalous scattering term according to the measurements of fluorescence EXAFS of iron. Detection system of fluorescence from crystal must be necessary to construct for anomalous dispersion technique.

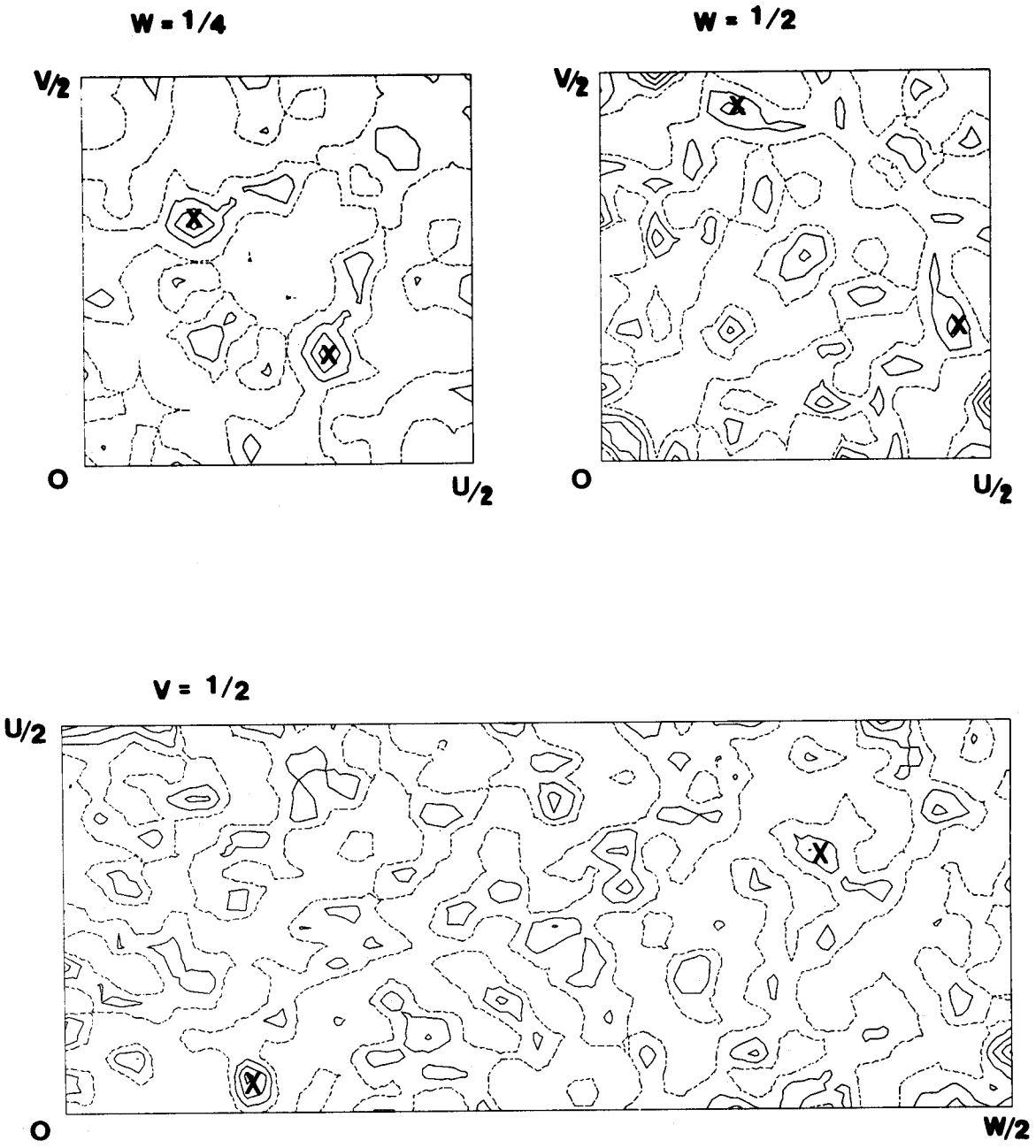

Figure 5-16

Native anomalous difference Patterson
of data collected at 1.04 Å
with coefficient of $|F_P(+)-F_P(-)|^2$

Dashed line shows zero level and these maps are contouring
of equal intervals in arbitrary unit

CONCLUDING REMARKS

Crystal of cytochrome c_{553} diffracts better than 1.5 Å resolution. And it is neccesary to continue refining the structure to elucidate its solvent structure and side chain conformations much precisely.

The multi-wavelength anomalous dispersion technique is one of the powerful technique to determine the crystallographic phases without using any other derivatives. In this study, this technique was applied to relatively small protein with one anomalous scatterer, and modified technique of isomorphous replacement method was successfully applied to determine the crystallographic phases. According to many advantages of multi-wavelength anomalous dispersion method, such as, 1) does not necessary to make isomorphous derivatives, 2)it has no lack of isomorphism, it must be neccesary to try determining structure of another protein which is larger than cytochrome c_{553} by multi-wavelength anomalous dispersion method.

Karle proposed a general algebraic analysis with no approximations for any number and type of anomalous scatterer (Karle, 1980), and Hendrickson proposed somewhat deviation of components that lends itself to direct analysis of the crystal structure at hand (Hendrickson, 1985). If $|^{\lambda}F(h)|$ is denoted the complete structure factors for reflection h at a particular wavelength λ, then the diffracted intensity, $I=K\cdot|F|^2$, is directly proportion to

$$
\begin{aligned}
|^{\lambda}F(\pm h)|^2 = {} & |^{0}F_T|^2 + a(\lambda)\cdot|^{0}F_A|^2 \\
& + b(\lambda)\cdot|^{0}F_T|\cdot|^{0}F_A|\cdot\cos(^{0}\phi_T - {}^{0}\phi_A) \\
& \pm c(\lambda)\cdot|^{0}F_T|\cdot|^{0}F_A|\cdot\sin(^{0}\phi_T - {}^{0}\phi_A)
\end{aligned}
$$

Here, ${}^0F_T=|{}^0F_T|\exp(i\cdot{}^0\phi_T)$ is the normal scattering (f^0) contribution from all atoms in the structure and $|{}^0F_A|$ is the corresponding contribution just from the anomalous centers. These factors are ratios of anomalous to normal scattering components,

$$a(\lambda) = (f'^2+f''^2)/f^{0\,2}$$

$$b(\lambda) = 2\cdot(f'/f^0)$$

$$c(\lambda) = 2\cdot(f''/f^0)$$

his new treatment will be applied to calculate the crystallographic phases of cytochrome c_{553} for check. In this treatment, it is neccesary to determine the parameters, $a(\lambda)$, $b(\lambda)$, $c(\lambda)$. These parameters will be calculates from the measurement of fluorescence EXAFS of the crystal. The author want to construct this measurement system.

And furthermore, another monochromators, such as Si(311) or double crystal monochromator, of which wavelength dispersion is better than Si(111) may be needed to measure the much precise data near absorption edge.

REFERENCES

Ahmed,A.J., Smith,H.T., Smith,M.B. and Millett,F.S. (1978) *Biochemistry*, **17**, 2479-2483

Amemiya,Y., Matsushita,T., Nakagawa,A., Satow,Y., Miyahara,J., and Chikawa,J. (1988) *Nucl. Instrum. Methods*, **A266**, 645-653

Ardnot,V.W. and Wonacott,A.J. (1977) In *The Rotation Method in Crystallography*, Amsterdam : North-Holland

Argos,P. and Mathews,F.S. (1973) *Acta Crystallogr.*, **B29**, 1604-1611

Beijerink,M.W. (1895) *Zentbl. Bakt. Parasitkde (abt.2)*, **1**, 1-9, 49-59, 104-114

Bernstein,F.C., Koetzle,T.F., Williams,G.J.B., Meyer,F.F., Bruce Jr.,M.D., Rodgers,J.R., Kennerd,O., Simanouchi,T., and Tasumi,M. (1977) *J. Mol. Biol.*, **112**, 535-542

Blow,D. (1960) *Acta Crystallogr.*, **13**, 168

Blow,D. and Crick,F.H.C. (1959) *Acta Crystallogr.*, **12**, 794-802

Bruschi,M. and Le Gall,J. (1972) *Biochim. Biophys. Acta*, **271**,48-60

Bruschi,M., Le Gall,J. and Dus,K. (1970) *Biochem. Biophys. Res. Commun.*, **38**, 607-616

Carter,D.C., Melis,K.A., O'Donnell,S.E., Burgess,B.K., Furey Jr.W.F., Wang,B.C. and Stout,C.D. (1985) *J. Mol. Biol.*, **184**, 279-295

Chou,P.Y. and Fasman,G.D. (1977) *J. Mol. Biol.*, **115**, 135-175

Conolly,M. (1983) *J. Appl. Crystallogr.*, **16**, 548-558

Dickerson,R.E., Timkovich,R. and Almassy,R.J. (1976) *J. Mol. Biol.*, **100**, 473-491

Dickerson,R.E. (1980) In *The Evolution of Protein Structure and Function*, pp.173-202, Academic Press,N.Y.

Ferguson-Miller,S., Brautigan,D.L. and Margoliash,E. (1979) In *The Porphyrins*, Vol.Ⅶ B (D.Dolphin eds.), pp.149-240, Academic Press,N.Y.

Ferguson-Miller,S., Brautigan,D.L. and Margoliash,E. (1978) *J. Biol. Chem.*, **253**, 5369-5372

Friedrich,W. Knipping,P. and von Laue,M. (1912) *Sitzb. math-phys. Klasse*, bayer.Akad.Wiss.München, pp.303

Guss,J.M., Merritt,E.A., Phizackerley,R.P., Hedman,B., Murata,M. Hodgson,K.O. and Freeman,H.C. (1988) *Science*, **741**, 806-811

Haser,R., Pierrot,M., Frey,M., Payan,F., Astier,J.P., Bruschi,M. and Le Gall J. (1979) *Nature (London)*, **282**, 806-810

Hendrickson,W.A., Pähler,A., Smith,J.L., Satow,Y., Merritt,E.A. and Phizackerley,R.P. (1989) *Proc. Natl. Acad. Sci.*, **86**, 2190-2194

Hendrickson,W.A. (1985) *Trans. Amer. Cryst. Ass.*, **21**, 11-21

Hendrickson,W.A. and Konnert,J.H. (1980) In *Biomolecular Structure, Function,Conformation and Evolution* (Srinivasan,R., eds.), vol.1, pp.43-57, Pregamon Press, Oxford

Hendrickson,W.A. and Teeter,M.M. (1981) *Nature (London)*, **290**, 107-113

Higashi,T. (1989) *J. Appl. Crystallgr.*, **22**, 9-18

Higuchi,Y., Bando,S., Kusunoki,M., Matsuura,Y., Yasuoka,N., Kakudo,M., Yamanaka,T., Yagi,T. and Inokuchi,H. (1981) *J. Biochem.(Tokyo)* **89**, 1659-1662

Higuchi,Y., Inaka,K., Yasuoka,N. and Yagi,T. (1987) *Biochim. Biophys. Acta*, **911**, 341-348

Higuchi,Y., Kusunoki,M., Matsuura,Y., Yasuoka,N. and Kakudo,M. (1984) *J. Mol. Biol.*, **172**, 109-139

Higuchi,Y., Kusunoki,M., Yasuoka,N., Kakudo,M. and Yagi,T. (1981) *J. Biochem. (Tokyo)*, **90**, 1715-1723

Ishimoto,M. and Koyama,J. (1953) *Nippon Kagaku Kaishi*, **74**, 853-857

Ishimoto,M., Koyama,J. and Nagai Y. (1954) *Bull. Chem. Soc. Japan*, **27**, 564-565

Jones,T.A. (1978) *J. Appl. Crystallogr.*, **11**, 268-272

Karle,J. (1980) *Int. J. Quantum Chem. Quantim Biol. Symp.*, **7**, 357-367

Katayama,C., Sakabe,N. and Sakabe,K. (1972) *Acta Crstallogr.*, **A28**, 293-295

Kobayashi,K. and Fox,J.L. (1978) In *Evolution of Protein Molecules* (Matsubara,H. and Yamanaka,T. eds) pp.233-242, Japan Scientific Society Press, Tokyo

Kobayashi,K. and Skyring,G.W. (1982) *J. Gen. Appl. Microbiol.*, **28**, 45-54

Le Gall,J. and Bruschi-Heriand,M. (1968) In *Structure and Function of cytochromes* (Okunuki,K., Kamen,M.D. and Sekuzu,I., eds.), pp.467-470, The University of Tokyo Press, Tokyo

Mathews,F.S. (1985) *Prog. Biophys. Molec. Biol.*, **45**, 1-56

Matsuura,Y., Takano,T. and Dickerson,R.E. (1982) *J. Mol. Biol.*, **156**, 389-410

Matthews,B.W. (1966) *Acta Crystallogr.*, **20**, 82-86

Matthews,B.W. (1968) *J. Mol. Biol.*, **33**, 491-497

Matthews,B.W. and Czerwinski,E.W. (1975) *Acta Crystallogr.*, **A31**, 480-487

Miyahara,J., Takahashi,K., Amemiya,Y. Kamiya,N. and Satow,Y. (1986) *Nucl. Instrum. Methods*, **A246**, 572-578

Nakagawa,A., Nagashima,E., Higuchi,Y., Kusunoki,M., Matsuura,Y., Yasuoka,N., Katsube,Y., Chihara,H. and Yagi,T. (1986) *J. Biochem. (Tokyo)*, **99**, 605-606

Nakano,K., Kikumoto,Y. and Yagi,T. (1983) *J. Biol. Chem.*, **258**, 12409-12412

North,A.C.T. (1965) *Acta Crystallogr.*, **18**, 212-216

North,A.C.T., Philips,D.C. and Mathews,F.S. (1968) *Acta Crystallogr.*, **A24**, 351-359

Ochi,H., Hata,Y., Tanaka,N., Kakudo,M., Sakuri,T., Aihara,S. and Morita,Y. (1983) *J. Mol. Biol.*, **166**, 407-418

Ogata,M., Arihara,K. and Yagi,T. (1981) *J. Biochem. (Tokyo)*, **89**, 1423-1431

Oshieroff,N., Brautigan,D.L. and Margoliash,E. (1980) *J. Biol. Chem.*, **255**, 4732-4739

Peck,H.D. and Le Gall,J. (1982) *Phil. Trans. R. Soc. Lond.*, **B.298**, 443-446

Pierrot,M., Haser,R., Frey,M., Payan,F. and Astier,J.P. (1982) *J. Biol. Chem.* **257**, 14341-14348

Postgate,J.R. (1954) *Biochem. J.*, **58**, xi

Ramakrishnan,C. and Ramachandran,G.N. (1965) *Bio. Phys. J.*, **5**, 909-933

Reider,R. and Bosshard,H.R. (1980) *J. Biol. Chem.*, **255**, 4732-4739

Rossmann,M.G. (1979) *J. Appl. Crystallogr.*, **12**, 2555-238

Sakabe,N. (1983) *J. Appl. Crystallogr.*, **16**, 542-547

Sakabe,N., Nakagawa,A., Sasaki,K., Sakabe,K., Watanabe,N., Kondo,H. and Shimonura,M. (1989) *Rev. Sci. Instrum.*, **60(7)**, 2440-2441

Salemme,F.R., Freer,S.T., Xuong,N.H., Alden,R.A. and Kraut,J. (1973) *J. Biol. Chem.*, **248**, 3910-3921

Sasaki,S. (1984) In *Anomalous Scattering Factors for Synchrotron Users*, KEK Report, 83-22

Satow,Y., Mikuni,A., Kamiya,N. and Ando,M. (1989) *Rev. Sci. Instrum.*, **60(7)**, 2394-2397

Senn,H., Guerlesquin,F., Bruschi,M. and Wüthrich,K. (1983) *Biochim. Biophys. Acta*, **748**, 194-204

Smith,H.T., Staudenmayer,N. and Millett,F. (1977) *Biochemistry*, **16**, 4971-4974

Smith,M.B., Stonehuerner,J., Ahmed,A.J., Staudenmeyer,N. and Millett,F. (1980) *Biochim. Biophys. Acta*, **592**, 303-313

Stellwagen,E. (1978) *Nature (London)*, **275**, 73-74

Takano,T. and Dickerson,R.E. (1980) *Proc. Natl. Acad. Sci.*, **77**, 6371-6375

Weissenberg,K. (1924) *Z. Phys.*, **23**, 229-238

Wilson,A.J.C. (1949) *Acta Crystallogr.*, **2**, 318-321

Yagi,T. (1969) *J. Biochem. (Tokyo)*, **66**, 473-478

Yagi,T. (1979) *Biochim. Biophy. Acta*, **548**, 96-105

Yagi,T. and Maruyama,K. (1971) *Biochim. Biophys. Acta*, **243**, 214-224

Appendix

A. Imaging Plate system at Photon Factory and its software system

The imaging plate system at Photon Factory was designed and constructed by Amemiya *et al.* (Amemiya *et al.*, 1988). A conventional drum-type film densitometer, which has two drums with a common rotating axis, has been modified into a laser scanner for the image read-out. One drum is used to read out X-ray image on the imaging plate, and the other is used to imprint the image on normal photographic film. The imaging plate is attached to the outer surface of the drum by using Scotch tape. A 20mW He-Ne laser source and a focusing optical system are adapted in a shaded box which moves along the direction of the drum axis together with device to collect the photostimulable luminescence and two photomultiplier tubes. The outputs of the photomultiplier tubes are logarithmically amplified and digitized by 100KHz, 12-bit A/D converters. The digitized data are sent directly to disk memories *via* three buffer memories of a host computer, ECLIPSE MV/4000 made by Nippon Data General. The operation of the system is controlled by this computer. The digital image can be displayed on a color graphic display terminal immediately after the image is read out. The image on the graphic terminal is photocopied on instant film or 35mm roll film by hard copy machine. For more precise reproduction of the X-ray image, the digital data are reconverted by 100KHz, 12-bit D/A converter into a time-series of analogue signals which modify the intensity of a glow lamp to imprint the image on a photographic film attached on the other drum. The digital data

are finally stored on a magnetic tape (6250/1600bpi) for further data processing by another computers.

The following points are to be improved in comparison with the one which is commercially available.

(a) The pixel sizes of 25μm^2 and 50μm^2 in addition to 100μm^2 are available by making both a focus size and a scanning pitch of the laser beam changeable.

(b) The output signals from a photomultiplier tube are digitized by a 12-bit A/D converter in place of a 8-bit A/D to improve the precision in X-ray intensity measurement.

(c) In order to fully utilize a wide dynamic range (1:10^5) of the photostimulated luminescence, two photomultiplier tubes are used simultaneously to detect the intensities of the luminescence with different sensitivities. The second multiplier tube receives roughly 1% of the total amount of the luminescence and convert a higher intensity range where the first one is saturated.

(d) Arbitrary size of the imaging plate are available simply by taping and the maximum size of the imaging plate is 200X380mm^2.

(e) In order to decrease the image distortion, a drum-type film densitometer is utilized which provides more precise scanning pitches than the flat-type one.

(f) The non-uniformity of response is reduced as the incident angle of the laser beam is always constant by using a drum-type film densitometer. The phosphor can be stimulated more uniformly by the laser beam.

(g) A high-resolution graphic display system (1280X1024 pixels, 8-bit

color depth, 19-inch) is also available in addition to a system for imprinting the image to get a visible image immediately.

Host computer, ECLIPSE MV/4000, has 4MB main memory, 354MB hard disk and magnetic tape unit (6250/1600bpi) as data storage system. The color raster graphic display, 1280$1024 pixels, 8-bit color depth (256 colors from 16 million color table can be displayed at a same time), hard copy machine for graphic display (Multi Color, Dunn Instruments) and X-Y plotter (7475A, YHP) are also available as image processing. Figure (A-1) shows a block diagram of the data handling components of the imaging plate system based on ECLIPSE MV/4000.

All software programs are coded using JIS Fortran (Fortran 77) and some subroutines are supported by Nippon Data General and runs under the AOS/VS operating system. Figure (A-2) shows a tree structure of the software system for the imaging plate system.

I. File Format

This imaging plate system can read any size of imaging plate. But five typical sizes and one arbitrary size are chosen in this program system. As it is neccesary to make a file which has continuous region on the physical disk to get high speed for writing data on the disk. All this kind of files are only used to input the data read out by image reader.

Standard format file of this system has a header block at the beginning of the file. This header block is 512byte size and it contains some informations about data in the file (Table (A-1)). Almost all programs in this

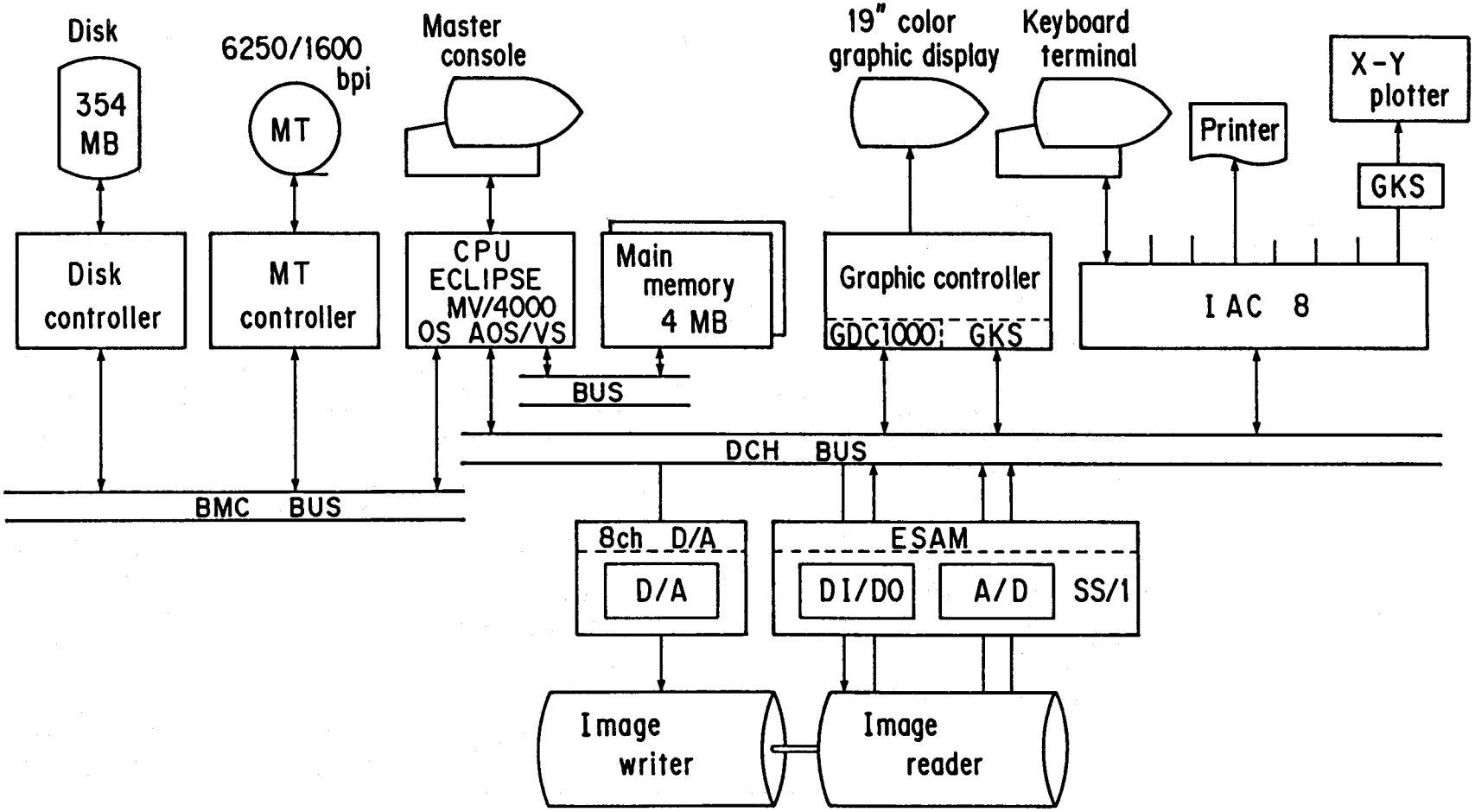

Figure A-1

Block diagram of the data handling components of the imaging plate system based on ECLIPSE MV/4000

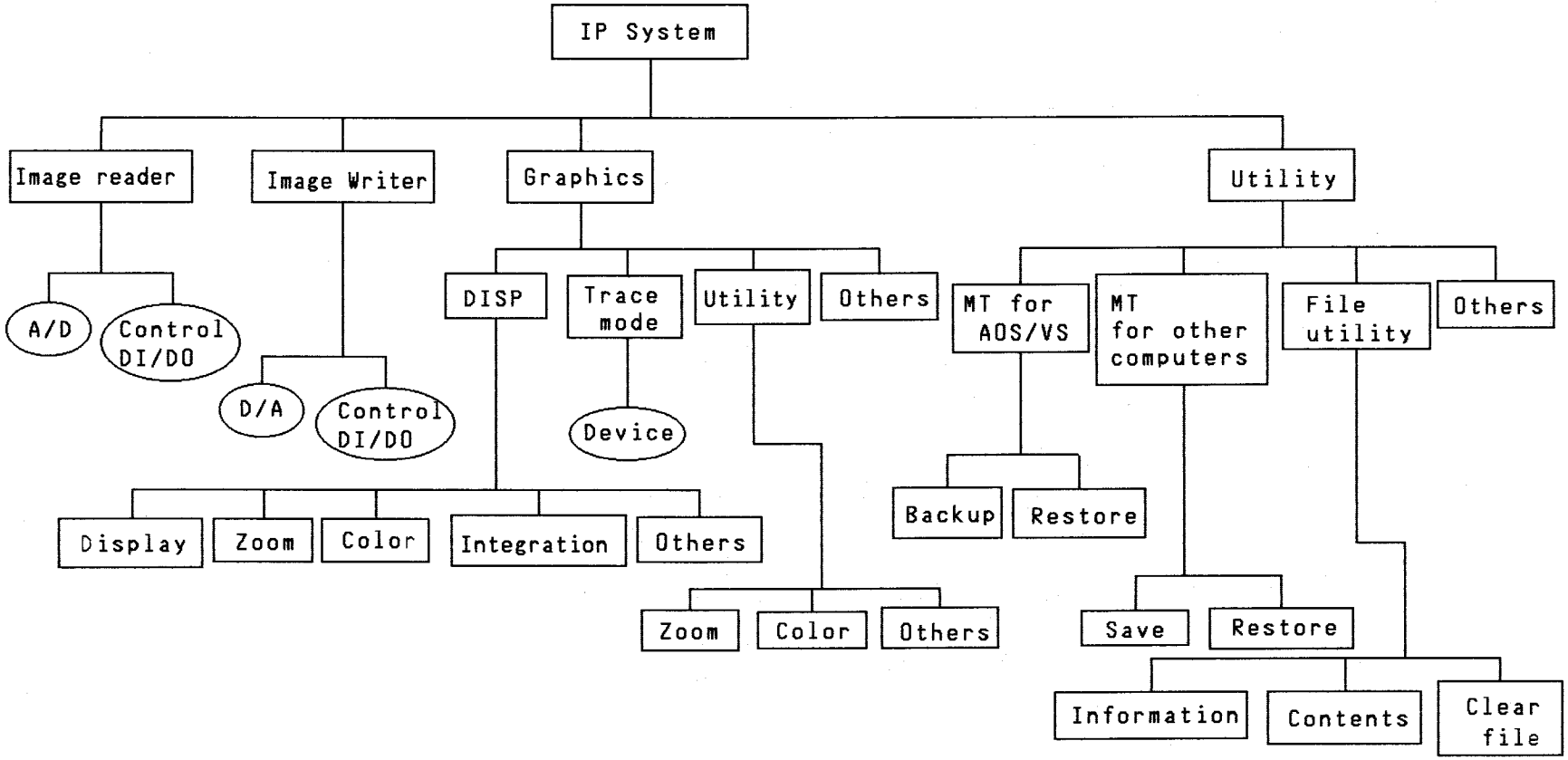

Figure A-2

Tree structure of the software system for the imaging plate system at Photon Factory

·MT format

1. AOS/VS DUMP_II format
2. ANSI standard (ASCII Code)
   No Label, 6250bpi
   Record length : 512 byte
   Block size : 8192 byte

·Header record (Type 1) (512 byte)

1.	HEAD	Character*4	'HDR1'[1]
2.	*null*	Character*4	(0000)h
3.	SAMPLE	Character*64	Sample name
4.	TITLE	Character*128	Title
5.	DATE(3)	Integer*4	Date
6.	TIME(3)	Integer*4	Time
7.	IXPIX	Integer*4	Pixel number along X-direction
8.	IYPIX	Integer*4	Pixel number along Y-direction
9.	IPIXEL	Integer*4	Total pixel number
10.	ISTEP	Integer*2	Raster step size[2]
11.	ISPEED	Integer*2	Scanning speed[3]
12.	IHV	Integer*2	High voltage for Main-PMT
13.	IGAIN	Integer*2	A/D gain[4] for Main-PMT
14.	ISUB	Integer*2	Use Sub-PMT[5]
15.	IHV2	Integer*2	High voltage for Sub-PMT
16.	IGAIN2	Integer*2	A/D gain[4] for Sub-PMT
17.	*others*	282 byte	Keep for future use (must be 0)

[1] Indicate IP-data file TYPE1.

[2] = 0 ... 250 (line/inch)
= 1 ... 500
= 2 ... 1000

[3] = 0 ... 2.5 (r.p.s)
= 1 ... 5.0
= 2 ... 10.0

[4] = 0 ... ± 10 V
= 1 ... ± 5
= 2 ... ± 2.5
= 3 ... ± 1.25

[5] = 0 ... Only Main-PMT
= 1 ... Use Main- and Sub-PMT

Table A-1

MT Format of Imaging Plate Data

system read header block at the begging of the program and determine the default conditions for the data on the file.

II. Image Reader

The output of the photomultiplier tubes are logarithmically amplified and digitized by 100KHz, 12bit A/D converters. The digitized data are sent to disk memories *via* triple chaining buffer. A user must input only 1)sample name, 2)comment, 3)size of the imaging plate which is selected from menu. As the pixel size of the data is limited by the character of the imaging plate itself, only 100mm^2 pixel size can be read now. And even now, the data detected by sub-photomultiplier cannot read-out according to the limitation of sampling clock and only one photomultiplier mode can be used. As following operations; a)opening the shutter of the laser beam, b)operating the switch of high voltage power suppliers for photomultipliers, c)starting and stopping rotation of drum and d)reset and start of digital counter to count number of pixels are controlled by the host computer automatically using DI/DO (digital input and output) functions, users must be needed just mounting the imaging plate onto the drum. The SS/1 board on the computer and ESAM which is a software to control SS/1 board are used for both A/D and DI/DO functions.

III. Image Writer

The digital data on the computer are reconstructed by 100KHz, 12bit D/A converter into a time-series of analogue signals, which modify the intensity of a glow lamp, and it implements the image on a photographic film to get a precise reproduction of the X-ray image. D/A converter is used HSDA

board and 8ch D/A converter which is a software system to control HSDA board.

Present version of the software for the image writer reconstructs the image data as stored in the computer and does not do anything such as enhancement of image and so on.

Ⅳ. Graphics

19-inch raster-type color graphic display and X-Y plotter are connected with the host computer and the graphics system is used to support the interpretation of stored data.

Graphic system is roughly speaking composed of image display program and image scanning program. Image display program displays two-dimensional image data as two-dimensional graphics and intensities are expressed according to blackness or special color tables. Image scanning program displays intensities of one-direction scanning of data using line graph. Image display program is used the graphics package, GDC1000, which is a graphics system to support a raster graphics of AOS/VS system, and image scanning program is using the graphics package, GKS, graphic kernel system. AOS/VS operating system supports the GKS as a graphics package to control many kind of devices. 19-inch color raster graphics display, X-Y plotter and Kanji terminal can be used as output devices of this system.

Image display program is useful to recognize the images on the file which image reader has read-out. A users must input both the threshold value and the latitude to determine the color table at first. These two values are always determined at first considering the output monitor, which is a synchronous scope, connected with the output of the image reader. This

program also supports some display utilities, zooming, translation, changing color level and/or color table, integration of pixel data. These functions are selected from menu or by using the optical mouse. Image scanning mode is useful to recognize the one-dimensional data, such as powder diffraction or compton scattering and so on, on the imaging plate as as a two-dimensional detector. A user chooses data scanning direction, either drum scanning direction or drum rotating direction, and which lines to be sum up. And a user can select the output device, graphics display, X-Y plotter or Kanji terminal.

V . Utilities

This system has utilities for displaying or changing of file header block. And the utilities to save the data on the disk to the magnetic tape and restore the data on magnetic tape to the disk are also available using both AOS/VS backup format and no label ANSI standard format tape for other computers.

All these programs in the system are connected by using CLI (command line interpreter) and all of them can be executed by just only selected the item from menu-style dialogue command to be possible to use this system by anyone who does not familiar to both/either AOS/VS operating system and/or ECLIPSE MV/4000 hardware system.

B. Atomic Paramters of Cytochrome *c*553

```
COMPND    CYTOCHROME $C=553= (OXIDIZED)
SOURCE    (DESULFOVIBRIO VULGARIS) MIYAZAKI F
CRYST   42.700   42.700  103.400  90.00  90.00  90.00 P 43 21 2      8
ORIGX1      1.000000  0.000000  0.000000        0.00000
ORIGX2      0.000000  1.000000  0.000000        0.00000
ORIGX3      0.000000  0.000000  1.000000        0.00000
SCALE1      0.023419  0.000000  0.000000        0.00000
SCALE2      0.000000  0.023419  0.000000        0.00000
SCALE3      0.000000  0.000000  0.009671        0.00000
ATOM      1  N    ALA     1      15.669   0.963  34.494  1.00 23.53
ATOM      2  CA   ALA     1      15.919  -0.028  33.417  1.00 19.56
ATOM      3  C    ALA     1      17.323  -0.575  33.455  1.00  7.27
ATOM      4  O    ALA     1      18.374   0.073  33.290  1.00 18.81
ATOM      5  CB   ALA     1      15.554   0.719  32.096  1.00 21.69
ATOM      6  N    ASP     2      17.324  -1.836  33.815  1.00 11.41
ATOM      7  CA   ASP     2      18.513  -2.628  34.018  1.00 12.07
ATOM      8  C    ASP     2      18.843  -3.473  32.752  1.00 12.53
ATOM      9  O    ASP     2      18.183  -4.489  32.605  1.00 13.93
ATOM     10  CB   ASP     2      18.256  -3.582  35.202  1.00 19.29
ATOM     11  CG   ASP     2      19.356  -4.410  35.738  1.00 31.41
ATOM     12  OD1  ASP     2      19.430  -4.720  36.980  1.00 25.93
ATOM     13  OD2  ASP     2      20.240  -4.813  34.956  1.00 22.76
ATOM     14  N    GLY     3      19.855  -2.927  32.107  1.00 17.16
ATOM     15  CA   GLY     3      20.243  -3.572  30.815  1.00 21.94
ATOM     16  C    GLY     3      20.489  -5.034  30.929  1.00 25.11
ATOM     17  O    GLY     3      20.052  -5.864  30.106  1.00 20.00
ATOM     18  N    ALA     4      21.343  -5.439  31.880  1.00 15.65
ATOM     19  CA   ALA     4      21.625  -6.829  32.119  1.00 14.44
ATOM     20  C    ALA     4      20.413  -7.694  32.388  1.00 16.41
ATOM     21  O    ALA     4      20.372  -8.858  31.925  1.00 17.83
ATOM     22  CB   ALA     4      22.692  -6.812  33.224  1.00 17.89
ATOM     23  N    ALA     5      19.385  -7.329  33.222  1.00 12.75
ATOM     24  CA   ALA     5      18.241  -8.170  33.473  1.00 13.32
ATOM     25  C    ALA     5      17.335  -8.264  32.159  1.00 13.16
ATOM     26  O    ALA     5      16.826  -9.360  32.011  1.00 16.68
ATOM     27  CB   ALA     5      17.366  -7.515  34.568  1.00 21.96
ATOM     28  N    LEU     6      17.221  -7.074  31.573  1.00 16.47
ATOM     29  CA   LEU     6      16.336  -7.144  30.312  1.00 14.79
ATOM     30  C    LEU     6      17.010  -8.058  29.268  1.00 14.44
ATOM     31  O    LEU     6      16.232  -8.784  28.606  1.00 14.77
ATOM     32  CB   LEU     6      16.278  -5.683  29.892  1.00 15.76
ATOM     33  CG   LEU     6      15.412  -4.781  30.777  1.00 17.07
ATOM     34  CD1  LEU     6      15.660  -3.335  30.432  1.00 16.71
ATOM     35  CD2  LEU     6      13.943  -5.186  30.625  1.00 22.75
ATOM     36  N    TYR     7      18.297  -7.963  29.191  1.00 17.57
ATOM     37  CA   TYR     7      19.016  -8.819  28.191  1.00 12.58
ATOM     38  C    TYR     7      18.775 -10.271  28.329  1.00 20.19
ATOM     39  O    TYR     7      19.006 -11.101  27.385  1.00 17.04
ATOM     40  CB   TYR     7      20.463  -8.377  28.006  1.00 17.69
```

```
ATOM     41  CG  TYR     7      21.165  -9.154  26.882  1.00 13.21
ATOM     42  CD1 TYR     7      21.993 -10.238  27.082  1.00 11.32
ATOM     43  CD2 TYR     7      20.993  -8.721  25.544  1.00 29.50
ATOM     44  CE1 TYR     7      22.680 -10.953  26.109  1.00 22.51
ATOM     45  CE2 TYR     7      21.697  -9.395  24.563  1.00 14.96
ATOM     46  CZ  TYR     7      22.448 -10.506  24.767  1.00 20.06
ATOM     47  OH  TYR     7      23.189 -11.163  23.812  1.00 20.09
ATOM     48  N   LYS     8      18.349 -10.827  29.529  1.00 14.11
ATOM     49  CA  LYS     8      18.153 -12.221  29.620  1.00  9.37
ATOM     50  C   LYS     8      17.102 -12.834  28.665  1.00 10.42
ATOM     51  O   LYS     8      17.186 -14.034  28.534  1.00 16.68
ATOM     52  CB  LYS     8      17.712 -12.582  31.112  1.00 16.54
ATOM     53  CG  LYS     8      18.842 -11.967  31.974  1.00 22.76
ATOM     54  CD  LYS     8      19.845 -13.046  32.324  1.00 31.43
ATOM     55  CE  LYS     8      20.629 -12.683  33.571  1.00 62.66
ATOM     56  NZ  LYS     8      21.698 -11.716  33.204  1.00 64.53
ATOM     57  N   SER     9      16.198 -11.985  28.193  1.00  9.11
ATOM     58  CA  SER     9      15.120 -12.432  27.293  1.00 13.20
ATOM     59  C   SER     9      15.773 -12.529  25.840  1.00 16.01
ATOM     60  O   SER     9      15.017 -13.139  25.053  1.00 20.50
ATOM     61  CB  SER     9      14.093 -11.316  27.203  1.00 13.74
ATOM     62  OG  SER     9      13.270 -11.387  28.401  1.00 26.24
ATOM     63  N   CYS    10      16.940 -12.073  25.692  1.00 20.89
ATOM     64  CA  CYS    10      17.613 -12.025  24.368  1.00 16.43
ATOM     65  C   CYS    10      18.584 -13.120  24.064  1.00 39.01
ATOM     66  O   CYS    10      18.941 -13.361  22.908  1.00 21.05
ATOM     67  CB  CYS    10      18.401 -10.690  24.357  1.00 12.51
ATOM     68  SG  CYS    10      17.403  -9.292  24.785  1.00 16.26
ATOM     69  N   VAL    11      19.103 -13.803  25.027  1.00 17.21
ATOM     70  CA  VAL    11      20.126 -14.809  25.039  1.00 17.82
ATOM     71  C   VAL    11      19.890 -16.048  24.218  1.00 16.34
ATOM     72  O   VAL    11      20.905 -16.607  23.757  1.00 27.82
ATOM     73  CB  VAL    11      20.283 -15.103  26.613  1.00 18.62
ATOM     74  CG1 VAL    11      20.655 -16.521  26.865  1.00 23.51
ATOM     75  CG2 VAL    11      21.228 -14.071  27.164  1.00 23.25
ATOM     76  N   GLY    12      18.698 -16.509  24.061  1.00 18.74
ATOM     77  CA  GLY    12      18.329 -17.705  23.308  1.00 28.61
ATOM     78  C   GLY    12      18.938 -17.500  21.873  1.00 21.02
ATOM     79  O   GLY    12      19.680 -18.385  21.475  1.00 27.55
ATOM     80  N   CYS    13      18.622 -16.343  21.356  1.00 23.06
ATOM     81  CA  CYS    13      19.130 -16.035  19.974  1.00 22.72
ATOM     82  C   CYS    13      20.453 -15.336  19.848  1.00 31.02
ATOM     83  O   CYS    13      21.206 -15.639  18.880  1.00 26.86
ATOM     84  CB  CYS    13      18.002 -15.267  19.285  1.00 23.72
ATOM     85  SG  CYS    13      16.398 -16.102  19.252  1.00 24.12
ATOM     86  N   HIS    14      20.809 -14.401  20.726  1.00 17.83
ATOM     87  CA  HIS    14      22.033 -13.610  20.639  1.00 12.25
ATOM     88  C   HIS    14      23.275 -14.106  21.360  1.00 17.12
ATOM     89  O   HIS    14      24.398 -13.579  21.238  1.00 20.88
ATOM     90  CB  HIS    14      21.648 -12.180  20.984  1.00 13.30
ATOM     91  CG  HIS    14      20.673 -11.588  20.008  1.00 14.19
ATOM     92  ND1 HIS    14      21.314 -11.139  18.825  1.00 23.80
```

```
ATOM     93  CE1 HIS    14      20.369 -10.625  18.111  1.00 15.10
ATOM     94  NE2 HIS    14      19.124 -10.731  18.573  1.00 14.03
ATOM     95  CD2 HIS    14      19.385 -11.392  19.837  1.00 15.65
ATOM     96  N   GLY    15      23.018 -15.121  22.199  1.00 25.55
ATOM     97  CA  GLY    15      24.082 -15.655  23.082  1.00 35.15
ATOM     98  C   GLY    15      24.300 -14.749  24.310  1.00 27.32
ATOM     99  O   GLY    15      24.048 -13.546  24.386  1.00 22.59
ATOM    100  N   ALA    16      24.888 -15.381  25.325  1.00 43.31
ATOM    101  CA  ALA    16      25.199 -14.686  26.595  1.00 22.18
ATOM    102  C   ALA    16      26.279 -13.683  26.390  1.00 24.77
ATOM    103  O   ALA    16      26.372 -12.670  27.109  1.00 24.70
ATOM    104  CB  ALA    16      25.638 -15.738  27.616  1.00 38.06
ATOM    105  N   ASP    17      27.130 -13.936  25.369  1.00 25.66
ATOM    106  CA  ASP    17      28.191 -12.965  25.081  1.00 21.67
ATOM    107  C   ASP    17      27.838 -12.056  23.867  1.00 24.07
ATOM    108  O   ASP    17      28.628 -11.158  23.537  1.00 31.01
ATOM    109  CB  ASP    17      29.591 -13.523  24.961  1.00 29.96
ATOM    110  CG  ASP    17      29.765 -14.525  23.838  1.00 28.82
ATOM    111  OD1 ASP    17      28.799 -15.038  23.263  1.00 35.69
ATOM    112  OD2 ASP    17      30.959 -14.810  23.614  1.00 47.96
ATOM    113  N   GLY    18      26.681 -12.286  23.315  1.00 27.34
ATOM    114  CA  GLY    18      26.135 -11.505  22.188  1.00 21.78
ATOM    115  C   GLY    18      26.895 -11.778  20.900  1.00 36.39
ATOM    116  O   GLY    18      26.673 -10.972  19.971  1.00 23.40
ATOM    117  N   SER    19      27.669 -12.833  20.861  1.00 27.09
ATOM    118  CA  SER    19      28.472 -13.051  19.623  1.00 37.70
ATOM    119  C   SER    19      27.810 -13.927  18.589  1.00 31.97
ATOM    120  O   SER    19      28.400 -14.245  17.523  1.00 31.34
ATOM    121  CB  SER    19      29.808 -13.656  20.068  1.00 33.40
ATOM    122  OG  SER    19      29.488 -14.996  20.440  1.00 28.40
ATOM    123  N   LYS    20      26.598 -14.345  18.837  1.00 24.11
ATOM    124  CA  LYS    20      25.882 -15.272  17.927  1.00 28.97
ATOM    125  C   LYS    20      25.179 -14.541  16.800  1.00 31.14
ATOM    126  O   LYS    20      24.678 -13.420  16.927  1.00 29.03
ATOM    127  CB  LYS    20      25.005 -16.118  18.790  1.00 27.86
ATOM    128  CG  LYS    20      24.290 -17.379  18.395  1.00 74.42
ATOM    129  CD  LYS    20      23.742 -18.049  19.662  1.00 59.70
ATOM    130  CE  LYS    20      22.744 -19.143  19.343  1.00 74.66
ATOM    131  NZ  LYS    20      22.215 -19.746  20.595  1.00100.03
ATOM    132  N   GLN    21      25.225 -15.167  15.624  1.00 29.45
ATOM    133  CA  GLN    21      24.528 -14.595  14.431  1.00 24.26
ATOM    134  C   GLN    21      23.129 -15.177  14.595  1.00 18.58
ATOM    135  O   GLN    21      22.888 -16.375  14.299  1.00 27.06
ATOM    136  CB  GLN    21      25.206 -15.083  13.131  1.00 28.19
ATOM    137  CG  GLN    21      25.124 -14.033  12.050  1.00 32.30
ATOM    138  CD  GLN    21      25.356 -14.591  10.643  1.00 30.17
ATOM    139  OE1 GLN    21      25.176 -13.862   9.669  1.00 30.05
ATOM    140  NE2 GLN    21      25.576 -15.886  10.646  1.00 19.57
ATOM    141  N   ALA    22      22.239 -14.327  15.065  1.00 21.08
ATOM    142  CA  ALA    22      20.878 -14.781  15.439  1.00 23.89
ATOM    143  C   ALA    22      20.158 -15.419  14.251  1.00 29.50
ATOM    144  O   ALA    22      20.005 -14.763  13.215  1.00 23.33
```

```
ATOM    145  CB  ALA    22      20.074 -13.641  16.039  1.00 23.60
ATOM    146  N   MET    23      19.738 -16.638  14.410  1.00 19.61
ATOM    147  CA  MET    23      18.956 -17.411  13.433  1.00 20.92
ATOM    148  C   MET    23      19.714 -17.457  12.065  1.00 21.07
ATOM    149  O   MET    23      19.050 -17.484  11.031  1.00 32.83
ATOM    150  CB  MET    23      17.554 -16.850  13.284  1.00 20.97
ATOM    151  CG  MET    23      16.853 -16.752  14.632  1.00 30.91
ATOM    152  SD  MET    23      15.141 -16.216  14.414  1.00 29.90
ATOM    153  CE  MET    23      14.263 -17.728  14.704  1.00 36.20
ATOM    154  N   GLY    24      21.004 -17.393  12.154  1.00 24.60
ATOM    155  CA  GLY    24      21.979 -17.404  11.074  1.00 29.56
ATOM    156  C   GLY    24      21.866 -16.294  10.057  1.00 29.76
ATOM    157  O   GLY    24      22.196 -16.541   8.883  1.00 35.36
ATOM    158  N   VAL    25      21.440 -15.111  10.372  1.00 21.17
ATOM    159  CA  VAL    25      21.281 -13.927   9.512  1.00 20.21
ATOM    160  C   VAL    25      21.873 -12.727  10.241  1.00 50.87
ATOM    161  O   VAL    25      21.859 -12.698  11.487  1.00 21.77
ATOM    162  CB  VAL    25      19.752 -13.762   9.342  1.00 22.90
ATOM    163  CG1 VAL    25      19.256 -12.410   8.872  1.00 31.11
ATOM    164  CG2 VAL    25      19.204 -14.913   8.522  1.00 26.05
ATOM    165  N   GLY    26      22.359 -11.758   9.505  1.00 22.94
ATOM    166  CA  GLY    26      22.802 -10.489  10.069  1.00 20.20
ATOM    167  C   GLY    26      24.059 -10.424  10.880  1.00 20.41
ATOM    168  O   GLY    26      24.987 -11.223  10.714  1.00 24.68
ATOM    169  N   HIS    27      24.090  -9.447  11.802  1.00 20.15
ATOM    170  CA  HIS    27      25.295  -9.134  12.548  1.00 17.08
ATOM    171  C   HIS    27      25.100  -9.385  14.092  1.00 19.80
ATOM    172  O   HIS    27      23.977  -9.150  14.505  1.00 20.06
ATOM    173  CB  HIS    27      25.542  -7.643  12.315  1.00 14.84
ATOM    174  CG  HIS    27      25.482  -7.277  10.817  1.00 28.82
ATOM    175  ND1 HIS    27      26.615  -7.372  10.030  1.00 28.86
ATOM    176  CE1 HIS    27      26.228  -6.925   8.824  1.00 22.19
ATOM    177  NE2 HIS    27      24.943  -6.611   8.759  1.00 19.15
ATOM    178  CD2 HIS    27      24.454  -6.837  10.054  1.00 27.66
ATOM    179  N   ALA    28      26.129  -9.866  14.707  1.00 32.77
ATOM    180  CA  ALA    28      26.090 -10.150  16.180  1.00 15.59
ATOM    181  C   ALA    28      26.097  -8.830  16.893  1.00 33.48
ATOM    182  O   ALA    28      26.684  -7.901  16.339  1.00 21.69
ATOM    183  CB  ALA    28      27.310 -11.016  16.492  1.00 18.23
ATOM    184  N   VAL    29      25.506  -8.703  18.083  1.00 20.76
ATOM    185  CA  VAL    29      25.467  -7.361  18.733  1.00 19.62
ATOM    186  C   VAL    29      26.794  -6.980  19.384  1.00 13.08
ATOM    187  O   VAL    29      27.020  -5.799  19.603  1.00 21.13
ATOM    188  CB  VAL    29      24.247  -7.373  19.677  1.00 23.63
ATOM    189  CG1 VAL    29      22.969  -7.755  18.920  1.00 18.68
ATOM    190  CG2 VAL    29      24.497  -8.440  20.777  1.00 18.26
ATOM    191  N   LYS    30      27.556  -7.992  19.667  1.00 23.01
ATOM    192  CA  LYS    30      28.848  -7.878  20.341  1.00 26.61
ATOM    193  C   LYS    30      29.839  -7.107  19.482  1.00 30.94
ATOM    194  O   LYS    30      30.078  -7.447  18.313  1.00 52.69
ATOM    195  CB  LYS    30      29.431  -9.254  20.663  1.00 28.14
ATOM    196  CG  LYS    30      30.805  -9.255  21.339  1.00 29.95
```

ATOM	197	CD	LYS	30	31.387	-10.665	21.401	1.00	32.34
ATOM	198	CE	LYS	30	32.726	-10.664	22.175	1.00	28.50
ATOM	199	NZ	LYS	30	32.920	-12.061	22.659	1.00	94.77
ATOM	200	N	GLY	31	30.322	-6.040	20.062	1.00	26.03
ATOM	201	CA	GLY	31	31.363	-5.181	19.498	1.00	33.42
ATOM	202	C	GLY	31	30.841	-3.840	19.026	1.00	36.56
ATOM	203	O	GLY	31	31.646	-2.950	18.703	1.00	52.68
ATOM	204	N	GLN	32	29.533	-3.717	18.981	1.00	26.87
ATOM	205	CA	GLN	32	28.870	-2.506	18.485	1.00	21.32
ATOM	206	C	GLN	32	28.754	-1.445	19.560	1.00	41.90
ATOM	207	O	GLN	32	28.745	-1.735	20.761	1.00	37.65
ATOM	208	CB	GLN	32	27.539	-2.865	17.801	1.00	28.78
ATOM	209	CG	GLN	32	27.636	-3.882	16.654	1.00	30.30
ATOM	210	CD	GLN	32	26.328	-3.940	15.889	1.00	14.83
ATOM	211	OE1	GLN	32	25.788	-2.897	15.519	1.00	24.33
ATOM	212	NE2	GLN	32	25.702	-5.087	15.670	1.00	21.86
ATOM	213	N	LYS	33	28.669	-0.215	19.136	1.00	27.08
ATOM	214	CA	LYS	33	28.560	0.990	19.942	1.00	29.49
ATOM	215	C	LYS	33	27.125	1.133	20.418	1.00	40.09
ATOM	216	O	LYS	33	26.189	0.938	19.638	1.00	27.52
ATOM	217	CB	LYS	33	28.981	2.234	19.157	1.00	38.70
ATOM	218	CG	LYS	33	30.481	2.252	18.910	1.00	39.05
ATOM	219	CD	LYS	33	30.980	3.613	18.446	1.00	64.26
ATOM	220	CE	LYS	33	32.416	3.538	17.957	1.00	108.72
ATOM	221	NZ	LYS	33	32.745	4.733	17.116	1.00	104.93
ATOM	222	N	ALA	34	26.921	1.527	21.664	1.00	23.76
ATOM	223	CA	ALA	34	25.562	1.667	22.173	1.00	26.24
ATOM	224	CB	ALA	34	25.628	2.257	23.579	1.00	29.56
ATOM	225	C	ALA	34	24.672	2.506	21.275	1.00	16.86
ATOM	226	O	ALA	34	23.488	2.213	21.138	1.00	20.35
ATOM	227	N	ASP	35	25.141	3.669	20.884	1.00	21.25
ATOM	228	CA	ASP	35	24.339	4.567	20.027	1.00	23.50
ATOM	229	CB	ASP	35	25.253	5.749	19.617	1.00	24.78
ATOM	230	CG	ASP	35	25.254	6.874	20.637	1.00	114.95
ATOM	231	OD1	ASP	35	24.507	6.826	21.631	1.00	82.07
ATOM	232	OD2	ASP	35	26.033	7.827	20.394	1.00	91.56
ATOM	233	C	ASP	35	23.854	3.766	18.777	1.00	15.56
ATOM	234	O	ASP	35	22.666	3.930	18.419	1.00	23.34
ATOM	235	N	GLU	36	24.788	3.001	18.278	1.00	28.75
ATOM	236	CA	GLU	36	24.494	2.201	17.058	1.00	35.03
ATOM	237	CB	GLU	36	25.751	1.614	16.482	1.00	25.68
ATOM	238	CG	GLU	36	25.872	0.172	16.038	1.00	106.65
ATOM	239	CD	GLU	36	27.004	-0.164	15.108	1.00	118.71
ATOM	240	OE1	GLU	36	27.011	0.064	13.907	1.00	81.37
ATOM	241	OE2	GLU	36	27.952	-0.727	15.698	1.00	91.68
ATOM	242	C	GLU	36	23.460	1.143	17.326	1.00	34.60
ATOM	243	O	GLU	36	22.476	1.039	16.605	1.00	20.81
ATOM	244	N	LEU	37	23.599	0.370	18.386	1.00	18.97
ATOM	245	CA	LEU	37	22.635	-0.660	18.786	1.00	24.73
ATOM	246	CB	LEU	37	23.334	-1.466	19.893	1.00	18.32
ATOM	247	CG	LEU	37	24.519	-2.317	19.524	1.00	16.73
ATOM	248	CD1	LEU	37	25.275	-2.741	20.805	1.00	32.07

```
ATOM    249  CD2 LEU    37      24.050  -3.598  18.828  1.00 18.93
ATOM    250  C   LEU    37      21.313  -0.020  19.085  1.00 13.62
ATOM    251  O   LEU    37      20.243  -0.572  18.778  1.00 18.94
ATOM    252  N   PHE    38      21.263   1.165  19.724  1.00 16.32
ATOM    253  CA  PHE    38      20.001   1.808  20.045  1.00 17.83
ATOM    254  CB  PHE    38      20.234   2.917  21.081  1.00 17.23
ATOM    255  CG  PHE    38      18.972   3.640  21.424  1.00 23.40
ATOM    256  CD1 PHE    38      17.874   2.946  21.896  1.00 28.19
ATOM    257  CE1 PHE    38      16.682   3.595  22.173  1.00 32.71
ATOM    258  CZ  PHE    38      16.580   4.970  21.988  1.00 45.81
ATOM    259  CE2 PHE    38      17.686   5.695  21.520  1.00 50.17
ATOM    260  CD2 PHE    38      18.876   5.014  21.241  1.00 40.33
ATOM    261  C   PHE    38      19.211   2.240  18.804  1.00 15.92
ATOM    262  O   PHE    38      18.002   1.992  18.715  1.00 18.46
ATOM    263  N   LYS    39      19.960   2.784  17.854  1.00 32.70
ATOM    264  CA  LYS    39      19.338   3.200  16.579  1.00 19.13
ATOM    265  CB  LYS    39      20.419   3.775  15.660  1.00 23.10
ATOM    266  CG  LYS    39      20.365   5.278  15.410  1.00 57.99
ATOM    267  CD  LYS    39      20.777   5.567  13.970  1.00 73.23
ATOM    268  CE  LYS    39      21.773   6.698  13.841  1.00102.75
ATOM    269  NZ  LYS    39      22.137   6.928  12.413  1.00 99.02
ATOM    270  C   LYS    39      18.711   2.014  15.856  1.00 20.80
ATOM    271  O   LYS    39      17.601   2.128  15.281  1.00 23.54
ATOM    272  N   LYS    40      19.433   0.901  15.926  1.00 16.94
ATOM    273  CA  LYS    40      18.948  -0.345  15.289  1.00 17.33
ATOM    274  CB  LYS    40      19.980  -1.424  15.172  1.00 21.37
ATOM    275  CG  LYS    40      21.126  -1.065  14.203  1.00 14.59
ATOM    276  CD  LYS    40      22.292  -1.969  14.262  1.00 14.71
ATOM    277  CE  LYS    40      23.315  -1.604  13.173  1.00 16.76
ATOM    278  NZ  LYS    40      24.411  -2.586  13.174  1.00 17.75
ATOM    279  C   LYS    40      17.675  -0.829  15.948  1.00 39.03
ATOM    280  O   LYS    40      16.712  -1.180  15.246  1.00 19.82
ATOM    281  N   LEU    41      17.629  -0.834  17.288  1.00 19.61
ATOM    282  CA  LEU    41      16.401  -1.269  17.981  1.00 17.46
ATOM    283  CB  LEU    41      16.684  -1.300  19.529  1.00 17.39
ATOM    284  CG  LEU    41      17.704  -2.284  19.989  1.00 18.49
ATOM    285  CD1 LEU    41      18.095  -2.046  21.471  1.00 22.18
ATOM    286  CD2 LEU    41      17.243  -3.732  19.809  1.00 19.21
ATOM    287  C   LEU    41      15.200  -0.429  17.620  1.00  7.85
ATOM    288  O   LEU    41      14.107  -0.954  17.356  1.00 17.45
ATOM    289  N   LYS    42      15.399   0.858  17.610  1.00 13.10
ATOM    290  CA  LYS    42      14.359   1.828  17.247  1.00 23.58
ATOM    291  CB  LYS    42      14.769   3.268  17.436  1.00 24.02
ATOM    292  CG  LYS    42      15.036   3.625  18.914  1.00 34.89
ATOM    293  CD  LYS    42      14.195   4.827  19.323  1.00 43.46
ATOM    294  CE  LYS    42      12.715   4.460  19.289  1.00 52.82
ATOM    295  NZ  LYS    42      11.906   5.710  19.363  1.00 62.13
ATOM    296  C   LYS    42      14.001   1.574  15.760  1.00 19.87
ATOM    297  O   LYS    42      12.810   1.609  15.510  1.00 20.69
ATOM    298  N   GLY    43      14.985   1.210  14.971  1.00 30.27
ATOM    299  CA  GLY    43      14.718   0.891  13.551  1.00 20.59
ATOM    300  C   GLY    43      13.765  -0.264  13.370  1.00 19.43
```

ATOM	301	O	GLY	43	12.938	-0.327	12.455	1.00	35.24
ATOM	302	N	TYR	44	13.938	-1.285	14.183	1.00	21.44
ATOM	303	CA	TYR	44	13.099	-2.474	14.157	1.00	19.10
ATOM	304	CB	TYR	44	13.653	-3.587	15.035	1.00	16.58
ATOM	305	CG	TYR	44	14.780	-4.407	14.472	1.00	19.32
ATOM	306	CD1	TYR	44	14.584	-5.138	13.268	1.00	22.17
ATOM	307	CE1	TYR	44	15.600	-5.918	12.798	1.00	18.13
ATOM	308	CZ	TYR	44	16.881	-5.896	13.311	1.00	16.17
ATOM	309	OH	TYR	44	17.892	-6.660	12.850	1.00	18.89
ATOM	310	CE2	TYR	44	17.117	-5.166	14.499	1.00	21.30
ATOM	311	CD2	TYR	44	16.055	-4.406	14.966	1.00	12.49
ATOM	312	C	TYR	44	11.665	-2.081	14.501	1.00	31.72
ATOM	313	O	TYR	44	10.699	-2.714	14.041	1.00	34.88
ATOM	314	N	ALA	45	11.567	-1.046	15.317	1.00	40.74
ATOM	315	CA	ALA	45	10.296	-0.485	15.785	1.00	56.96
ATOM	316	CB	ALA	45	10.442	0.371	17.029	1.00	46.36
ATOM	317	C	ALA	45	9.563	0.238	14.660	1.00	31.51
ATOM	318	O	ALA	45	8.395	-0.171	14.499	1.00	53.74
ATOM	319	N	ASP	46	10.162	1.165	13.929	1.00	45.22
ATOM	320	CA	ASP	46	9.520	1.851	12.803	1.00	41.37
ATOM	321	CB	ASP	46	10.183	3.139	12.307	1.00	44.23
ATOM	322	CG	ASP	46	11.665	3.195	12.621	1.00	38.68
ATOM	323	OD1	ASP	46	12.204	4.238	13.027	1.00	71.33
ATOM	324	OD2	ASP	46	12.262	2.106	12.503	1.00	77.86
ATOM	325	C	ASP	46	9.386	0.919	11.586	1.00	45.54
ATOM	326	O	ASP	46	8.501	1.146	10.755	1.00	96.85
ATOM	327	N	GLY	47	10.265	-0.047	11.501	1.00	51.07
ATOM	328	CA	GLY	47	10.333	-1.015	10.402	1.00	44.64
ATOM	329	C	GLY	47	11.464	-0.602	9.446	1.00	49.78
ATOM	330	O	GLY	47	11.818	-1.309	8.489	1.00	64.96
ATOM	331	N	SER	48	12.033	0.546	9.735	1.00	43.30
ATOM	332	CA	SER	48	13.118	1.202	8.997	1.00	27.69
ATOM	333	CB	SER	48	13.185	2.642	9.495	1.00	32.40
ATOM	334	OG	SER	48	14.276	2.977	10.319	1.00	44.67
ATOM	335	C	SER	48	14.471	0.522	9.002	1.00	46.26
ATOM	336	O	SER	48	15.372	0.933	8.231	1.00	32.60
ATOM	337	N	TYR	49	14.684	-0.472	9.847	1.00	28.07
ATOM	338	CA	TYR	49	15.963	-1.188	9.900	1.00	28.48
ATOM	339	CB	TYR	49	16.808	-0.797	11.168	1.00	17.61
ATOM	340	CG	TYR	49	18.094	-1.594	11.204	1.00	14.72
ATOM	341	CD1	TYR	49	19.232	-1.122	10.518	1.00	15.49
ATOM	342	CE1	TYR	49	20.405	-1.830	10.475	1.00	11.49
ATOM	343	CZ	TYR	49	20.601	-3.059	11.136	1.00	8.76
ATOM	344	OH	TYR	49	21.776	-3.687	11.123	1.00	17.30
ATOM	345	CE2	TYR	49	19.458	-3.514	11.861	1.00	16.46
ATOM	346	CD2	TYR	49	18.277	-2.778	11.900	1.00	15.15
ATOM	347	C	TYR	49	15.726	-2.676	9.814	1.00	20.43
ATOM	349	N	GLY	50	16.553	-3.475	9.138	1.00	16.74
ATOM	350	CA	GLY	50	16.403	-4.890	9.160	1.00	17.82
ATOM	351	C	GLY	50	16.633	-5.676	7.880	1.00	19.03
ATOM	352	O	GLY	50	16.432	-5.147	6.771	1.00	34.85
ATOM	353	N	GLY	51	16.977	-6.885	8.119	1.00	17.79

ATOM	354	CA	GLY	51	17.317	-7.891	7.072	1.00	26.60
ATOM	355	C	GLY	51	16.117	-8.737	6.759	1.00	10.29
ATOM	356	O	GLY	51	14.919	-8.351	6.963	1.00	18.32
ATOM	357	N	GLU	52	16.348	-9.963	6.309	1.00	13.03
ATOM	358	CA	GLU	52	15.320	-10.888	5.914	1.00	17.91
ATOM	359	C	GLU	52	14.407	-11.413	7.008	1.00	28.37
ATOM	360	O	GLU	52	13.301	-11.871	6.730	1.00	19.20
ATOM	361	CB	GLU	52	15.891	-12.055	5.115	1.00	23.93
ATOM	362	CG	GLU	52	17.087	-12.705	5.791	1.00	48.07
ATOM	363	CD	GLU	52	17.928	-13.568	4.889	1.00	57.60
ATOM	364	OE1	GLU	52	17.453	-14.595	4.431	1.00	50.50
ATOM	365	OE2	GLU	52	19.076	-13.069	4.767	1.00	35.66
ATOM	366	N	LYS	53	14.931	-11.353	8.235	1.00	22.11
ATOM	367	CA	LYS	53	14.096	-11.842	9.383	1.00	21.68
ATOM	368	C	LYS	53	13.758	-10.687	10.309	1.00	33.49
ATOM	369	O	LYS	53	13.504	-10.951	11.503	1.00	26.91
ATOM	370	CB	LYS	53	14.894	-12.845	10.171	1.00	19.86
ATOM	371	CG	LYS	53	15.528	-14.001	9.430	1.00	30.93
ATOM	372	CD	LYS	53	15.358	-15.315	10.154	1.00	34.04
ATOM	373	CE	LYS	53	14.832	-16.421	9.262	1.00	63.23
ATOM	374	NZ	LYS	53	13.343	-16.417	9.286	1.00	55.73
ATOM	375	N	LYS	54	13.738	-9.470	9.842	1.00	18.73
ATOM	376	CA	LYS	54	13.455	-8.255	10.554	1.00	18.10
ATOM	377	C	LYS	54	12.212	-8.364	11.422	1.00	30.51
ATOM	378	O	LYS	54	12.224	-7.867	12.570	1.00	20.81
ATOM	379	CB	LYS	54	13.504	-6.983	9.761	1.00	25.11
ATOM	380	CG	LYS	54	12.350	-6.790	8.781	1.00	30.54
ATOM	381	CD	LYS	54	12.352	-5.342	8.290	1.00	31.82
ATOM	382	CE	LYS	54	11.781	-5.234	6.888	1.00	64.13
ATOM	383	NZ	LYS	54	11.815	-3.809	6.475	1.00	58.42
ATOM	384	N	ALA	55	11.165	-8.991	10.980	1.00	22.40
ATOM	385	CA	ALA	55	9.885	-9.136	11.667	1.00	34.21
ATOM	386	C	ALA	55	10.058	-9.821	13.031	1.00	20.33
ATOM	387	O	ALA	55	9.239	-9.477	13.905	1.00	23.99
ATOM	388	CB	ALA	55	8.806	-9.838	10.859	1.00	25.63
ATOM	389	N	VAL	56	10.971	-10.735	13.143	1.00	21.69
ATOM	390	CA	VAL	56	11.197	-11.427	14.432	1.00	24.30
ATOM	391	C	VAL	56	11.556	-10.400	15.508	1.00	44.52
ATOM	392	O	VAL	56	11.086	-10.448	16.657	1.00	22.85
ATOM	393	CB	VAL	56	12.234	-12.522	14.208	1.00	19.52
ATOM	394	CG1	VAL	56	12.991	-12.961	15.455	1.00	26.49
ATOM	395	CG2	VAL	56	11.571	-13.719	13.544	1.00	27.99
ATOM	396	N	MET	57	12.345	-9.427	15.113	1.00	16.88
ATOM	397	CA	MET	57	12.808	-8.365	16.052	1.00	16.86
ATOM	398	C	MET	57	11.728	-7.332	16.257	1.00	29.35
ATOM	399	O	MET	57	11.533	-6.787	17.372	1.00	20.70
ATOM	400	CB	MET	57	14.148	-7.772	15.710	1.00	8.99
ATOM	401	CG	MET	57	15.309	-8.666	15.822	1.00	7.79
ATOM	402	SD	MET	57	15.529	-8.739	17.731	1.00	17.60
ATOM	403	CE	MET	57	15.666	-7.078	18.113	1.00	14.84
ATOM	404	N	THR	58	10.989	-6.949	15.222	1.00	20.65
ATOM	405	CA	THR	58	9.902	-5.996	15.312	1.00	17.09

```
ATOM    406  C   THR  58       8.852  -6.410  16.391  1.00 18.08
ATOM    407  O   THR  58       8.422  -5.533  17.182  1.00 21.07
ATOM    408  CB  THR  58       9.139  -5.797  13.928  1.00 22.97
ATOM    409  OG1 THR  58      10.116  -5.005  13.183  1.00 26.60
ATOM    410  CG2 THR  58       7.871  -4.979  14.139  1.00 23.70
ATOM    411  N   ASN  59       8.495  -7.643  16.393  1.00 16.81
ATOM    412  CA  ASN  59       7.473  -8.219  17.277  1.00 17.22
ATOM    413  C   ASN  59       7.965  -8.060  18.772  1.00 22.47
ATOM    414  O   ASN  59       7.049  -7.881  19.601  1.00 20.94
ATOM    415  CB  ASN  59       7.226  -9.642  16.948  1.00 15.95
ATOM    416  CG  ASN  59       6.289 -10.387  17.865  1.00 26.82
ATOM    417  OD1 ASN  59       6.795 -10.859  18.915  1.00 23.21
ATOM    418  ND2 ASN  59       5.044 -10.591  17.543  1.00 18.33
ATOM    419  N   LEU  60       9.257  -8.174  18.901  1.00 20.94
ATOM    420  CA  LEU  60       9.860  -8.024  20.261  1.00 19.42
ATOM    421  C   LEU  60      10.060  -6.625  20.765  1.00 29.98
ATOM    422  O   LEU  60       9.576  -6.336  21.887  1.00 22.66
ATOM    423  CB  LEU  60      11.196  -8.752  20.229  1.00 18.07
ATOM    424  CG  LEU  60      11.132 -10.245  20.030  1.00 29.40
ATOM    425  CD1 LEU  60      12.543 -10.825  20.064  1.00 30.18
ATOM    426  CD2 LEU  60      10.183 -10.831  21.070  1.00 31.87
ATOM    427  N   VAL  61      10.817  -5.818  20.058  1.00 22.39
ATOM    428  CA  VAL  61      11.136  -4.463  20.452  1.00 23.96
ATOM    429  C   VAL  61       9.922  -3.598  20.706  1.00 20.00
ATOM    430  O   VAL  61      10.091  -2.530  21.369  1.00 20.99
ATOM    431  CB  VAL  61      12.023  -3.701  19.424  1.00 29.03
ATOM    432  CG1 VAL  61      13.288  -4.372  19.037  1.00 21.16
ATOM    433  CG2 VAL  61      11.188  -3.256  18.234  1.00 28.50
ATOM    434  N   LYS  62       8.743  -3.882  20.205  1.00 14.46
ATOM    435  CA  LYS  62       7.610  -3.015  20.403  1.00 19.32
ATOM    436  C   LYS  62       7.104  -3.187  21.896  1.00 12.24
ATOM    437  O   LYS  62       6.249  -2.368  22.201  1.00 19.36
ATOM    438  CB  LYS  62       6.470  -3.459  19.459  1.00 23.37
ATOM    439  CG  LYS  62       6.737  -2.723  18.106  1.00 39.58
ATOM    440  CD  LYS  62       5.638  -3.080  17.121  1.00 33.74
ATOM    441  CE  LYS  62       4.261  -2.780  17.683  1.00116.98
ATOM    442  NZ  LYS  62       3.185  -3.417  16.883  1.00 79.49
ATOM    443  N   ARG  63       7.682  -4.239  22.450  1.00 16.31
ATOM    444  CA  ARG  63       7.190  -4.489  23.899  1.00 16.98
ATOM    445  C   ARG  63       8.022  -3.741  24.898  1.00 27.14
ATOM    446  O   ARG  63       7.796  -3.885  26.132  1.00 21.60
ATOM    447  CB  ARG  63       7.343  -5.977  24.076  1.00 13.71
ATOM    448  CG  ARG  63       6.398  -6.842  23.246  1.00 17.25
ATOM    449  CD  ARG  63       6.941  -8.211  23.174  1.00 25.37
ATOM    450  NE  ARG  63       6.249  -9.092  22.242  1.00 16.38
ATOM    451  CZ  ARG  63       5.039  -9.541  22.164  1.00 17.63
ATOM    452  NH1 ARG  63       3.983  -9.304  22.968  1.00 13.60
ATOM    453  NH2 ARG  63       4.597 -10.250  21.047  1.00 18.05
ATOM    454  N   TYR  64       8.979  -2.986  24.473  1.00 17.46
ATOM    455  CA  TYR  64       9.946  -2.224  25.231  1.00 17.91
ATOM    456  C   TYR  64       9.892  -0.740  25.072  1.00 25.89
ATOM    457  O   TYR  64       9.522  -0.146  24.042  1.00 21.87
```

ATOM	458	CB	TYR	64	11.383	-2.739	25.087	1.00	20.93
ATOM	459	CG	TYR	64	11.588	-4.160	25.489	1.00	22.48
ATOM	460	CD1	TYR	64	12.068	-4.476	26.795	1.00	17.52
ATOM	461	CD2	TYR	64	11.276	-5.227	24.655	1.00	18.01
ATOM	462	CE1	TYR	64	12.249	-5.795	27.122	1.00	11.66
ATOM	463	CE2	TYR	64	11.426	-6.572	24.986	1.00	15.21
ATOM	464	CZ	TYR	64	11.896	-6.863	26.322	1.00	20.64
ATOM	465	OH	TYR	64	12.031	-8.138	26.685	1.00	19.60
ATOM	466	N	SER	65	10.305	-0.038	26.158	1.00	18.24
ATOM	467	CA	SER	65	10.302	1.410	26.098	1.00	15.19
ATOM	468	C	SER	65	11.646	1.860	25.564	1.00	7.79
ATOM	469	O	SER	65	12.669	1.133	25.546	1.00	17.41
ATOM	470	CB	SER	65	10.038	2.072	27.466	1.00	21.94
ATOM	471	OG	SER	65	11.213	1.803	28.240	1.00	21.28
ATOM	472	N	ASP	66	11.671	3.126	25.153	1.00	16.84
ATOM	473	CA	ASP	66	12.914	3.713	24.678	1.00	19.95
ATOM	474	C	ASP	66	14.006	3.583	25.735	1.00	25.79
ATOM	475	O	ASP	66	15.139	3.274	25.386	1.00	18.09
ATOM	476	CB	ASP	66	12.806	5.138	24.183	1.00	27.02
ATOM	477	CG	ASP	66	12.143	5.301	22.824	1.00	36.59
ATOM	478	OD1	ASP	66	11.371	4.482	22.333	1.00	27.49
ATOM	479	OD2	ASP	66	12.415	6.379	22.269	1.00	43.72
ATOM	480	N	GLU	67	13.700	3.894	27.029	1.00	19.39
ATOM	481	CA	GLU	67	14.789	3.781	28.015	1.00	21.46
ATOM	482	C	GLU	67	15.241	2.350	28.221	1.00	9.83
ATOM	483	O	GLU	67	16.427	2.120	28.478	1.00	13.77
ATOM	484	CB	GLU	67	14.275	4.453	29.325	1.00	24.18
ATOM	485	CG	GLU	67	13.902	5.948	29.209	1.00	16.90
ATOM	486	CD	GLU	67	12.574	6.214	28.598	1.00	21.99
ATOM	487	OE1	GLU	67	11.659	5.446	28.329	1.00	32.90
ATOM	488	OE2	GLU	67	12.444	7.425	28.282	1.00	52.26
ATOM	489	N	GLU	68	14.367	1.383	28.117	1.00	13.20
ATOM	490	CA	GLU	68	14.639	-0.034	28.195	1.00	10.94
ATOM	491	C	GLU	68	15.620	-0.424	27.047	1.00	15.65
ATOM	492	O	GLU	68	16.684	-1.015	27.142	1.00	14.00
ATOM	493	CB	GLU	68	13.465	-0.948	28.246	1.00	16.97
ATOM	494	CG	GLU	68	12.736	-0.783	29.640	1.00	14.62
ATOM	495	CD	GLU	68	11.473	-1.532	29.680	1.00	27.02
ATOM	496	OE1	GLU	68	11.112	-2.074	30.725	1.00	22.09
ATOM	497	OE2	GLU	68	10.739	-1.533	28.664	1.00	18.45
ATOM	498	N	MET	69	15.228	0.120	25.852	1.00	18.89
ATOM	499	CA	MET	69	16.174	-0.159	24.699	1.00	17.19
ATOM	500	C	MET	69	17.555	0.366	24.856	1.00	8.25
ATOM	501	O	MET	69	18.642	-0.258	24.659	1.00	19.50
ATOM	502	CB	MET	69	15.483	0.415	23.413	1.00	12.14
ATOM	503	CG	MET	69	14.248	-0.369	23.135	1.00	11.91
ATOM	504	SD	MET	69	13.661	0.374	21.511	1.00	30.10
ATOM	505	CE	MET	69	12.400	-0.843	21.263	1.00	32.61
ATOM	506	N	LYS	70	17.698	1.612	25.369	1.00	16.93
ATOM	507	CA	LYS	70	18.872	2.403	25.651	1.00	18.44
ATOM	508	C	LYS	70	19.747	1.622	26.638	1.00	16.24
ATOM	509	O	LYS	70	20.925	1.349	26.482	1.00	16.38

ATOM	510	CB	LYS	70	18.578	3.782	26.173	1.00	21.15
ATOM	511	CG	LYS	70	19.668	4.822	26.029	1.00	41.91
ATOM	512	CD	LYS	70	21.072	4.291	25.828	1.00	80.78
ATOM	513	CE	LYS	70	21.429	4.094	24.371	1.00	86.91
ATOM	515	N	ALA	71	18.995	1.095	27.654	1.00	17.56
ATOM	516	CA	ALA	71	19.741	0.258	28.632	1.00	16.15
ATOM	517	C	ALA	71	20.284	-1.024	28.079	1.00	12.30
ATOM	518	O	ALA	71	21.391	-1.481	28.448	1.00	17.80
ATOM	519	CB	ALA	71	18.844	0.010	29.880	1.00	17.17
ATOM	520	N	MET	72	19.484	-1.725	27.237	1.00	12.96
ATOM	521	CA	MET	72	19.958	-2.988	26.590	1.00	18.84
ATOM	522	C	MET	72	21.149	-2.623	25.660	1.00	17.37
ATOM	523	O	MET	72	22.096	-3.421	25.624	1.00	18.30
ATOM	524	CB	MET	72	18.800	-3.661	25.890	1.00	16.46
ATOM	525	CG	MET	72	17.909	-4.369	26.858	1.00	16.08
ATOM	526	SD	MET	72	16.588	-5.357	26.159	1.00	21.27
ATOM	527	CE	MET	72	15.581	-4.111	25.420	1.00	20.06
ATOM	528	N	ALA	73	21.032	-1.508	24.964	1.00	21.95
ATOM	529	CA	ALA	73	22.114	-1.096	24.032	1.00	20.03
ATOM	530	C	ALA	73	23.429	-0.877	24.754	1.00	16.05
ATOM	531	O	ALA	73	24.499	-1.374	24.434	1.00	19.55
ATOM	532	CB	ALA	73	21.655	0.160	23.298	1.00	21.16
ATOM	533	N	ASP	74	23.226	-0.129	25.897	1.00	22.79
ATOM	534	CA	ASP	74	24.433	0.062	26.755	1.00	19.94
ATOM	535	C	ASP	74	25.062	-1.241	27.121	1.00	10.93
ATOM	536	O	ASP	74	26.285	-1.416	27.039	1.00	18.32
ATOM	537	CB	ASP	74	24.086	1.060	27.880	1.00	31.87
ATOM	538	CG	ASP	74	24.374	2.454	27.316	1.00	90.18
ATOM	539	OD1	ASP	74	25.549	2.843	27.215	1.00	87.93
ATOM	540	OD2	ASP	74	23.386	3.099	26.915	1.00	74.31
ATOM	541	N	TYR	75	24.320	-2.188	27.689	1.00	17.97
ATOM	542	CA	TYR	75	24.725	-3.509	28.143	1.00	16.32
ATOM	543	C	TYR	75	25.416	-4.300	27.026	1.00	21.85
ATOM	544	O	TYR	75	26.513	-4.819	27.151	1.00	20.14
ATOM	545	CB	TYR	75	23.539	-4.300	28.747	1.00	21.70
ATOM	546	CG	TYR	75	23.940	-5.657	29.245	1.00	17.27
ATOM	547	CD1	TYR	75	23.694	-6.815	28.513	1.00	22.09
ATOM	548	CD2	TYR	75	24.705	-5.851	30.432	1.00	17.13
ATOM	549	CE1	TYR	75	24.074	-8.071	28.893	1.00	23.40
ATOM	550	CE2	TYR	75	25.123	-7.118	30.800	1.00	17.54
ATOM	551	CZ	TYR	75	24.824	-8.243	30.083	1.00	17.82
ATOM	552	OH	TYR	75	25.141	-9.505	30.445	1.00	23.77
ATOM	553	N	MET	76	24.725	-4.346	25.880	1.00	23.41
ATOM	554	CA	MET	76	25.272	-5.112	24.741	1.00	23.60
ATOM	555	C	MET	76	26.631	-4.526	24.325	1.00	14.91
ATOM	556	O	MET	76	27.531	-5.326	24.024	1.00	23.72
ATOM	557	CB	MET	76	24.190	-5.178	23.663	1.00	19.07
ATOM	558	CG	MET	76	23.080	-6.147	23.943	1.00	15.35
ATOM	559	SD	MET	76	22.006	-6.189	22.407	1.00	21.02
ATOM	560	CE	MET	76	21.313	-4.604	22.371	1.00	16.60
ATOM	561	N	SER	77	26.778	-3.242	24.356	1.00	15.16
ATOM	562	CA	SER	77	27.954	-2.463	24.017	1.00	20.88

```
ATOM    563  C   SER   77      29.147  -2.832  24.892  1.00 32.99
ATOM    564  O   SER   77      30.301  -2.688  24.437  1.00 27.83
ATOM    565  CB  SER   77      27.632  -1.008  23.973  1.00 22.59
ATOM    566  OG  SER   77      27.934  -0.357  25.188  1.00 41.41
ATOM    567  N   LYS   78      28.854  -3.401  26.064  1.00 30.31
ATOM    568  CA  LYS   78      29.907  -3.843  26.984  1.00 27.15
ATOM    569  C   LYS   78      30.188  -5.311  26.897  1.00 30.91
ATOM    570  O   LYS   78      31.135  -5.812  27.532  1.00 30.33
ATOM    571  CB  LYS   78      29.571  -3.404  28.418  1.00 36.23
ATOM    572  CG  LYS   78      29.607  -1.874  28.525  1.00 37.56
ATOM    573  CD  LYS   78      28.909  -1.373  29.780  1.00 62.12
ATOM    574  CE  LYS   78      28.954   0.143  29.866  1.00 38.12
ATOM    575  NZ  LYS   78      27.633   0.666  30.308  1.00 67.07
ATOM    576  N   LEU   79      29.433  -6.073  26.124  1.00 22.86
ATOM    577  CA  LEU   79      29.716  -7.492  25.958  1.00 18.50
ATOM    578  C   LEU   79      31.061  -7.721  25.259  1.00 39.59
ATOM    579  O   LEU   79      31.622  -8.784  25.592  1.00 37.51
ATOM    580  CB  LEU   79      28.528  -8.170  25.296  1.00 36.02
ATOM    581  CG  LEU   79      27.234  -8.291  26.077  1.00 38.32
ATOM    582  CD1 LEU   79      26.234  -8.993  25.153  1.00 25.28
ATOM    583  CD2 LEU   79      27.409  -9.141  27.343  1.00 26.53
ATOM    584  OXT LEU   79      31.500  -6.855  24.487  1.00 32.12
ATOM    585  FE  HEM   80      17.581  -9.819  18.175  1.00 16.80
ATOM    586  CHA HEM   80      18.823  -8.651  15.271  1.00 16.62
ATOM    587  CHB HEM   80      18.888  -7.144  19.848  1.00 14.44
ATOM    588  CHC HEM   80      15.892 -10.800  20.992  1.00 15.01
ATOM    589  CHD HEM   80      16.667 -12.821  16.636  1.00 20.82
ATOM    590  N A HEM   80      18.601  -8.233  17.715  1.00 17.89
ATOM    591  C1A HEM   80      19.086  -7.817  16.385  1.00 11.64
ATOM    592  C2A HEM   80      19.873  -6.652  16.422  1.00 15.00
ATOM    593  C3A HEM   80      19.898  -6.192  17.731  1.00 17.63
ATOM    594  C4A HEM   80      19.132  -7.165  18.426  1.00 13.12
ATOM    595  CMA HEM   80      20.602  -4.960  18.272  1.00 16.58
ATOM    596  CAA HEM   80      20.617  -6.021  15.227  1.00 15.34
ATOM    597  CBA HEM   80      22.038  -6.497  14.957  1.00 16.49
ATOM    598  CGA HEM   80      22.619  -5.691  13.753  1.00 14.06
ATOM    599  O1A HEM   80      23.631  -5.009  13.910  1.00 16.72
ATOM    600  O2A HEM   80      21.752  -5.780  12.818  1.00 20.26
ATOM    601  N B HEM   80      17.414  -9.095  20.110  1.00  6.35
ATOM    602  C1B HEM   80      18.020  -7.974  20.438  1.00 12.73
ATOM    603  C2B HEM   80      17.644  -7.811  21.910  1.00 12.77
ATOM    604  C3B HEM   80      16.777  -8.757  22.183  1.00 14.25
ATOM    605  C4B HEM   80      16.611  -9.678  21.083  1.00 14.66
ATOM    606  CMB HEM   80      18.179  -6.609  22.678  1.00 17.50
ATOM    607  CAB HEM   80      16.056  -9.004  23.575  1.00 17.21
ATOM    608  CBB HEM   80      15.181  -7.987  23.925  1.00 19.16
ATOM    609  N C HEM   80      16.514 -11.388  18.618  1.00 19.47
ATOM    610  C1C HEM   80      15.969 -11.713  19.914  1.00 16.31
ATOM    611  C2C HEM   80      15.413 -13.010  19.950  1.00 19.16
ATOM    612  C3C HEM   80      15.585 -13.579  18.734  1.00 19.75
ATOM    613  C4C HEM   80      16.310 -12.595  17.990  1.00 12.49
ATOM    614  CMC HEM   80      14.771 -13.617  21.247  1.00 17.12
```

```
ATOM    615  CAC HEM    80      15.254 -15.029  18.329  1.00 17.89
ATOM    616  CBC HEM    80      13.995 -15.467  18.258  1.00 16.91
ATOM    617  N  D HEM    80      17.731 -10.577  16.276  1.00  7.16
ATOM    618  C1D HEM    80      17.199 -11.777  15.961  1.00 13.60
ATOM    619  C2D HEM    80      17.420 -11.859  14.447  1.00 13.16
ATOM    620  C3D HEM    80      17.951 -10.718  14.110  1.00 15.80
ATOM    621  C4D HEM    80      18.215  -9.854  15.228  1.00 28.85
ATOM    622  CMD HEM    80      16.877 -13.048  13.622  1.00 14.68
ATOM    623  CAD HEM    80      18.261 -10.184  12.610  1.00 12.58
ATOM    624  CBD HEM    80      16.920  -9.723  12.022  1.00 13.32
ATOM    625  CGD HEM    80      17.132  -8.993  10.655  1.00 16.98
ATOM    626  O1D HEM    80      16.800  -9.764   9.713  1.00 22.19
ATOM    627  O2D HEM    80      17.513  -7.832  10.654  1.00 16.77
ATOM    628  O    WAT    81      21.185  -0.619  33.042  1.00 32.58
ATOM    629  O    WAT    82      13.222   1.294  35.169  1.00 24.01
ATOM    630  O    WAT    83      12.233  -2.707  33.177  1.00 19.76
ATOM    631  O    WAT    84      10.654 -10.092   8.338  1.00 31.78
ATOM    632  O    WAT    85      19.101 -10.450   5.173  1.00 26.05
ATOM    633  O    WAT    86       3.278  -5.160  21.384  1.00 40.18
ATOM    634  O    WAT    87       4.444  -7.045  19.155  1.00 23.24
ATOM    635  O    WAT    88      13.351  -8.597  28.873  1.00 19.19
ATOM    636  O    WAT    89      28.727  -7.919  10.754  1.00 34.32
ATOM    637  O    WAT    90      33.699 -13.010  19.924  1.00 36.39
ATOM    638  O    WAT    91      27.763   4.829  21.882  1.00 43.95
ATOM    639  O    WAT    92      18.173   3.455  30.316  1.00 24.39
ATOM    640  O    WAT    93      21.286  -8.246  11.952  1.00 26.00
ATOM    641  O    WAT    94       9.608 -12.889  17.365  1.00 34.80
ATOM    642  O    WAT    95      20.097 -18.047  16.983  1.00 31.88
ATOM    643  O    WAT    96      18.867   2.747  33.126  1.00 23.77
ATOM    644  O    WAT    97      24.163 -11.383  18.607  1.00 24.72
ATOM    645  O    WAT    98      15.753 -10.562  34.027  1.00 27.73
ATOM    646  O    WAT    99      15.993 -15.698  24.496  1.00 36.67
ATOM    647  O    WAT   100       9.005   4.682  25.102  1.00 35.01
ATOM    648  O    WAT   101       7.830  -0.687  29.268  1.00 37.82
ATOM    649  O    WAT   102      22.483 -10.467  31.345  1.00 38.95
ATOM    650  O    WAT   103      11.822   0.479  32.879  1.00 27.37
ATOM    651  O    WAT   104       5.092  -3.230  27.124  1.00 36.57
ATOM    652  O    WAT   105       8.910  -1.957  32.511  1.00 29.05
ATOM    653  O    WAT   106      20.924   3.764  29.722  1.00 36.97
ATOM    654  O    WAT   107      24.823 -18.771  25.060  1.00 51.29
ATOM    655  O    WAT   108      12.911 -11.305  23.734  1.00 31.08
ATOM    656  O    WAT   109      29.610   2.182  23.142  1.00 39.93
ATOM    657  O    WAT   110      29.890  -5.394  22.706  1.00 32.26
ATOM    658  O    WAT   111      22.415 -11.273  15.858  1.00 29.69
ATOM    659  O    WAT   112      20.191   2.293  11.974  1.00 52.69
ATOM    660  O    WAT   113      15.749  -8.137  38.277  1.00 49.22
ATOM    661  O    WAT   114      21.050 -11.025  13.633  1.00 27.43
ATOM    662  O    WAT   115      10.995  -9.928  24.829  1.00 32.51
ATOM    663  O    WAT   116       9.910   6.337  27.553  1.00 42.08
ATOM    664  O    WAT   117       6.626  -0.141  27.066  1.00 42.13
ATOM    665  O    WAT   118      16.439   6.048  29.359  1.00 43.33
ATOM    666  O    WAT   119       9.391   2.196  22.553  1.00 47.26
```

```
ATOM    667  O   WAT   120      24.833 -11.803  29.288  1.00 36.70
ATOM    668  O   WAT   121      22.825 -13.167  30.121  1.00 49.20
ATOM    669  O   WAT   122      27.794  -6.247  29.382  1.00 46.25
ATOM    670  O   WAT   123      14.836  -3.532   6.121  1.00 42.19
ATOM    671  O   WAT   124      12.735  -8.188  31.677  1.00 34.17
ATOM    672  O   WAT   125      16.138   4.176  13.977  1.00 41.10
ATOM    673  O   WAT   126      18.524  -6.817  38.638  1.00 43.91
ATOM    674  O   WAT   127      33.448  -7.188  22.713  1.00 47.37
ATOM    675  O   WAT   128      33.310 -14.451  21.791  1.00 44.92
ATOM    676  O   WAT   129      18.772 -15.748  29.993  1.00 37.62
ATOM    677  O   WAT   130       5.332  -0.003  21.206  1.00 66.42
ATOM    678  O   WAT   131      28.713  -9.693  30.358  1.00 43.30
ATOM    679  O   WAT   132      14.193 -10.563  31.711  1.00 65.35
ATOM    681  O   WAT   134       6.524   0.935  18.929  1.00 62.24
ATOM    682  O   WAT   135       6.708  -0.571  31.549  1.00 50.99
ATOM    683  O   WAT   136       8.778   7.150  18.757  1.00 66.91
ATOM    684  O   WAT   137      19.346 -17.049  33.467  1.00 77.15
ATOM    685  O   WAT   138       7.213   2.709  17.230  1.00 60.94
ATOM    686  O   WAT   139      20.281 -22.137  17.117  1.00 72.37
ATOM    687  O   WAT   140      27.162 -17.609  15.266  1.00 52.56
ATOM    688  O   WAT   141      28.769  -7.352  14.873  1.00 45.14
ATOM    689  O   WAT   142      17.077 -10.725  36.734  1.00 45.41
ATOM    690  O   WAT   143      10.215 -16.354  10.876  1.00 64.95
```

LIST OF PUBLICATIONS

(1) Crystallographic study of Cytochrome c_{553} from *Desulfovibrio vulgaris* Miyazaki

Atsushi Nakagawa, Etsuro Nagashima, Yoshiki Higuchi, Masami Kusunoki, Yoshiki Matsuura, Noritake Yasuoka, Yukiteru Katsube, Hideaki Chihara, and Tatsuhiko Yagi (1986) *J.Biochem. (Tokyo)*, **99**, 605-606

(2) Design and performance of an Imaging Plate system for X-ray diffraction study

Yoshiyuki Amemiya, Tadashi Matsushita, Atsushi Nakagawa, Yoshinori Satow, Junji Miyahara and Jun-ichi Chikawa, (1988) *Nucl.Instrum.Methods*, **A266**, 645-653

(3) Structure determination of Cytochrome c_{553} by the multi-wavelength anomalous dispersion method

(in preparation)